THE UNIVERSITY OF CHICAGO

DEVELOPMENT OF DNA BASED VOLTAGE SENSORS FOR INTRACELLULAR ORGANELLES

A DISSERTATION SUBMITTED TO

THE FACULTY OF THE DIVISION OF THE PHYSICAL SCIENCES

IN CANDIDACY FOR THE DEGREE OF

DOCTOR OF PHILOSOPHY

DEPARTMENT OF CHEMISTRY

BY

ANAND SAMINATHAN

CHICAGO, ILLINOIS

MARCH 2021

Table of Contents

List of Figures:

List of Tables:

List of publications:

1. Saminathan, A., Devany, J., Veetil, A.T., Suresh, B., Pillai, K.S., Schwake, M. and Krishnan, Y., 2021. A DNA-based voltmeter for organelles. ***Nature Nanotechnology***, 16(1), pp.96-103.
2. Suresh, B., Saminathan, A., Chakraborty, K., Cui, C., Becker, L. and Krishnan, Y., 2020. Tubular lysosomes harbor active ion gradients and poise macrophages for phagocytosis. ***bioRxiv***.
3. Saminathan, A., Noyola, V.S. and Krishnan, Y., 2020. Chemically Resolving Lysosome Populations in Live Cells. ***Trends in biochemical sciences***, 45(4), p.365.
4. Sayresmith, N.A., Saminathan, A., Sailer, J.K., Patberg, S.M., Sandor, K., Krishnan, Y. and Walter, M.G., 2019. Photostable Voltage-Sensitive Dyes Based on Simple, Solvatofluorochromic, Asymmetric Thiazolothiazoles. ***Journal of the American Chemical Society***, 141(47), pp.18780-18790.
5. Leung, K., Chakraborty, K., Saminathan, A. and Krishnan, Y., 2019. A DNA nanomachine chemically resolves lysosomes in live cells. ***Nature nanotechnology***, 14(2), p.176.
6. Narayanaswamy, N., Chakraborty, K., Saminathan, A., Zeichner, E., Leung, K., Devany, J. and Krishnan, Y., 2019. A pH-correctable, DNA-based fluorescent reporter for organellar calcium. ***Nature methods***, 16(1), p.95.
7. Banerjee, A., Bhatia, D., Saminathan, A., Chakraborty, S., Kar, S. and Krishnan, Y., 2013. Controlled release of encapsulated cargo from a DNA icosahedron using a chemical trigger. ***Angewandte Chemie International Edition***, 52(27), pp.6854-6857.

Abstract:

The role of membrane potential as a source of energy and as a signaling cue remains unexplored in most intracellular organelles. Here, we introduce DNA based voltage sensors, (i) Voltair, a fluorescent nanodevice that quantitatively reports the absolute membrane potential and (ii) mVivo, a photoactivable nanodevice that reports changes in membrane potential, across intracellular membrane. DNA based voltage probes consists of a voltage-sensitive fluorophore, a reference fluorophore as ratiometric and fiducial marker, and a targeting moiety that localizes the probe to specific organellar membranes. Using Voltair, we could quantify the resting membrane potential of different organelles in situ. DNA based voltage probes can potentially guide the rational design of biocompatible electronics and further enhance our understanding of how intracellular organelles use membrane potential as a battery source and as a transmission signal.

Acknowledgments:

I consider the possibility to understand, probe or even witness science as a noble prospect and I would not have had this opportunity if not for my mentors, friends and family. First and foremost, I would like to thank my doctoral advisor Prof. Yamuna Krishnan for her constant support and encouragement. A summer internship with Yamuna had seeded the excitement and passion for science, in me. I was fortunate to have an advisor like Yamuna, who stood by me thorough all my unsuccessful experiments, projects, presentations and proposals. She made me realize that curiosity is endless and has always encouraged me to pursue curiosity driven science every single day. I am grateful for all of her efforts, time, patience and energy in making my Ph.D. experience fun, stimulating and successful.

I would also like to take this opportunity to thank all my lab seniors Saikat, Shabana, Sonali, Sunaina, Dhiraj, Saheli and Masood for showing by example what is expected out of you as a scientist and how to push boundaries. I would like to specifically thank Suruchi and Aneesh, who mentored me during my first and second year, respectively. Suruchi showed me that experiments can be as fun as interpreting results and Aneesh taught me how to deconstruct a scientific idea to understand its value. I would also like to thank my lab peers Shareefa, Junyi, Matt, Krishna, Maulik, Anees, Nagarjun, Ved, Kate, Ellie, John for not going easy on me during our lab presentations or discussions and pushing me to be a better version of myself. I owe special thanks to Bhavya and Kaho who spent countless hours listening and criticizing my scientific ideas or proposals. I would also like to thank Prof. Dickinson lab and Prof. He lab for various reagents and protocols, Prof. Bezanilla lab (Joao L. C. Souza), Jary Delgado and Prof. Tian lab (Yuanwen Jiang) for discussions and assistance with electrophysiology. I would like to specifically thank Xiaoli Zhang and Prof. Haoxing Xu (University of Michigan) for teaching lysosome electrophysiology.

Finally, I would also like to thank Prof. Tomas Kirchhausen at Boston Children Hospital, Prof. Michael Walter at University of North Carolina and Dr. Michael Schwake at Bielefeld University for critical contributions in our collaborative research.

I would like to thank Kasturi, my best friend, lab mate, inspiration and partner, for all her love and support. She had my back personally and professionally, and immensely helped me refine my scientific ideas and experiments. I would also like to thank my undergraduate friends, especially Shaunak who primarily inspired me to explore science passionately. Last but not the least, I sincerely thank my parents for their constant support and belief in me. They trusted my passion to pursue Ph.D. and supported my journey, despite being thousands of miles away. I also thank my loving brother for being there for me and taking care of my parents while I focused on my research.

I. Introduction

I.A: Membrane potential – property of all biological membranes

The cell membrane is primarily made of phospholipid bilayers and is an electrical insulator bathed in conductive electrolytes, with selective proteins embedded in the membranes providing semi permeability to physiological ions. Membrane potential is defined as the voltage difference across any semipermeable membrane, but physiologically, it is only characterized across the plasma membrane of select cell types, such as neurons and cardiac cells[1–3]. Electrophysiological measurements on these excitable cells have been relatively feasible due to their ability to generate large amplitude, fast electrical spikes[4]. This development can also be attributed due to the accessibility of the plasma membrane to external electrodes[5]. Pioneering experiments from Leonor Michaelis and Kenneth Cole demonstrated that an artificial or biological membrane can sustain membrane potential in the presence of electrolytes[6–8]. In 1943, Kenneth Cole's graduate student, David E. Goldman used the Nernst-Planck theory to formulate voltage difference across the plasma membrane with different ion mobilities[9]. The Nernst-Planck equation, now known as the constant field equation, describes the current density due to single ionic species and is dependent on chemical and voltage gradient. This was further expanded to the well-known Goldman-Hodgkin-Katz equation (1) in 1949, when Hodgkin and Katz investigated the effect of sodium ions on the activity of giant squid axon[10].

$$V = \frac{RT}{F} \ln \left[\frac{P_{Na}[Na]_o + P_K[K]_o + P_{Cl}[Cl]_i}{P_{Na}[Na]_i + P_K[K]_i + P_{Cl}[Cl]_o}\right] \quad (1)$$

Where the voltage difference (V) is given by relative permeability (P_{Na}, P_K, P_{Cl}) and concentration of the ions across the membrane of neurons or muscles.

Although Goldman and Nernst equations are well suited to address membrane potential across plasma membrane of excitable cells, they do not explain the voltage difference across other membranes such as the mitochondrial inner membrane[11]. The membrane potential across the mitochondrial inner membrane has been shown to be in the range of -150 to -180 mV (lumen negative) and changes in membrane potential are related to cellular metabolism and mitochondrial fission and fusion[12–14]. A Nernst potential of -180 mV cannot be generated by the ionic gradient of well-known ions such as H^+, K^+, Na^+ or Ca^{2+}. Further, the mitochondrial membrane contains ionic fluxes due to the electrogenic pump F_0F_1 ATPase, electrogenic transporters such as calcium uniporter (MCU) and electrogenic exchangers such as ATP/ADP exchanger (ANT) and mitochondrial sodium/calcium exchanger (NCLX), which are not considered in Nernst or Goldman equations[15].

Mitochondria, similar to bacteria, convert the chemical energy from membrane-localized redox reactions to electrical potential across their membranes, which in addition to the proton gradient provides the necessary proton motive force to generate intracellular ATP[11]. This negative membrane potential accounts for the function of F_0F_1 ATP synthase on these membranes, which imports ~12 protons and synthesizes three ATP molecules[16]. The resting membrane potential of mitochondria determines if ATP synthase consumes ATP to export protons or if protons are imported to synthesize ATP. The equilibrium membrane potential (V_{eq}) is given by the Nernst equation (2) from electrochemistry as follows,

$$V_{eq} = V_0 + \frac{RT}{zF} lnQ \qquad (2)$$

Where V_0 is the membrane potential at their standard states, z is the number of positive charges transferred across the membrane per reaction, and Q is the reaction quotient. At room temperature,

RT/F is ~59.0 mV. Thermodynamic analysis for F_0F_1 ATP synthase provides equilibrium membrane potential to be -70 mV[17]. For membrane potentials lower than -70 mV, the ATP synthase imports protons and produces ATP; for membrane potential higher than -70 mV, the ATPase exports protons and consumes ATP. Hence, the resting membrane potential of -150 mV suggests the mitochondria produces ATP in its native state.

Similarly, other intracellular organelles are also known to possess various sources for generating membrane potential. For instance, electrogenic V-ATPases in acidic organelles could generate voltage across the organellar membrane[18]. Membrane potential with the largest amplitude of -300 mV are found in plants, due to the activity of ATP driven proton pumps[19]. Donnan potential could form due to the presence of membrane impermeant charged species on one side of the membrane, thereby affecting the distribution of other membrane permeant ions. Donnan potential due to packaging of DNA (~200 mM) within the nuclear envelope is calculated to be approximately -36 mV and measured to be -15 mV[20]. Phagocytic cells use electron transport to maintain redox homeostasis and, in the process, generate membrane potential at the phagosomal membrane[21].

I.B: Double life of membrane potential:

Cells use electric potential as a source of energy to perform chemical and mechanical functions across a membrane. In a simpler system such as bacteria, membrane potential has been considered as a conventional battery. Bacteria use this resting membrane potential, in addition to ionic gradient, as ion motive force (proton or sodium) to synthesize ATP, to fuel flagella movement for motility and to uptake important metabolic factors[22,23]. Bacterial membrane potential (BMP) has generally been considered to be a homeostatic battery, but recent studies revealed that BMP is dynamic and can act as a physical signaling cue[24]. Recent work from Gürol M. Süel, shows that

electrical signaling within biofilms attracts other motile cells of different species, thereby increasing the diversity of biofilms[25] (Fig I.1).

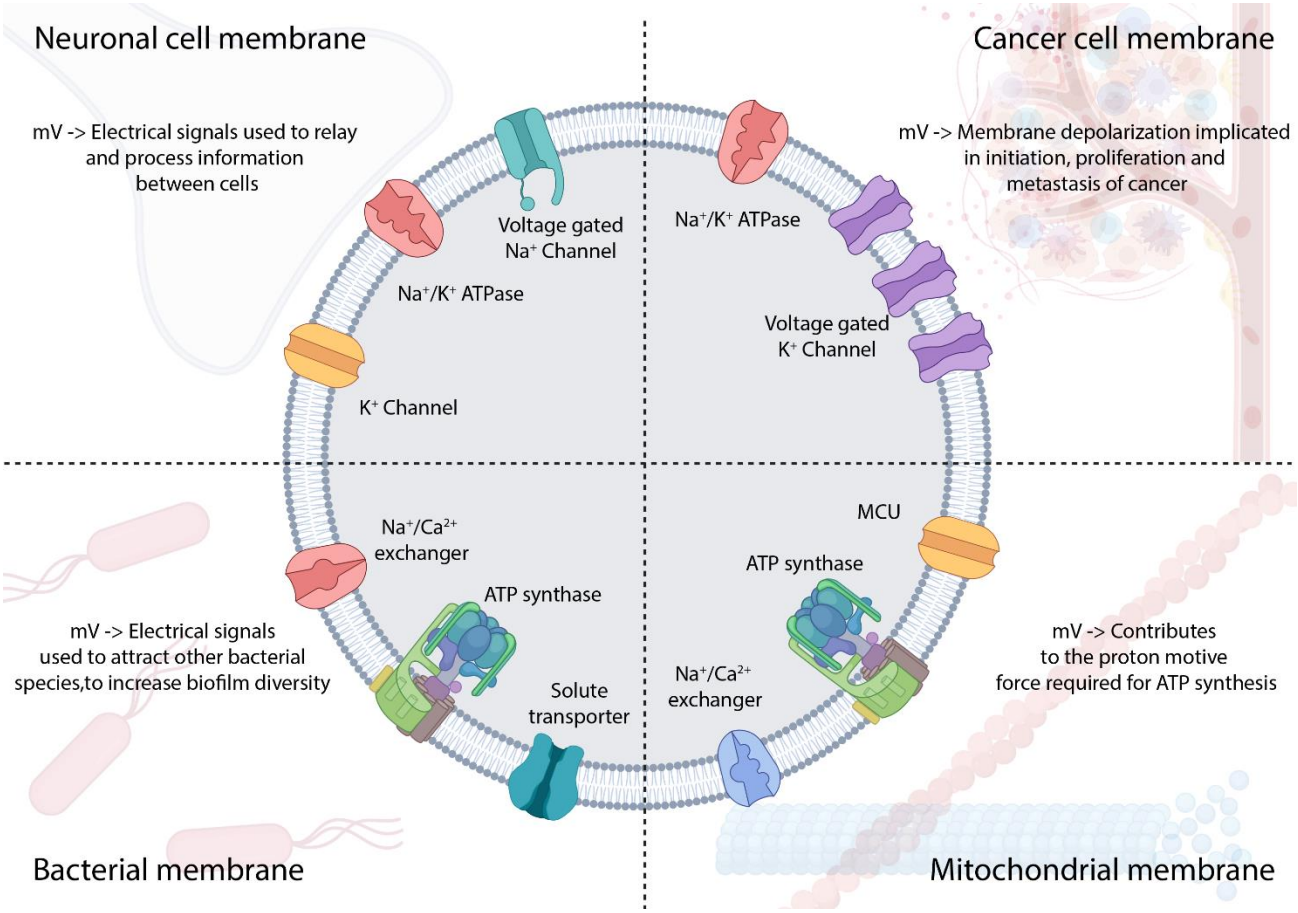

Figure I.1: Biological membranes sustaining membrane potential.

In higher order organisms, membrane potential regulates numerous cellular functions, such as cell growth and proliferation, differentiation, gene expression, apoptosis and migration[26]. Ideally cells tend to maintain a negative membrane potential (cytosol is negative), whereas stem cells, embryonic and cancerous cells are found to be relatively depolarized. It is not surprising that several ion channels and pumps, such as NaV1.5, KCNE2, SCN5A etc. are classified as oncogenes and implicated in dysregulation of cancer[27]. In many genetic experiments, loss of ion channels or transporters results in loss of specific functions such as spatial patterning or tail regeneration in model organisms, but it has been shown that membrane potential as a physical cue cannot be

reduced to a single protein[28]. Studies relevant to developmental biology such as eye induction, tail regeneration and head determination, reveal that the identity of an ion channel is not necessary as long as the appropriate resting membrane potential is maintained[28]. Similar to development, formation of tumors due to mutations in oncogenes KRAS and p53, can be reduced by inhibiting the depolarization during oncogenic transformation[29]. Thus, plasma membrane potential as a bioelectric signaling code is not just to limited to cell types, but to one step higher, at the level of organs.

Membrane potential as a physical signaling cue is very well understood in one of the most complicated tissue of higher organisms, the brain[30]. Neuronal cells in our brain use this electrical signal called action potential, spatiotemporally to relay and process information. The relative accessibility of the plasma membrane and robust electrical signals started a bioelectricity revolution to spatiotemporally map these changes in intact brain[31–33]. This ongoing revolution resulted in numerous fluorescent probes, voltage sensitive dyes and genetically encoded voltage indicators[34,35]. With an arsenal of such techniques, researchers are expanding their attention from one neuron to multiple neurons, and from whole organ to whole organism level[36]. Conversely, this cannot be said about the membrane potential at the intracellular or intraorganellar level.

I.C: Organelle membrane potential – Historical timeline

To quote Stephen W. Hawking, “The whole history of science has been the gradual realization that events do not happen in an arbitrary manner, but that they reflect a certain underlying order, which may or may not be divinely inspired”.

1950s: In 1952, Alan Hodgkin and Andrew Huxley published a set of five articles, detailing the conductance-based model that describes how action potential are generated and propagated in neurons[37–41]. More than a century long hunt in understanding electrical excitability was put to rest by their quantitative description of this phenomenon and in the process revealed physical mechanisms that started the modern era of biophysics. The underlying experimental technique of two electrode voltage clamp proved to be robust in recording the ionic currents across the membrane of giant squid axons[42]. This resulted in the use of this technique in other cell types and eventually led to the birth of electrophysiology[43].

The diffraction limit of light microscopy forwarded the development of electron microscopy, providing the high-resolution images of intracellular organelles such as mitochondria and Golgi complex[44]. In parallel, organelles were chemically investigated by Albert Claude, who pioneered the cell fractionation by differential centrifugation[45]. This resulted in purification of various intracellular organelles in its intact, preserved form. In 1955, Christian De Duve purified one such intracellular organelle called lysosome in an effort to isolate liver phosphatase[46].

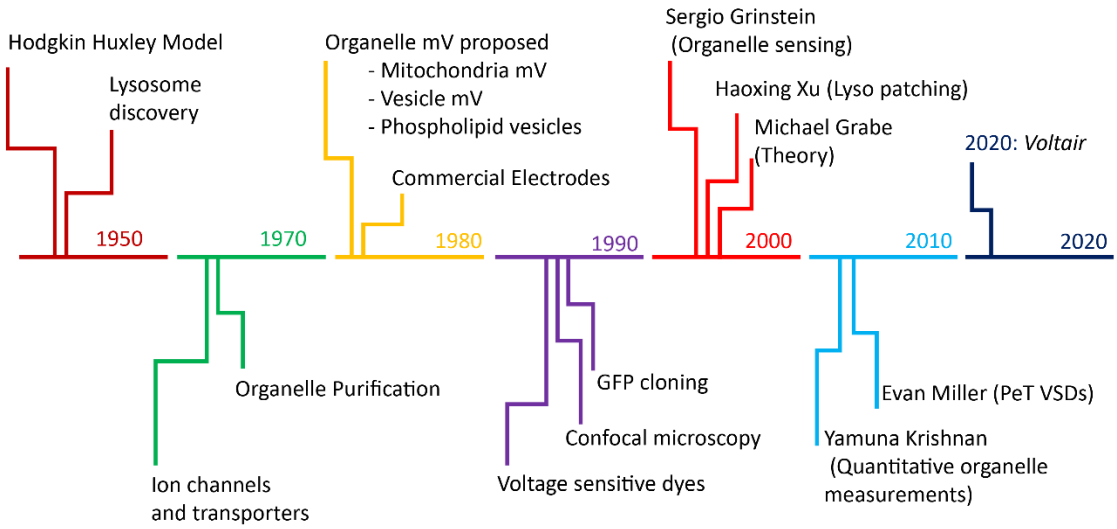

Figure I.2: Historical events leading up to organelle membrane potential measurements.

1970s: Erwin Neher and Bert Sakmann developed the patch clamp technique that allowed them to record ionic currents from a single ion channel, and this was feasible due to the development of electronics and Hodgkin-Huxley's pioneering electrophysiological experiments[47]. Neher and Sakmann's patch clamp technique confirmed ion permeable pores formed by proteins, and further allowed the discovery of voltage and ligand gated conductance across these membranes[48].

Discovering the existence of lysosomes without imaging revealed the importance of organelle purification techniques and revolutionized organelle specific interrogation[49]. This can be seen with the crucial experiments, performed to prove Peter Mitchell's "chemiosmotic coupling", that ATP synthesis was coupled to the electrochemical gradient of inner mitochondrial membrane [50]. This revealed the existence of ion transport mechanism in intracellular organelles, similar to neuronal membranes.

1980s: Molecular level characterization of ion channels and transporters required development in another field, "recombinant DNA technology". This led to the first characterization of the primary structure of the α-subunit precursor of the nicotinic acetylcholine receptor from the electric ray (Torpedo californica) and voltage-gated sodium channel from eel (Electrophorus electricus)[51,52]. The important feature of recombinant DNA technology is site directed mutagenesis and led to number of ground breaking discoveries uncovering the mechanism of voltage sensing in ion channels[53].

A serendipitous discovery that cationic hydrophobic dyes accumulate at mitochondria due to its negative membrane potential w.r.t. cytoplasm, resulted in a semiquantitative method to investigate mitochondrial membrane potential[54,55]. Due to the development of electrochemistry

and quantitative electrodes, membrane potential across other purified organelles were proposed and investigated[56]. For instance, membrane potential of purified chromaffin granules was found to be +50 mV (lumen positive), based on thiocyanate (SCN-) distributions across the vesicle membrane[57].

1990s: Development of fluorescent imaging techniques as well as introduction of fluorescent proteins and biosensors made the electrochemical method of probing organellar membrane potential obsolete[58]. The scientific community's demand for physiological and non-invasive methods to explore cell biology led to the development of numerous fluorescent sensors to image physiological ions such as calcium and protons, as well as voltage sensitive dyes for imaging action potential[59,60].

2000s: The organellar community shifted their interest in probing the biogenesis of various intracellular organelles and uncovering their physiological functions. Very few scientists were still in pursuit of quantitative interrogation of intracellular membranes. Sergio Grinstein's crucial work on sensing pH in intracellular vesicles and null point titration using selective ionophores, shed light into the complexity of intracellular membranes with hidden transporters and ion channels[61,62]. In parallel, Joseph Mindell mechanistically characterized the lysosomal chloride exchanger, ClC7 on purified lysosomes, with fluorescent pH sensor and voltage clamp using valinomycin selective K^+ diffusion potential[63].

With growing interest in intracellular ion channels and transporters, theoretical scientists like Michael Grabe, were able to model the electrophysiology of intracellular organelles with limited knowledge on the identity of resident channels and transporters[64]. A more quantitative approach soon took over, as Haoxing Xu developed the lysosome electrophysiology technique directly investigating endolysosomal channels and transporters[65].

2010s: In addition to the increasing discovery of intracellular channels and transporters, probe developers such as Yamuna Krishnan, had developed a sensing platform that can be used to make quantitative measurements of lumenal ions such as H^+, Cl^- and Ca^{2+} in various intracellular compartments[66]. Simultaneously, the race to develop robust voltage sensors in order to map neural activity resulted in more than a dozen novel genetically encoded probes and a new class of voltage sensitive dyes based on photoinduced electron transfer, designed by Evan Miller[34,67].

2020: Now, with all of the work done by our predecessors to quantify membrane potential and deliver quantitative probes to intracellular membranes, we have created a DNA-based nanodevice, called Voltair, that functions as a non-invasive, organelle-targetable, ratiometric reporter of absolute organellar membrane potential in live cells[68]. Membrane enclosed compartments harbor numerous ion channels and transporters, whose functions are known to be dependent on membrane potential and could even regulate membrane voltage for signaling[69]. Physiological processes such as nutrient starvation have been shown to perturb lysosomal channels and transporters, thereby affecting resting membrane potential[70]. Organelle voltage has also been hypothesized to regulate membrane fusion, either directly or indirectly by assisting calcium release[71]. Hence, a technology such as Voltair is very important to investigate the physiological role of organelle membrane potential. Voltair probes could unravel the significance of voltage across all membrane bound organelles, similar to what rhodamine probes did to decades of mitochondrial research.

I.D: DNA – a platform for quantitative intracellular measurements

In addition to being the genetic code of life, the physical and chemical properties of DNA have been used to design synthetic nano-scaffolds with complex functions and structural features[72]. Yamuna Krishnan pioneered the use of DNA scaffolds to construct a multitude of fluorescent sensors that can quantitatively report chemical events occurring at single organelle level. By leveraging the 1:1 stoichiometry of dyes attached to double-stranded DNA, organelle specific DNA sensors incorporate three primary modules: (i) a sensing module that comprises a fluorescent dye sensitive to a chemical or physical cue, (ii) a normalizing module that comprises a spectrally orthogonal fluorescent dye insensitive to the specific cue and (iii) a targeting module that localizes the DNA sensor to a specific organelle within a live cell. The reporting domain, made up of (i) and (ii) allows for quantitative ratiometric measurements[73]. DNA based probes bridge the best of the two worlds: high sensitivity and brightness from fluorescent dye space and organelle specific targeting from protein space. DNA-based nano sensors have been used to measure chemical analytes such as ions (H^+, Ca^{2+}, Cl^-), reactive molecules (HOCl, NO, H_2S) and second messengers (cAMP, Ca^{2+})[66]. Using the same principles, we designed a DNA based nanodevice to measure a physical cue, voltage, across membranes of intracellular organelles.

I.E: Thesis outline

The role of membrane potential in the function of several intracellular organelles remains unaddressed as they are refractory to electrophysiology and there is a paucity of organelle-specific probes. The pH sensitivity in fluorescent proteins limits their applicability in organelles where lumenal pH and membrane potential are co-dependent. Alternatively, electrochromic hemicyanine dyes or photoinduced electron transfer (PeT) based voltage sensitive dyes are particularly attractive for organelles due to their low capacitive loads, high temporal resolution, photostability

and response range[74]. However, unlike proteins, voltage sensitive dyes cannot be targeted to specific organelles other than mitochondria.

Chapter 2 outlines the necessity of new technology for probing intracellular voltage of various organelles. Unlike chemical cues, physical cues such as membrane potential must be investigated in situ to understand their physiological implications. Importantly, the role of membrane potential in the function of several intracellular organelles cannot be addressed due to their inaccessibility by electrophysiological and fluorescent-based methods. The chapter discusses the design and characterization of a new category of voltage sensors (Voltair, mVivo) which combine voltage sensitive dyes with the DNA nanotechnology-based quantitative imaging platform of the Krishnan Lab.

In Chapter 3, I describe the development of new variants of DNA probes that specifically target endocytic vesicles along the degradative pathway, recycling pathway, and retrograde trafficking pathway. Targeting modules incorporated in the DNA probe reprogram the voltage sensing domain to specific intracellular membranes.

Chapter 4 describes the functional characterization of Voltair and mVivo variants on the plasma membrane and intracellular membrane of mammalian cells. Characterization of the voltage-sensitive response of DNA probes on the plasma membrane was done using whole-cell voltage clamping performed on a home-built electrophysiology-fluorescence imaging set up. Characterization on intracellular membranes was done using whole-lysosome voltage clamping techniques, performed on Vacuolin-1 treated enlarged lysosomes.

Chapter 5 describes the quantification of resting membrane potential of early and late endosomes, recycling endosomes, lysosomes, and the Trans Golgi Network. Quantitative measurements show

the contribution of V-ATPase towards organelle membrane potential across different acidic compartments and also report dynamic changes in lysosomal mV upon physiological perturbations.

I.F: References

1. Schuetze, S. M. The discovery of the action potential. *Trends Neurosci.* **6,** 164–168 (1983).
2. Stojilkovic, S. S., Tabak, J. & Bertram, R. Ion channels and signaling in the pituitary gland. *Endocr. Rev.* **31,** 845–915 (2010).
3. Wei, X., Yohannan, S. & Richards, J. R. in *StatPearls* (StatPearls Publishing, 2020).
4. Seyfarth, E.-A. Julius Bernstein (1839-1917): pioneer neurobiologist and biophysicist. *Biol. Cybern.* **94,** 2–8 (2006).
5. Curtis, H. J. & Cole, K. S. Membrane action potentials from the squid giant axon. *J Cell Comp Physiol* **15,** 147–157 (1940).
6. Cole, K. S. & Curtis, H. J. Electric impedance of the squid giant axon during activity. *J. Gen. Physiol.* **22,** 649–670 (1939).
7. Green, A. A., Weech, A. A. & Michaelis, L. Studies on permeability of membranes : vii. conductivity of electrolytes within the membrane. *J. Gen. Physiol.* **12,** 473–485 (1929).
8. Hille, B. The founding of Journal of General Physiology: Membrane permeation and ion selectivity. *J. Gen. Physiol.* **150,** 389–400 (2018).
9. Goldman, D. E. Potential, impedance, and rectification in membranes. *J. Gen. Physiol.* **27,** 37–60 (1943).
10. Hodgkin, A. L. & Katz, B. The effect of sodium ions on the electrical activity of giant axon of the squid. *J. Physiol. (Lond)* **108,** 37–77 (1949).
11. Mitchell, P. Chemiosmotic coupling in oxidative and photosynthetic phosphorylation. *Biol. Rev. Camb. Philos. Soc.* **41,** 445–502 (1966).
12. Zorova, L. D. *et al.* Mitochondrial membrane potential. *Anal. Biochem.* **552,** 50–59 (2018).
13. Meeusen, S., McCaffery, J. M. & Nunnari, J. Mitochondrial fusion intermediates revealed in vitro. *Science (80-.).* **305,** 1747–1752 (2004).

14. Ramzan, R., Staniek, K., Kadenbach, B. & Vogt, S. Mitochondrial respiration and membrane potential are regulated by the allosteric ATP-inhibition of cytochrome c oxidase. *Biochim. Biophys. Acta* **1797,** 1672–1680 (2010).

15. Bernardi, P. Mitochondrial transport of cations: channels, exchangers, and permeability transition. *Physiol. Rev.* **79,** 1127–1155 (1999).

16. Ferguson, S. J. ATP synthase: what dictates the size of a ring? *Curr. Biol.* **10,** R804–8 (2000).

17. Cohen, A. E. & Venkatachalam, V. Bringing bioelectricity to light. *Annu. Rev. Biophys.* **43,** 211–232 (2014).

18. Farsi, Z. *et al.* Single-vesicle imaging reveals different transport mechanisms between glutamatergic and GABAergic vesicles. *Science (80-.).* **351,** 981–984 (2016).

19. Sanders, D., Hansen, U. P. & Slayman, C. L. Role of the plasma membrane proton pump in pH regulation in non-animal cells. *Proc. Natl. Acad. Sci. USA* **78,** 5903–5907 (1981).

20. Loewenstein, W. R. & Kanno, Y. SOME ELECTRICAL PROPERTIES OF A NUCLEAR MEMBRANE EXAMINED WITH A MICROELECTRODE. *J. Gen. Physiol.* **46,** 1123–1140 (1963).

21. Steinberg, B. E., Touret, N., Vargas-Caballero, M. & Grinstein, S. In situ measurement of the electrical potential across the phagosomal membrane using FRET and its contribution to the proton-motive force. *Proc. Natl. Acad. Sci. USA* **104,** 9523–9528 (2007).

22. Manson, M. D., Tedesco, P., Berg, H. C., Harold, F. M. & Van der Drift, C. A protonmotive force drives bacterial flagella. *Proc. Natl. Acad. Sci. USA* **74,** 3060–3064 (1977).

23. Stratford, J. P. *et al.* Electrically induced bacterial membrane-potential dynamics correspond to cellular proliferation capacity. *Proc. Natl. Acad. Sci. USA* **116,** 9552–9557 (2019).

24. Prindle, A. *et al.* Ion channels enable electrical communication in bacterial communities. *Nature* **527,** 59–63 (2015).

25. Humphries, J. *et al.* Species-Independent Attraction to Biofilms through Electrical Signaling. *Cell* **168,** 200–209.e12 (2017).

26. Levin, M., Selberg, J. & Rolandi, M. Endogenous bioelectrics in development, cancer, and regeneration: drugs and bioelectronic devices as electroceuticals for regenerative medicine. *iScience* **22,** 519–533 (2019).

27. Peruzzo, R., Biasutto, L., Szabò, I. & Leanza, L. Impact of intracellular ion channels on cancer development and progression. *Eur Biophys J* **45,** 685–707 (2016).

28. Levin, M. Molecular bioelectricity: how endogenous voltage potentials control cell behavior and instruct pattern regulation in vivo. *Mol. Biol. Cell* **25,** 3835–3850 (2014).

29. Chernet, B. T. & Levin, M. Transmembrane voltage potential is an essential cellular parameter for the detection and control of tumor development in a Xenopus model. *Dis. Model. Mech.* **6,** 595–607 (2013).

30. Knöpfel, T. Genetically encoded optical indicators for the analysis of neuronal circuits. *Nat. Rev. Neurosci.* **13,** 687–700 (2012).

31. Viventi, J. *et al.* Flexible, foldable, actively multiplexed, high-density electrode array for mapping brain activity in vivo. *Nat. Neurosci.* **14,** 1599–1605 (2011).

32. Hong, G. & Lieber, C. M. Novel electrode technologies for neural recordings. *Nat. Rev. Neurosci.* **20,** 330–345 (2019).

33. Peterka, D. S., Takahashi, H. & Yuste, R. Imaging voltage in neurons. *Neuron* **69,** 9–21 (2011).

34. Kulkarni, R. U. *et al.* A Rationally Designed, General Strategy for Membrane Orientation of Photoinduced Electron Transfer-Based Voltage-Sensitive Dyes. *ACS Chem. Biol.* **12,** 407–413 (2017).

35. Yang, H. H. & St-Pierre, F. Genetically encoded voltage indicators: opportunities and challenges. *J. Neurosci.* **36,** 9977–9989 (2016).

36. Knöpfel, T. & Song, C. Optical voltage imaging in neurons: moving from technology development to practical tool. *Nat. Rev. Neurosci.* **20,** 719–727 (2019).

37. Hodgkin, A. L. & Huxley, A. F. The dual effect of membrane potential on sodium conductance in the giant axon of Loligo. *J. Physiol. (Lond)* **116,** 497–506 (1952).

38. HODGKIN, A. L., HUXLEY, A. F. & KATZ, B. Measurement of current-voltage relations in the membrane of the giant axon of Loligo. *J. Physiol. (Lond)* **116,** 424–448 (1952).

39. Hodgkin, A. L. & Huxley, A. F. The components of membrane conductance in the giant axon of Loligo. *J. Physiol. (Lond)* **116,** 473–496 (1952).

40. Hodgkin, A. L. & Huxley, A. F. A quantitative description of membrane current and its application to conduction and excitation in nerve. *J. Physiol. (Lond)* **117,** 500–544 (1952).

41. Hodgkin, A. L. & Huxley, A. F. Currents carried by sodium and potassium ions through the membrane of the giant axon of Loligo. *J. Physiol. (Lond)* **116,** 449–472 (1952).

42. Chandler, W. K. & Meves, H. Voltage clamp experiments on internally perfused giant axons. *J. Physiol. (Lond)* **180,** 788–820 (1965).

43. Schwiening, C. J. A brief historical perspective: Hodgkin and Huxley. *J. Physiol. (Lond)* **590,** 2571–2575 (2012).

44. Sjostrand, F. S. Electron microscopy of mitochondria and cytoplasmic double membranes. *Nature* **171,** 30–32 (1953).

45. Claude, A. Fractionation of mammalian liver cells by differential centrifugation : ii. experimental procedures and results. *J. Exp. Med.* **84,** 61–89 (1946).

46. Sabatini, D. D. & Adesnik, M. Christian de Duve: Explorer of the cell who discovered new organelles by using a centrifuge. *Proc. Natl. Acad. Sci. USA* **110,** 13234–13235 (2013).

47. Neher, E. & Sakmann, B. Single-channel currents recorded from membrane of denervated frog muscle fibres. *Nature* **260,** 799–802 (1976).

48. Hamill, O. P., Marty, A., Neher, E., Sakmann, B. & Sigworth, F. J. Improved patch-clamp techniques for high-resolution current recording from cells and cell-free membrane patches. *Pflugers Arch.* **391,** 85–100 (1981).

49. Satori, C. P. *et al.* Bioanalysis of eukaryotic organelles. *Chem. Rev.* **113,** 2733–2811 (2013).

50. Tupper, J. T. & Tedeschi, H. Microelectrode studies on the membrane properties of isolated mitochondria. *Proc. Natl. Acad. Sci. USA* **63,** 370–377 (1969).

51. Noda, M. *et al.* Primary structure of alpha-subunit precursor of Torpedo californica acetylcholine receptor deduced from cDNA sequence. *Nature* **299,** 793–797 (1982).

52. Noda, M. *et al.* Primary structure of Electrophorus electricus sodium channel deduced from cDNA sequence. *Nature* **312,** 121–127 (1984).

53. Claudio, T. Recombinant DNA technology in the study of ion channels. *Trends Pharmacol. Sci.* **7,** 308–312 (1986).

54. Wong, J. & Bochen, L. Recent advances in the study of mitochondria in living cells. *Advances in Molecular and Cell Biology* **2,** 263–290 (1988).

55. Perry, S. W., Norman, J. P., Barbieri, J., Brown, E. B. & Gelbard, H. A. Mitochondrial membrane potential probes and the proton gradient: a practical usage guide. *BioTechniques* **50,** 98–115 (2011).

56. Karlovský, P. & Dadák, V. Tetraphenylborate-sensitive electrode for measuring membrane potential. *Folia Microbiol (Praha)* **27,** 460–464 (1982).

57. Johnson, R. G. & Scarpa, A. Protonmotive force and catecholamine transport in isolated chromaffin granules. *J. Biol. Chem.* **254,** 3750–3760 (1979).

58. Habib-E-Rasul Mullah, S. *et al.* Evaluation of voltage-sensitive fluorescence dyes for monitoring neuronal activity in the embryonic central nervous system. *J. Membr. Biol.* **246,** 679–688 (2013).

59. Yan, P. *et al.* Palette of fluorinated voltage-sensitive hemicyanine dyes. *Proc. Natl. Acad. Sci. USA* **109,** 20443–20448 (2012).

60. Terai, T. & Nagano, T. Small-molecule fluorophores and fluorescent probes for bioimaging. *Pflugers Arch.* **465,** 347–359 (2013).

61. Schapiro, F. B. & Grinstein, S. Determinants of the pH of the Golgi complex. *J. Biol. Chem.* **275,** 21025–21032 (2000).

62. Steinberg, B. E. *et al.* A cation counterflux supports lysosomal acidification. *J. Cell Biol.* **189,** 1171–1186 (2010).

63. Graves, A. R., Curran, P. K., Smith, C. L. & Mindell, J. A. The Cl-/H+ antiporter ClC-7 is the primary chloride permeation pathway in lysosomes. *Nature* **453,** 788–792 (2008).

64. Grabe, M. & Oster, G. Regulation of organelle acidity. *J. Gen. Physiol.* **117,** 329–344 (2001).

65. Dong, X.-P. *et al.* The type IV mucolipidosis-associated protein TRPML1 is an endolysosomal iron release channel. *Nature* **455,** 992–996 (2008).

66. Krishnan, Y., Zou, J. & Jani, M. S. Quantitative imaging of biochemistry *in situ* and at the nanoscale. *ACS Cent. Sci.* (2020). doi:10.1021/acscentsci.0c01076

67. Bando, Y., Grimm, C., Cornejo, V. H. & Yuste, R. Genetic voltage indicators. *BMC Biol.* **17,** 71 (2019).

68. Saminathan, A. *et al.* A DNA-based voltmeter for organelles: Supplementary information. *BioRxiv* (2019). doi:10.1101/523019

69. Li, P., Gu, M. & Xu, H. Lysosomal ion channels as decoders of cellular signals. *Trends Biochem. Sci.* **44,** 110–124 (2019).

70. Cang, C. *et al.* mTOR regulates lysosomal ATP-sensitive two-pore Na(+) channels to adapt to metabolic state. *Cell* **152,** 778–790 (2013).

71. Wang, X. *et al.* TPC proteins are phosphoinositide- activated sodium-selective ion channels in endosomes and lysosomes. *Cell* **151,** 372–383 (2012).

72. Ke, Y., Castro, C. & Choi, J. H. Structural DNA nanotechnology: artificial nanostructures for biomedical research. *Annu. Rev. Biomed. Eng.* **20,** 375–401 (2018).

73. Chakraborty, K., Veetil, A. T., Jaffrey, S. R. & Krishnan, Y. Nucleic Acid-Based Nanodevices in Biological Imaging. *Annu. Rev. Biochem.* **85,** 349–373 (2016).

74. Miller, E. W. *et al.* Optically monitoring voltage in neurons by photo-induced electron transfer through molecular wires. *Proc. Natl. Acad. Sci. USA* **109,** 2114–2119 (2012).

II. Development of DNA based organelle membrane potential sensor

II.A: Introduction

A great deal is known about membrane potential in neurons due to well established electrophysiological techniques[1,2]. Immense drive to understand this physical cue in a large number of neurons have steered the researchers in developing fluorescent imaging tools to directly or indirectly record voltage across neuronal membranes[3,4]. These voltage indicators can be broadly classified into two categories, (i) genetically encoded voltage indicators (GEVI)[5] and (ii) small molecule voltage sensitive dyes[6] (Fig II.1).

GEVI are further divided into three types as shown in figure 2.1: (a) Voltage sensitive domain (VSD) based GEVIs, where a fluorescent protein is fused directly to the voltage sensitive region of a phosphatase or ion channel that is sensitive to membrane potential [7,8]. (b) Opsin based voltage indicators, where the changes in membrane potential locally affect the protonation state of retinal Schiff base and thereby affects the fluorescence output from the chromophore[9]. (c) Chemogenetic sensors, that uses an exogenously added membrane potential sensitive molecule such as dipicrylamine (DPA), to quench the fluorescent protein recruited to a specific membrane in accordance to voltage difference[10] (Fig. II.1). Small molecule voltage sensitive dyes are of three types: (a) stark shift based electrochromic dyes such as ANEPPs, that change their spectral properties according to change in membrane potential difference[11]. (b) slow response oxonol dyes, which distributes across the transmembrane, dependent on membrane potential[12] and (c) Photoinduced electron transfer (PeT) based voltage indicators, comprising of a fluorophore coupled to molecular wire-quencher system, that quenches fluorescence via PeT mechanism and is dependent on membrane potential difference[13] (Fig. II.1).

Small molecule voltage indicators are mostly amphiphilic dyes with a hydrophilic head that prevents them from flipping across the membrane[6]. The direction of orientation is very important in measuring the direction of voltage difference across a membrane. But, this feature of voltage sensitive dyes makes it less feasible to target intracellular membranes, using strategies that currently target organelles such as morpholine group to target lysosomes[14] or triphenyl phosphonium group to target mitochondria[15]. Although GEVIs offer membrane targeting feature that lacks in small molecule voltage indicators, such targeting would not label membranes of organelles that dynamically mature over time, such as early, late and recycling endosomes. Importantly, the role of membrane potential in the function of several intracellular organelles remains unaddressed as they are refractory to electrophysiology and there is a paucity of organelle-specific probes. In addition, the pH sensitivity in fluorescent proteins limits their applicability in organelles where lumenal pH and membrane potential are co-dependent[16]. Thus, electrochromic hemicyanine dyes or photoinduced electron transfer (PeT) based voltage sensitive dyes are particularly attractive for organelles due to their low capacitive loads, high temporal resolution, photostability and response range[17].

Endocytic tracers such as DNA bind to receptor proteins at the plasma membrane and can specifically target endocytic organelles by vesicle mediated trafficking and can be further modified with other targeting motifs to reprogram DNA to other organellar membrane[18]. This chapter describes DNA-based nanodevices, called Voltair and mVivo, that functions as a non-invasive, organelle-targetable, reporter of organellar membrane potential in live cells. DNA is a versatile, programmable scaffold that is highly suited to imaging *in cellulo* and *in vivo*. The 1:1 stoichiometry of DNA hybridization incorporates a reference fluorophore and the PeT based voltage sensitive dye in a precise stoichiometry to yield ratiometric probes.

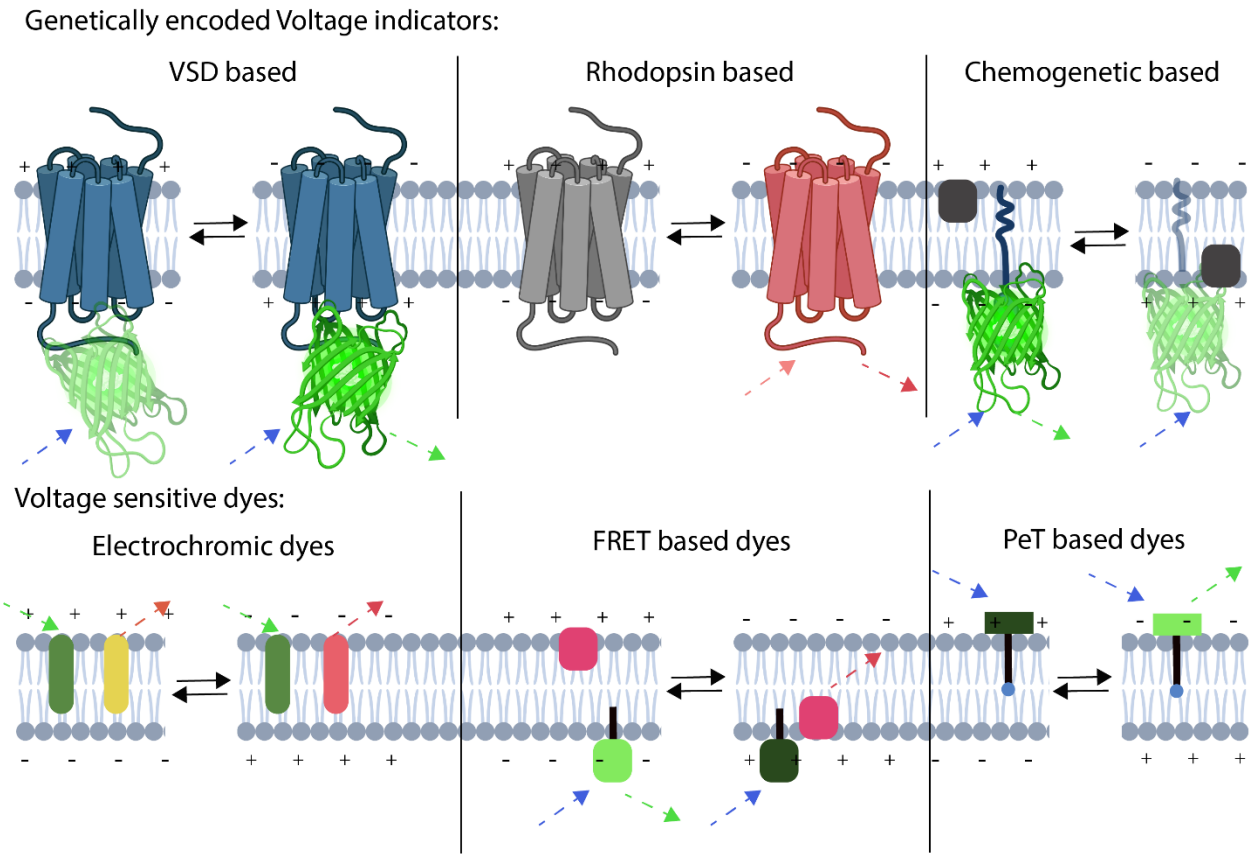

Figure II.1: General schematic of fluorescent voltage indicators. Sensors fall into two category, genetically encoded voltage indicators (GEVI, top), with three distinct families based on voltage sensing domains (VSD; left), microbial rhodopsins (middle), or chemogenetic probes (right) and voltage sensitive dyes, with three distinct types based on electrochromic shift (left), oxonol based FRET probes (middle), or photoinduced electron transfer based (PeT, right).

II.B: Materials and methods

1. Synthesis and characterization of RVF (*Voltair*)

Synthesis scheme is shown in figure II.2. Compound 1a13 (0.2 g, 0.36 mmol) was suspended in N,N-dimethylformamide (DMF) (1.4 mL) and cooled to 0°C . Triethylamine (2.7 mL) and Phenyl triflimide (0.25 g, 0.72 mmol, 2 eq.) were added dropwise. The ice bath was removed and the reaction was stirred at room temperature for 2 hours. The reaction mixture was then diluted in water and extracted with dichloromethane (DCM) twice. Organic extracts were washed three times

with brine and 1M HCl. The product was concentrated via rotor evaporation and dry DMSO was added (2mL). N-boc piperazine (3.72g, 20 mmol, 100eq.) was added and the reaction mixture was kept at 100ºC overnight. The reaction mixture was then diluted in water, extracted in DCM twice then washed with brine twice. The mixture was dried over anhydrous Na_2SO_4 and concentrated under reduced pressure. Silica gel column chromatography was performed in 5% methanol in chloroform to get 1b (0.08g, 28%). ESI-MS (-) Expected mass = 728.98, found = 729.0.

A reaction tube was charged with 1b (70 mg, 0.0956 mmol), $Pd(OAc)_2$ (6.87 mg, 0.0306 mmol, 0.32 eq.), tri-o-tolylphosphine (20.4 mg, 0.067 mmol, 0.7 eq.) and (E)-N,N-dimethyl-4-(4-vinylstyryl)aniline (26.23mg, 1.052 mmol, 1.1 eq.) which was previously synthesized according to literature[17]. The tube was evacuated and backfilled with N_2 three times. 1 mL of dry DMF and 500 µL dry triethylamine were added via syringe, and the reaction was stirred at 110ºC overnight. The reaction mixture was diluted in water and extracted with DCM twice. The organic extract was washed with brine twice and concentrated under reduce pressure. Silica gel column chromatography was performed in 5% methanol in DCM to get orangish brown solid 1c (20 mg, 25%). ESI-MS (+), Expected mass = 851.29, found = 851.2.

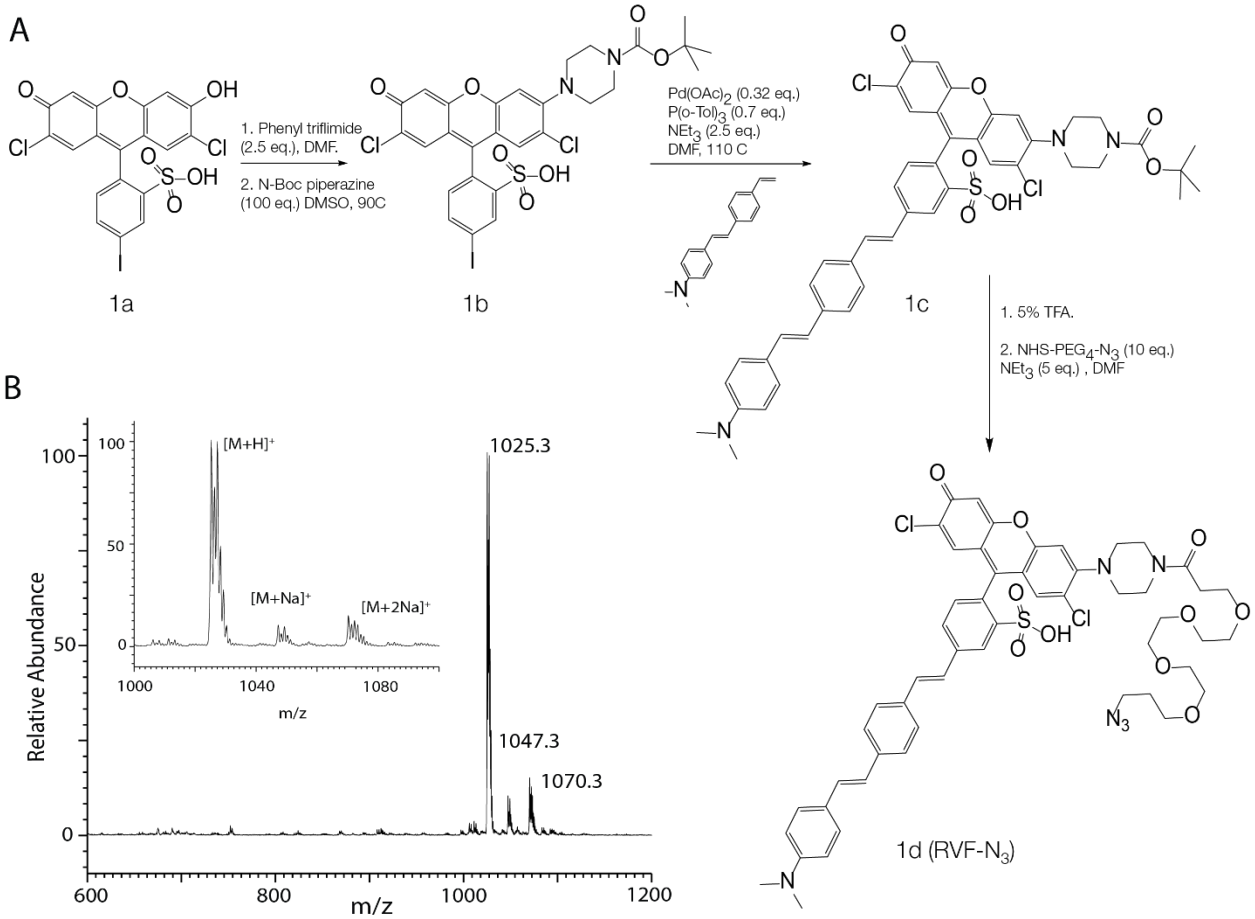

Figure II.2: Synthesis of conjugatable RVF-N_3. (a) Reaction scheme for synthesis of azido-RVF. The azido group in RVF is utilized to conjugate it to the DNA strand DV, the sensing component in the Voltair probes. (b) ESI-MS of RVF-N_3. Inset shows the region corresponding to the M+2 peaks arising from the Cl isotopes.

A reaction vial with 1c (5 mg, 6.7 nmol) was placed in 5% TFA in DCM overnight for deprotection. TFA was removed under reduced pressure and Azido-PEG_4-NHS ester (26mg, 6.7 nmol, 10.0 eq.), 300 µL dry DMF, and 200 µL triethylamine were added. The mixture was stirred for 4 hours at room temperature. The reaction mixture was then diluted in water, extracted to DCM twice, washed with brine three times, dried over anhydrous Na_2SO_4 and concentrated under reduced pressure. Silica gel column chromatography was performed with 2% methanol in DCM, slowly increasing the gradient to 10%, to get reddish brown solid 1d (2mg, 30%). ESI- MS(+), Expected mass = 1025.23, found = 1025.3.

2. Synthesis and characterization of Caged VF (mVivo)

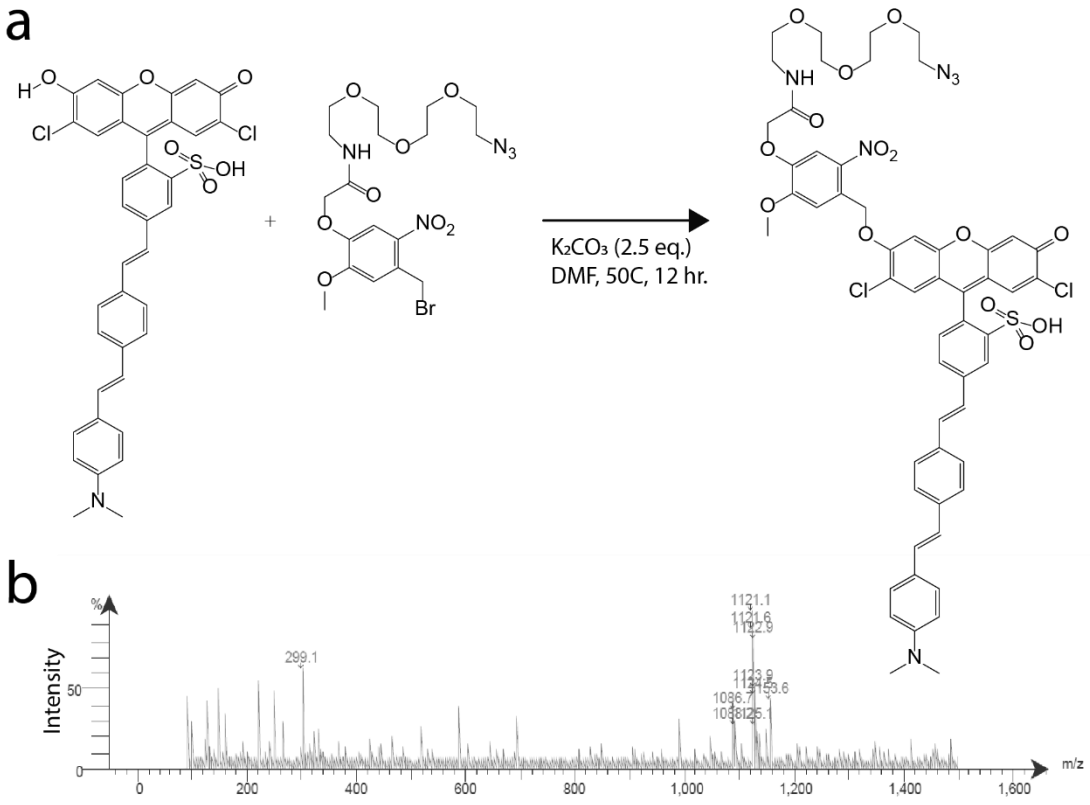

Figure II.3: Synthesis of CVF. (a) Reaction scheme for synthesis of caged Voltagefluor (CVF). The azido group in CVF is utilized to conjugate it to the DNA strand D_{CV}, the sensing component in the *mVivo* probes. (b) ESI-MS of CVF shows the M+2 peaks arising from the Cl isotopes.

VF2.1.Cl and clickable derivative of photocleavable 4,5-Dimethyxy-2-nitrobenzyl bromide (DMNB) was synthesized according to previous procedures[13,19,20]. Synthesis scheme is shown in figure II.3. A reaction vial with VF2.1.Cl (5 mg, 14.5 nmol), DMNB (17 mg, 29 nmol, 2 eq.) and potassium carbonate (5 mg, 36.3 nmol, 2.5 eq.) in 200 µL of dry DMF was stirred at 50°C overnight. The reaction mixture was diluted in water and extracted with DCM twice. The organic extract was washed with brine twice and concentrated under reduce pressure. Preparatory thin layer chromatography was performed in 5% methanol in DCM to get brown solid, caged VF (CVF). ESI-MS(-) 1121.0, found 1121.1.

3. Oligonucleotides

Modified DNA oligonucleotides were purchased from IDT (USA). PAGE purified and lyophilized oligonucleotides were dissolved in Milli-Q water of recommended volume to approximately prepare 100 µM stocks. Concentration of oligonucleotides are accurately quantified by collecting UV absorbance spectra and using Beer Lambert's law with absorbance at 260nm for DNA. In the case of fluorescently labeled oligonucleotides, equation 1 is used to quantify the concentration.

$$\text{Concentration} = (Abs_{260} \times \text{dilution factor}) / (\varepsilon_{oligo} - \varepsilon_{dye}) \quad \text{Eq. 1}$$

Where, molecular extinction coefficients of all oligonucleotides ε_{oligo} are provided in the specification sheet by IDT and molecular extinction coefficient of the fluorescent dye at 260nm ε_{odye} is referred from literature references.

Table II.1: List of modified oligonucleotides used in this study.

S. No	Strand	Sequence (5' to 3')	Comment
1	D_V or D_{CV}	ATCAACACTGCACACCAGACAGCAAGATCCTATATATA-ispacer18-DBCON	Sensing stand – conjugated to RVF or CVF
2	D_T	DBCO-TEG-TATATATAGGATCTTGCTGTCT	Targeting strand – conjugated to POPE
3	D_A	Atto647N – GGTGTGCAGTGTTGAT	Normalizing strand – PM
4	D_A'	TATATATAGGATCTTGCTGTCTGGTGTGCAGTGTTGAT-Atto647N	Normalizing strand – Intracellular Membrane (IM)

5	D_V^{RE}	DBCO-TEG-ispacer18-TATATATAGGATCTTGCTTCTGTGCCTGCAGTGTTGAT	RE sensing strand – conjugated to RVF
6	D_A^{RE}	Atto647N-ATCAACACTGCAGGCACAGAGTCTGGTG	RE normalizing stand
7	D_{Tf}	CACCAGACAGCAAGATCCTATATATAGGGGGA**UC**AA**UCC**AAGGGA**CCC**GGAAA**C**G**CUCCCUU**A**C**A**CCCC**	RE targeting strand – modified with RNA aptamer. The portion of sequence in red correspond to RNA aptamer against hTfR and bold letters indicate 2' fluoro modified bases.

Table II.1: List of modified oligonucleotides used in this study (continued).

4. DNA conjugation and purification

DBCO modified single stranded DNA was conjugated to RVF or CVF using copper free click chemistry protocol[21]. 10 µM of the 3'- DBCO modified 38 base strand (IDT, USA) was coupled to the azide containing RVF or CVF (50 µM, 5 eq.) in 20 mM sodium phosphate buffer, pH 7.4. The reaction mixture was stirred for 4 hours at room temperature (RT). Upon completion, 1/10th volume, 3M sodium acetate buffer is added (pH 5.2) to reaction mixture and vortexed vigorously. This is followed by adding 2.5 times volume of 100% ethanol and incubated at -20°C overnight. Precipitation of RVF or CVF conjugated DNA is collected using table top centrifugation (14K rpm) at 4°C. The orange colored precipitate is washed multiple times with 100% ethanol to remove unconjugated dye and final wash with 70% ethanol to remove excess salt. RVF conjugated DNA was reconstituted in 10 mM phosphate buffer, pH 7.4 and the final concentration was quantified using UV absorbance at 260 nm, as mentioned above.

1-palmitoyl-2-oleoyl-sn-glycero-3-phosphoethanolamine (POPE) was conjugated to NHS-PEG4-Azide using an established protocol[22]. 20 µM of the 5'-DBCO modified 22 base strand (IDT, USA) was coupled to azido-POPE (40 µM, 2eq.) in 20 mM sodium phosphate buffer, pH 7.4 and stirred for 4 hours at RT.

5. Sample preparation (Voltair and mVivo variants)

Stock solution of Voltair^{PM} was prepared at a final concentration of 10 µM by mixing D_V, D_T and D_A (Atto647N – 5' modified strand) at an equimolar ratio in 10 mM sodium phosphate buffer, pH 7.4. For Voltair^{IM} samples, D_V (Voltage sensing strand of Voltair^{PM}) and D_A' (Atto647N – 3' modified 38 mer strand) were mixed at an equimolar ratio with a final concentration of 10 µM (Table 2.1). For Voltair^{RE} samples, 10 µM of D_V^{RE}, D^{Tf} and D_A^{RE} were mixed at an equimolar ratio. Stock solution of mVivo was prepared at a final concentration of 10 µM by mixing D_{CV}, D_T and D_A (Atto647N – 5' modified strand) at an equimolar ratio in 10 mM sodium phosphate buffer, pH 7.4 (Fig 2.6, 2.7). For all samples, annealing was performed by heating the reaction mixture to 95°C for 15 min and gradually cooling to RT, at 1°C/ 3 min[23,24]. Annealed samples were equilibrated at 4°C overnight.

6. Gel electrophoresis

15% native polyacrylamide gels were used for visualizing the formation of annealed samples. Gels were run in 1X TBE buffer (100 mM Tris. HCl, 90 mM boric acid and 2 mM EDTA, pH 8.3) at RT,100V. Non-fluorescent samples were stained with ethidium bromide (1µg/mL) for 10 mins prior to visualization. Samples were observed by Biorad Universal Hood II Gel Doc system (Bio-Rad Laboratories, Inc.)

Denaturing polyacrylamide gels containing 12-15% acrylamide [38:2 acrylamide/ bisacrylamide] were used for visualizing the conjugation of RVF or CVF to DBCO ssDNA. Gel was allowed to pre run for 15 mins at 150 V and loading samples diluted with Bromophenol blue/ formamide were preheated to 95°C for 5 mins, to ensure complete denaturation of ssDNA. Gels were run in 1X TBE buffer (100 mM Tris. HCl, 90 mM boric acid and 2 mM EDTA, pH 8.3) at RT, 150 V. Non-fluorescent samples were stained with ethidium bromide (1µg/ mL) for 10 mins prior to visualization. Samples were observed by Biorad Universal Hood II Gel Doc system (Bio-Rad Laboratories, Inc.)

7. Spectral characterization of Voltair and mVivo

Fluorescence spectra was recorded on a FluoroMax-4 scanning Spectro-fluorometer (Horiba Scientific, Edison, NJ, USA). Voltair^{IM} and mVivo was diluted to 100 nM in universal buffer, UB4 buffer (20 mM HEPES, MES and sodium acetate, 150 mM KCl, 5 mM NaCl, 1 mM $CaCl_2$ and $MgCl_2$) of desired pH for all in vitro fluorescence experiments. The mVivo was photoactivated using a Thor lab irradiation system, equipped with 365 nm LED light source (180 mW). For recording spectra, Voltair^{IM} samples were excited at 520 nm (λ_{ex}^{RVF}) and 650 nm (λ_{ex}^{A647}) and emission spectra were collected between 525 – 600 nm and 655-750 nm respectively. Post irradiation, mVivo samples were excited at 500 nm (λ_{ex}^{CVF}) and 650 nm (λ_{ex}^{A647}), and emission spectra were collected between 510 – 600 nm and 655-750 nm respectively. In order to study the pH sensitivity of Voltair and mVivo probes, buffers of indicated pH (4 – 7) were incubated with Voltair^{IM} or mVivo for 30 mins prior recording. The pH sensitivity was obtained by plotting the ratio of RVF emission intensity (G, λ_{ex} = 520 nm) at 550 nm or CVF emission intensity (λ_{ex} = 500 nm) at 530 nm and emission intensity of normalizing dye (R, λ_{ex} = 650 nm) at 665 nm, as a function

of pH. Mean of G/R ratio from three independent experiments and their standard deviation were plotted for each pH value.

II.C: Results and Discussion:

1. Design and working principle of Voltair

Conventionally, resting voltage across a membrane is measured by the difference in electrical potential of two electrodes, a sample electrode inserted across the biological membrane and a reference electrode located outside the biological membrane of interest[25] (Fig. II.4a). The DNA nanodevice Voltair, is designed based on a similar concept, where the fluorescence of a reporter probe inserted into the biological membrane is compared to a reference probe at a different wavelength located outside the biological membrane (Fig II.4a).

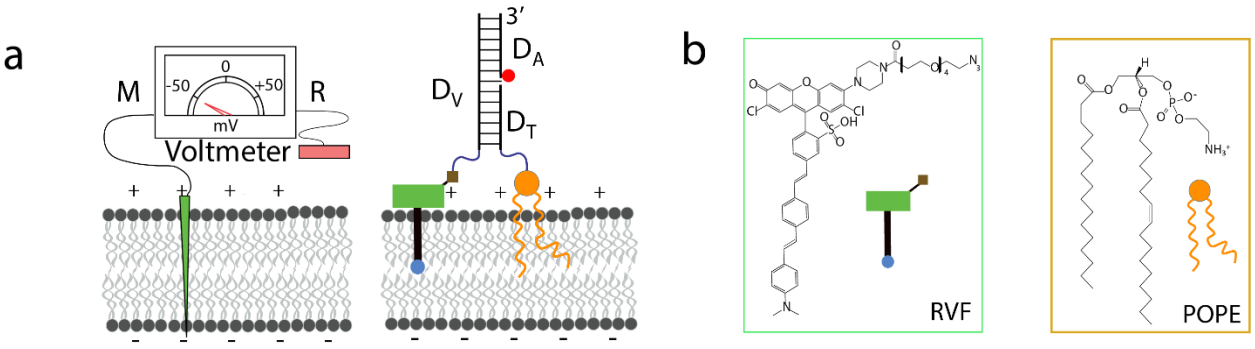

Figure II.4: Voltair schematic . (a) Schematic of the working principle of DNA voltmeter Voltair: Measuring probe (M, Green) is a voltage sensitive dye (RVF) conjugated to a DNA duplex that is membrane-tethered by attachment to a lipid anchor (POPE). Reference probe (R, red) is DNA duplex with a reference dye (Atto647N, red sphere) that together with RVF reports membrane potential ratiometrically. (b) Structure of a conjugatable version of RVF (RVF-N_3) and the lipid anchor POPE.

Voltair is based on nucleic acid scaffold that were previously shown to achieve ratiometric sensing of intracellular ions such as H^+, Ca^{2+}, Cl^- and reactive species such as NO, H_2S and HOCl

[23,26–31]. Voltair comprises a 38-base pair DNA duplex with three functional modules (Fig II.4a and Table II.1). The first module comprises the reporter probe, denoted Dv, is a 38-mer single-stranded DNA conjugated to a previously characterized voltage sensing dye (RVF) at the 3′ end. RVF belong to the class of voltage sensitive dyes that are based on fluorophore-bridge-quencher system designed by Evan W. Miller *et al.*[32]. RVF dye inserts into the biological membrane due to lipophilicity of molecular wire, phenylenevinylene (PPV) and the quencher. The fluorophore, 2,7-dichlorosulforhodol is quenched by photoinduced electron transfer (PeT) due to lone pair of electrons on its dimethyl aminobenzene moiety, extended via molecular wire PPV (Fig. II.4). When a potential difference is applied along the long axis of RVF, the local electric field modulates electron transfer, and therefore affects the fluorescence of RVF. For instance, plasma-membrane depolarization decreases electron transfer and increases fluorescence (Fig. II.4), whereas hyperpolarization increases electron transfer and decreases fluorescence.

The second module in Voltair, denoted as D_A, is the reference probe that is insensitive to membrane potential. The voltage insensitive reference dye corrects for intensity changes due to different sensor concentrations arising from non-uniform cellular uptake or inhomogeneous probe distribution. Thus, the ratio of fluorescence intensities from RVF and reference dye are proportional only to membrane potential across the membrane they are localized. The reference dye, Atto647N, is attached to the 5′ end of D_A and is chosen for its high photostability, minimal spectral overlap with RVF, insensitivity to pH, voltage and other ions (red circle, Fig. II.4).

The third functional module in Voltair, denoted as D_T, is a targeting moiety that can be changed to yield different variants for Voltair localization either at the plasma membrane, or in membranes of specific organelles[29,33]. The Voltair^{PM} variant has a targeting motif that localizes Voltair to the plasma-membrane by chemically conjugating the 5′ end of D_T to 1-palmitoyl-2-oleoyl-sn-glycero-

3-phosphoethanolamine (POPE) moiety via a tetra-ethylene glycol linker[22]. Other membrane anchors such as cholesterol are good alternatives for localizing DNA based probes onto plasma membrane of mammalian cells[33,34]. Thus, RVF is inserted in a defined orientation with respect to the membrane potential vector, and the anionic DNA duplex prevents any potential flipping of the RVF moiety in the membrane. Flipping of membrane potential probes can substantially perturb the measurement as the flipped probes would sense the electric field in the opposing direction.

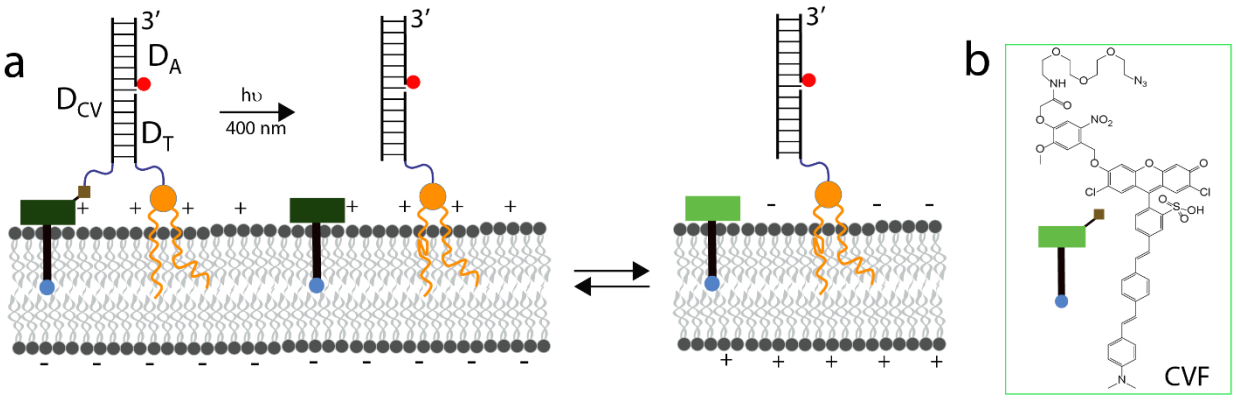

Figure II.5: mVivo schematic. (a) Schematic of the working principle of *mVivo*. Caged voltage sensitive dye (CVF) is conjugated to a DNA duplex that is membrane-tethered by attachment to a lipid anchor (POPE). Reference probe (R, red) is DNA duplex with a reference dye (Atto647N, red sphere) that is a fiducial marker, reveal the organelle location of mVivo. Irradiation with 400 nm light uncages the fluorescent VF to specific membrane of choice. The uncaged VF senses membrane potential based on PeT mechanism. (b) Structure of a conjugatable version of Caged VF (CVF).

Similar to Voltair, mVivo comprises of the same three functional modules discussed above. The reporter module of mVivo, denoted D_{CV}, is a 38-mer single-stranded DNA conjugated to a previously characterized photoactivable voltage sensing dye (CVF) at the 3′ end[20]. Photocaged VF (CVF) is coupled to DNA strand via photolabile 4,5-Dimethyxy-2-nitrobenzyl linker. Targeting module of mVivo localizes the probe to a specific membrane of choice and upon irradiation with

400 nm light, CVF is uncaged and released in the membrane as shown in figure II.5. Photoactivated CVF dye senses membrane potential via PeT mechanism as explained above. Ratio of fluorescence intensity from photoactivated VF to Atto647 corresponds to relative change in membrane potential (Fig. II.5).

2. Characterization of Voltair and mVivo assembly.

Assembly of DNA based probes are characterized using gel mobility shift assays[31]. Copper free click reaction of RVF to DBCO labeled strand (D_V) was validated by 15% Denaturing PAGE. Conjugation of 1 KDa (RVF) to 10 KDa (DBCO-strand) causes the slow mobility shift of D_V strand in Figure II.6. Furthermore, we confirmed that the lower mobility band contains RVF by fluorescence imaging in the rhodamine channel (excited by Epi-light and filtered by 560DF50). The D_V strand was purified and hybridized with the normalizing (D_A) and targeting module (D_T) as described in sample preparation section.

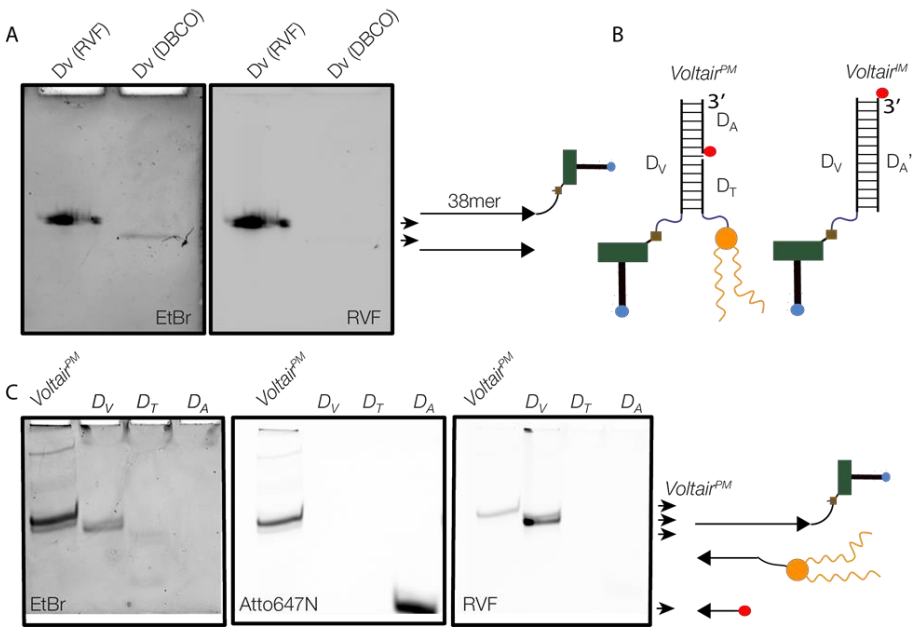

Figure II.6: Gel characterization of *Voltair*^{PM}. (a) 15% Denaturing polyacrylamide gel electrophoresis in 1X TBE, showing the conjugation of RVF-N_3 to the DNA strand DV bearing a 3' DBCO functionality. Gels are imaged in the EtBr channel that stains DNA as well as the rhodamine channel for RVF. (b) Schematic showing the components of Voltair^{PM} and Voltair^{IM}. (c) 15% Native polyacrylamide gel electrophoresis showing the formation of Voltair^{PM}. Gels were stained with Ethidium Bromide (EtBr) and imaged in the EtBr, Atto647N as well as RVF channels.

A 15% native PAGE was run to characterize the formation of complete sensor. In 15% acrylamide gels there is a large shift between duplex DNA and ssDNA. Under these conditions the increased persistence length of dsDNA leads to much slower mobility of Voltair^{PM} with respect to single strand components (D_V, D_T, D_A). This therefor validates the assembly of the full sensor at high yield. We again confirmed the slower mobility band contains RVF and the normalizing dye by imaging fluorescence in rhodamine channel (RVF) and Atto647N channel (Fig. II.6). Conjugation of CVF to DBCO modified DNA and assembly of mVivo was similarly characterized using 15% denaturing PAGE and 15% native PAGE, respectively (Fig. II.7)

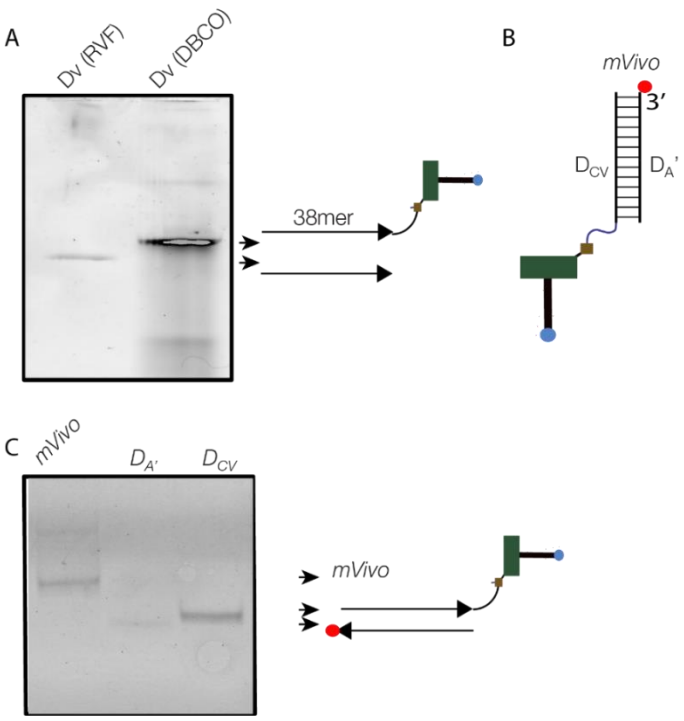

Figure II.7: Gel characterization of mVivo. (a) 15% Denaturing polyacrylamide gel electrophoresis in 1X TBE, showing the conjugation of CVF to the DNA strand D_{CV} bearing a 3' DBCO functionality. Gels are imaged in the EtBr channel that stains DNA. (b) 15% Native polyacrylamide gel electrophoresis showing the formation of mVivo. Gels were stained with EtBr and imaged in the EtBr channel.

3. Spectral characterization of Voltair and mVivo.

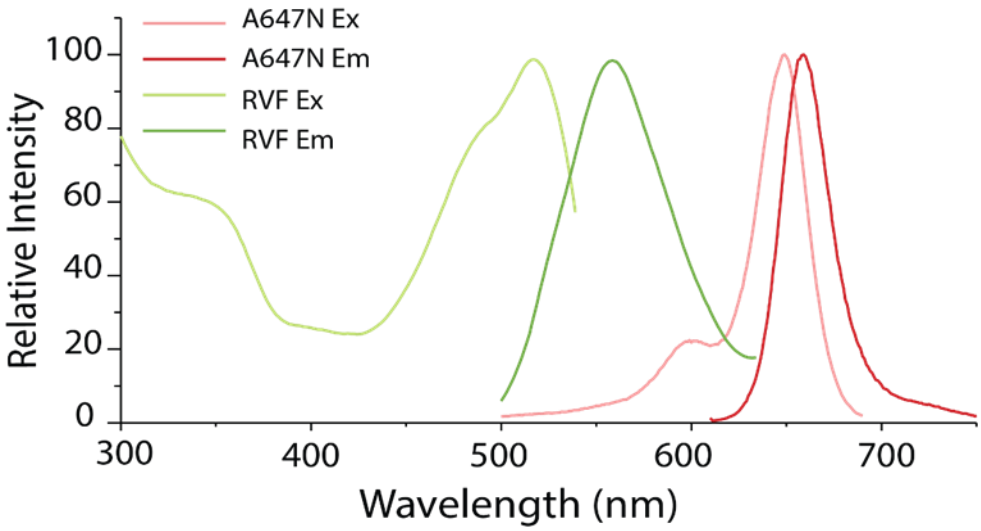

4. **Figure II.8: Spectral characteristics of Voltair**. Normalized excitation and emission spectra of RVF (green) and Atto647N (red). The reference dye (Atto647N) was chosen for the minimal overlap of its excitation spectra with the emission spectrum of the sensing (RVF) dye.

Fluorescence spectra of RVF dye show excitation λ_{max} at 510 nm and emission λ_{max} at 540 nm (Fig. II.8). Reference dye, Atto647N is chosen for its minimal spectral overlap as seen in figure II.8. UV light mediated photoactivation of mVivo is observed with the appearance of a strong absorption peak at 520 nm, characteristic of VF2.1.Cl (Fig 2.9a) and this further results in enhanced fluorescent intensity at 540 nm as a function of irradiation time[20] (Fig 2.9b-d).

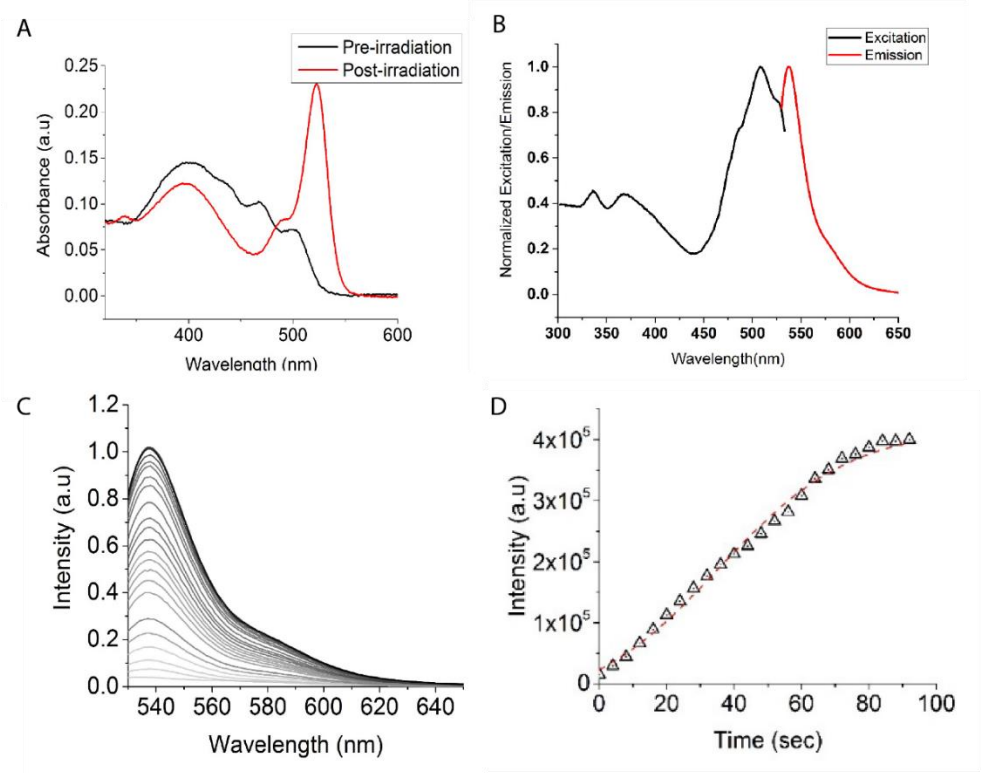

Figure II.9: Spectral characteristics of *mVivo*. (a) Absorption spectra of CVF before (black trace) and after (red trace) 400 nm irradiation. (b) Normalized excitation and emission spectra of CVF (black) and Atto647N (red). The reference dye (Atto647N) was chosen for the minimal overlap of its excitation spectra with the emission spectrum of the sensing (CVF) dye. (c) Exposure dependent increase in intensity of fluorescence spectra of CVF, upon irradiation with 400 nm light source. (d) Uncaging kinetics of CVF dye when irradiated with 400 nm light.

Intracellular compartments show increasing levels of lumenal acidity along the degradation pathway, ranging from pH 6.5 at early endosomes to pH 4.5 at lysosomes in mammalian cells. Most fluorescein and rhodol-based probes are sensitive to acidic pH and thus used as pH reporters in acidic organelles[35]. Protonation of phenolic -OH moiety (pKa = 6.4) of fluorescein chromophore decreases the fluorescence and hence used as well-established pH sensors. This aspect of pH interference makes it difficult to uncouple the probes ability to sense orthogonal signals such as membrane potential.

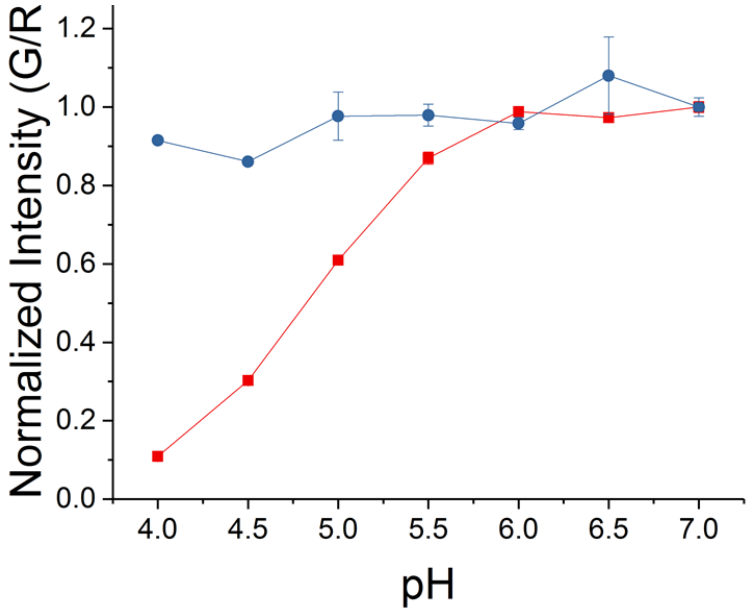

Figure II.10: Sensitivity of voltage sensitive dyes to physiological pH: Normalized G/R ratios of mVivo (red trace) and Voltair (blue trace) recorded in fluorescence spectrometer in UB4 buffers as a function of pH. Error bars indicate mean ± s.d.. of n = 3 measurements.

Thus, we chose a voltage sensitive dye (RVF) that could reliably sense at acidic pH. RVF comprise of dichlorosulforhodol dye, which is expected to have very low pKa due to two reasons. (i) dichlorofluorescein derivatives have lower pKa (~4.5) than fluorescein due to the negative inductive effect of chloro substitution at the ortho position of the phenolic OH. (ii) rhodol fluorophores have lower pKa than fluorescein (pKa of Rhodal = 5.5). To verify pH insensitivity of complete sensor Voltair^{IM}, fluorescence spectra of RVF and Atto647N were recorded at

different pH (4.0 – 7.0). G/R ratios were calculated by dividing the emission spectra maxima of RVF (550 nm) to that of Atto647N (665 nm) and plotted with respect to pH as shown in Figure 2.10. On the other hand, dichlorosulfofluorescein based VF dyes show pH sensitivity in the range 4.0 to 6.0, as shown by red trace in Figure II.10.

II.D: Conclusion

Protein-based voltage indicators while powerful, have limited applicability to acidic organelles, due to their pH sensitivity and cannot yet provide measures of absolute membrane potential using intensity-based measurements. Membrane localized voltage sensitive dyes are attractive due to their low capacitive loads and pH insensitivity but cannot be specifically targeted to organelles using conventional methods. Voltair, based on DNA scaffold, unites the advantages of voltage sensitive dyes with the organelle-targetability of proteins to non-invasively measure the membrane potential of organelles. Voltair leverages the 1:1 stoichiometry inherent in DNA duplexes along with functional and structural modularity, to integrate the following functions: (i) a voltage sensing probe (ii) an internal normalizing dye for ratiometric quantitation and (iii) an organelle targeting module for localization across intracellular membranes[18]. The modularity and structural precision allow Voltair modifications to target various intracellular membranes and quantify absolute membrane potential difference.

II.E: References

1. Petersen, C. C. H. Whole-Cell Recording of Neuronal Membrane Potential during Behavior. *Neuron* **95,** 1266–1281 (2017).
2. Bean, B. P. The action potential in mammalian central neurons. *Nat. Rev. Neurosci.* **8,** 451–465 (2007).
3. Broussard, G. J., Liang, R. & Tian, L. Monitoring activity in neural circuits with genetically encoded indicators. *Front. Mol. Neurosci.* **7,** 97 (2014).
4. Sepehri Rad, M. *et al.* Voltage and calcium imaging of brain activity. *Biophys. J.* **113,** 2160–2167 (2017).
5. Miller, E. W. Small molecule fluorescent voltage indicators for studying membrane potential. *Curr. Opin. Chem. Biol.* **33,** 74–80 (2016).
6. Knöpfel, T. & Song, C. Optical voltage imaging in neurons: moving from technology development to practical tool. *Nat. Rev. Neurosci.* **20,** 719–727 (2019).
7. Chamberland, S. *et al.* Fast two-photon imaging of subcellular voltage dynamics in neuronal tissue with genetically encoded indicators. *Elife* **6,** (2017).
8. Treger, J. S., Priest, M. F. & Bezanilla, F. Single-molecule fluorimetry and gating currents inspire an improved optical voltage indicator. *Elife* **4,** e10482 (2015).
9. Hochbaum, D. R. *et al.* All-optical electrophysiology in mammalian neurons using engineered microbial rhodopsins. *Nat. Methods* **11,** 825–833 (2014).
10. Chanda, B. *et al.* A hybrid approach to measuring electrical activity in genetically specified neurons. *Nat. Neurosci.* **8,** 1619–1626 (2005).
11. Yan, P. *et al.* Palette of fluorinated voltage-sensitive hemicyanine dyes. *Proc. Natl. Acad. Sci. USA* **109,** 20443–20448 (2012).
12. Ehrenberg, B., Montana, V., Wei, M. D., Wuskell, J. P. & Loew, L. M. Membrane potential can be determined in individual cells from the nernstian distribution of cationic dyes. *Biophys. J.* **53,** 785–794 (1988).
13. Miller, E. W. *et al.* Optically monitoring voltage in neurons by photo-induced electron transfer through molecular wires. *Proc. Natl. Acad. Sci. USA* **109,** 2114–2119 (2012).
14. Zhou, J. *et al.* A Lysosome-Targeting Fluorescence Off-On Probe for Imaging of Nitroreductase and Hypoxia in Live Cells. *Chem Asian J* **11,** 2719–2724 (2016).
15. Zielonka, J. *et al.* Mitochondria-Targeted Triphenylphosphonium-Based Compounds: Syntheses, Mechanisms of Action, and Therapeutic and Diagnostic Applications. *Chem. Rev.* **117,** 10043–10120 (2017).
16. Srivastava, J., Barber, D. L. & Jacobson, M. P. Intracellular pH sensors: design principles and functional significance. *Physiology (Bethesda)* **22,** 30–39 (2007).

17. Kulkarni, R. U. *et al.* A Rationally Designed, General Strategy for Membrane Orientation of Photoinduced Electron Transfer-Based Voltage-Sensitive Dyes. *ACS Chem. Biol.* **12,** 407–413 (2017).

18. Chakraborty, K., Veetil, A. T., Jaffrey, S. R. & Krishnan, Y. Nucleic Acid-Based Nanodevices in Biological Imaging. *Annu. Rev. Biochem.* **85,** 349–373 (2016).

19. Veetil, A. T. *et al.* Cell-targetable DNA nanocapsules for spatiotemporal release of caged bioactive small molecules. *Nat. Nanotechnol.* **12,** 1183–1189 (2017).

20. Grenier, V., Walker, A. S. & Miller, E. W. A Small-Molecule Photoactivatable Optical Sensor of Transmembrane Potential. *J. Am. Chem. Soc.* **137,** 10894–10897 (2015).

21. *Click chemistry for biotechnology and materials science*. (John Wiley & Sons, Ltd, 2009). doi:10.1002/9780470748862

22. Van Lengerich, B., Rawle, R. J. & Boxer, S. G. Covalent attachment of lipid vesicles to a fluid-supported bilayer allows observation of DNA-mediated vesicle interactions. *Langmuir* **26,** 8666–8672 (2010).

23. Modi, S. *et al.* A DNA nanomachine that maps spatial and temporal pH changes inside living cells. *Nat. Nanotechnol.* **4,** 325–330 (2009).

24. Modi, S., Nizak, C., Surana, S., Halder, S. & Krishnan, Y. Two DNA nanomachines map pH changes along intersecting endocytic pathways inside the same cell. *Nat. Nanotechnol.* **8,** 459–467 (2013).

25. Rubaiy, H. N. A short guide to electrophysiology and ion channels. *J. Pharm. Pharm. Sci.* **20,** 48–67 (2017).

26. Dan, K., Veetil, A. T., Chakraborty, K. & Krishnan, Y. DNA nanodevices map enzymatic activity in organelles. *Nat. Nanotechnol.* **14,** 252–259 (2019).

27. Leung, K., Chakraborty, K., Saminathan, A. & Krishnan, Y. A DNA nanomachine chemically resolves lysosomes in live cells. *Nat. Nanotechnol.* **14,** 176–183 (2019).

28. Veetil, A. T. *et al.* DNA-based fluorescent probes of NOS2 activity in live brains. *Proc. Natl. Acad. Sci. USA* **117,** 14694–14702 (2020).

29. Saha, S., Prakash, V., Halder, S., Chakraborty, K. & Krishnan, Y. A pH-independent DNA nanodevice for quantifying chloride transport in organelles of living cells. *Nat. Nanotechnol.* **10,** 645–651 (2015).

30. Thekkan, S. *et al.* A DNA-based fluorescent reporter maps HOCl production in the maturing phagosome. *Nat. Chem. Biol.* **15,** 1165–1172 (2019).

31. Narayanaswamy, N. *et al.* A pH-correctable, DNA-based fluorescent reporter for organellar calcium. *Nat. Methods* **16,** 95–102 (2019).

32. Woodford, C. R. *et al.* Improved PeT molecules for optically sensing voltage in neurons. *J. Am. Chem. Soc.* **137,** 1817–1824 (2015).

33. You, M. *et al.* DNA probes for monitoring dynamic and transient molecular encounters on live cell membranes. *Nat. Nanotechnol.* **12,** 453–459 (2017).

34. Jani, M. S., Zou, J., Veetil, A. T. & Krishnan, Y. A DNA-based fluorescent probe maps NOS3 activity with subcellular spatial resolution. *Nat. Chem. Biol.* **16,** 660–666 (2020).

35. Lanz, E., Gregor, M., Slavík, J. & Kotyk, A. Use of FITC as a Fluorescent Probe for Intracellular pH Measurement. *J Fluoresc* (1997).

III. Targeting DNA nanodevices to cellular membranes

III.A: Introduction

Exogenous nucleic acids are endocytic ligands to plasma membrane resident scavenger receptors[1]. Scavenger receptors are categorized into classes A-H according to their structural characteristics[2]. In general, they comprise a membrane anchored region and extracellular domain comprising positively charged lysines[3]. Scavenger receptor class A, found in macrophages comprise of a collagenase domain, formed by highly conserved amino acid repeats with multiple lysine residues[3]. The specific targeting of DNA nanodevices to scavenger receptors occurs by interaction of negative backbone of nucleic acids with anion ligand binding receptors (ALBRs), also known as scavenger receptors[4]. DNA based nanodevices such as I-switch and Clensor were targeted to endocytic vesicles, along the ALBR pathway in Drosophila hemocytes[4,5]. Similar principle allowed for targeting complex DNA nanostructures and functional DNA sensors to coelomoctyes of C. elegans *in vivo*[6,7]. Scavenger receptors are endogenously expressed in immune and fibroblast cells, which enabled the use of DNA based dual sensors ChloropHore and CalipHluor to diagnose severe lysosome centric diseases, such as Neiman pick disease type A, B, C and Parkinson diseased patient cells[8,9].

In addition to the endogenous trafficking pathway of nucleic acids, modularity of DNA enables further modification of DNA scaffold to reprogram intracellular trafficking[10]. Reprogramming DNA nanoprobes enabled targeting recycling endosomes, phagosomes and trans Golgi network in mammalian cells[5,11,12]. This is achieved by three strategies as shown in figure III.1,

(a) Endogenous ligand mediated targeting: DNA scaffold can be modified with receptor ligands such as transferrin or folic acids, that can engage receptors at the plasma membrane and

selectively traffic along their respective pathways[12,13]. This strategy can also be extended to selectively label plasma membrane by modifying DNA with lipid anchors such as cholesterol and phosphoethanolamine[14–16].

(b) Carrier protein targeting: Sequence-specific DNA binding protein is expressed as a chimera with an organelle trafficking protein, that binds DNA nanodevice at the plasma membrane and localizes within a given target organelle. This strategy was used to target I-switch to trans Golgi network, where the cells were expressed with a chimera of sequence specific DNA binding protein and proprotein convertase furin, that traffics I-switch in a retrograde pathway[12,17].

(c) Aptamer based targeting: DNA or RNA aptamers can be designed to specifically bind membrane resident proteins that are known to undergo recycling or retrograde trafficking pathway. An RNA aptamer designed to bind transferrin receptor, was used to localize Clensor in the recycling endosomes[5] and a DNA aptamer for MUC1 receptor was used to localize NOckout probes in the trans Golgi network of cancer cells[18].

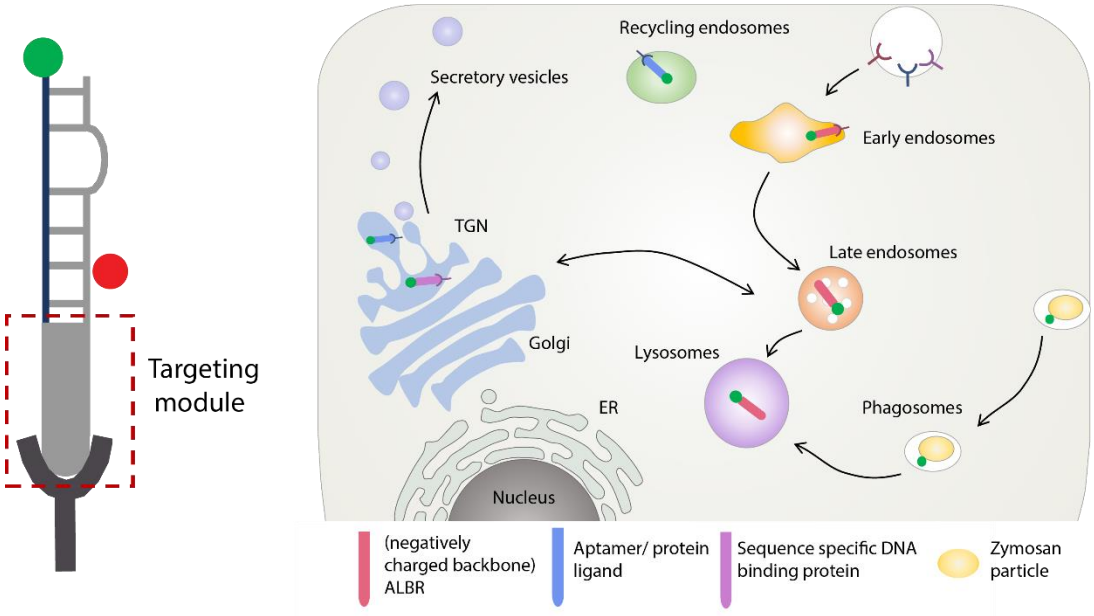

Figure III.1: Targeting DNA to intracellular compartments: DNA scaffold provides the "plug n play" feature to incorporate targeting modules that are modular and specifically labels intracellular organelles via. vesicle trafficking pathways.

In order to obtain voltage maps of various organelles within a given cell type, we are required to standardize all the above strategies in one specific cell type. Thus, we demonstrate targeting DNA nanodevice to different membrane compartments, such as plasma membrane, early, late and recycling endosomes, lysosomes and trans Golgi network in cell type that is commonly used to interrogate voltage sensors, HEK 293T cells.

III.B: Materials and methods

1. Oligonucleotides

Modified DNA oligonucleotides were purchased from IDT (USA). PAGE purified and lyophilized oligonucleotides were dissolved in Milli-Q water of recommended volume to approximately prepare 100 µM stocks. Concentration of oligonucleotides are accurately quantified by collecting UV absorbance spectra and using Beer Lambert's law with absorbance at 260nm for DNA. In the case of fluorescently labeled oligonucleotides, equation 1 is used to quantify the concentration.

$$\text{Concentration} = (Abs_{260} \times \text{dilution factor}) / (\varepsilon_{oligo} - \varepsilon_{dye}) \quad \text{Eq. 1}$$

Where, molecular extinction coefficients of all oligonucleotides ε_{oligo} are provided in the specification sheet by IDT and molecular extinction coefficient of the fluorescent dye at 260nm ε_{odye} is referred from literature references.

Table III.1. List of modified oligonucleotides used in chapter 3

S. No	Strand	Sequence (5' to 3')	Comment
1	D_V	ATCAACACTGCACACCAGACAGCAA GATCCTATATATA-ispacer18-DBCON	Sensing stand – conjugated to RVF

2	D_V^{POPE}	ATCAACACTGCACACCAGACAGCAA GATCCTATATATA-ispacer18-DBCON	PM labeling - conjugated to POPE
3	D_T	DBCO-TEG-TATATATAGGATCTTGCTGTCT	Targeting strand – conjugated to POPE
4	D_A	Atto647N – GGTGTGCAGTGTTGAT	Normalizing strand – PM
5	D_A’	TATATATAGGATCTTGCTGTCTGGTG TGCAGTGTTGAT-Atto647N	Normalizing strand – Intracellular Membrane (IM)
6	D_V^{RE}	DBCO-TEG-ispacer18-TATATATAGGATCTTGCTTCTGTGCC TGCAGTGTTGAT	RE sensing strand – conjugated to RVF
7	D_A^{RE}	Atto647NATCAACACTGCAGGCACAG AGTCTGGTG	RE normalizing stand
8	D_{Tf}	CACCAGACAGCAAGATCCTATATATA GGGGGA**UC**AA**UCC**AAGGGA**CCC**GG AAA**CG**C**UCCCUU**AC**A**CCCC**	RE targeting strand – modified with RNA aptamer. The portion of sequence in red correspond to RNA aptamer against hTfR and bold letters indicate 2’ fluoro modified bases.

Table III.1. List of modified oligonucleotides used in chapter 3 (continued).

2. Sample preparation

In order to study the targeting characteristics of Voltair, mono-labeled variant with only Atto647N label is used, $Voltair_{mono}^{IM}$. Stock solution of $Voltair_{mono}^{IM}$ was prepared at a final concentration

of 10 µM by mixing D_V (unlabeled) and D_A' (Atto647N – 3' modified 38 mer strand) at an equimolar ratio in 10 mM sodium phosphate buffer, pH 7.4. POPE-DNA complex is assembled at a final concentration of 10 µM by hybridizing D_v^{POPE} and D_A' (Atto647N – 3' modified 38 mer strand) at an equimolar ratio in 10 mM sodium phosphate buffer, pH 7.4. For $Voltair_{mono}^{RE}$ samples, 10 µM of D_V^{RE} (unlabeled), D^{Tf} and D_A^{RE} were mixed at an equimolar ratio. For all samples, annealing was performed by heating the reaction mixture to 95°C for 15 min and gradually cooling to RT, at 1°C/ 3 min. Annealed samples were equilibrated at 4°C overnight.

3. Gel electrophoresis

For gel electrophoresis 15% native polyacrylamide gels were used for annealed samples. Denaturing polyacrylamide gels containing 12-15% acrylamide [38:2 acrylamide/ bisacrylamide] were used for dye conjugated single strand samples. Gels were run in 1X TBE buffer (100 mM Tris. HCl, 90 mM boric acid and 2 mM EDTA, pH 8.3) at RT. Non-fluorescent samples were stained with ethidium bromide (1µg/mL) for 10 mins prior to visualization. Samples were observed by Biorad Universal Hood II Gel Doc system (Bio-Rad Laboratories, Inc.)

4. Cell culture

Human embryonic kidney cells (HEK 293T), BHK-21 cells, human dermal fibroblasts (HDF), RAW 264.7, THP-1 and T-47D cells were a kind gift from Dr. Bryan Dickinson (Department of Chemistry, University of Chicago), Dr. M. Gack (Department of Microbiology, the University of Chicago), J. Rowley's lab (University of Chicago), Dr. Christine A. Petersen (Department of Epidemiology, University of Iowa), Dr. D. Nelson (Department of Pharmacological and Physiological Sciences, the University of Chicago) and G. Greene (The Ben May Department for Cancer Research, the University of Chicago), respectively. COS-7 cells were purchased from

ATCC. Cells were cultured in Dulbecco's Modified Eagle's Medium (Invitrogen Corporation, USA) containing 10% heat inactivated Fetal Bovine Serum (FBS) (Invitrogen Corporation, USA), 100 U/mL penicillin and 100 µg/mL streptomycin and maintained at 37ºC under 5% CO_2. HEK 293T cells were passaged and plated at a confluency of 20 – 30% for electrophysiology experiments, and 50 – 70% for transfection and intracellular measurements.

5. Plasmids

The hMSR1 and hMSR1-ECFP plasmids were provided by Michael Schwake, Northwestern University. The hMSR1 sequence was cloned into the PCS2NXE vector (4,103 bp) containing the CMV promoter for overexpression in mammalian cell lines. The hMSR1-CFP plasmid (5973 bp) was constructed by cloning hMSR1 sequence into pECFP-C1 plasmid (4731 bp). The identity of each construct was confirmed by sequencing, using forward primer (5' to 3') GGGACATGGGAATGCAATAG and reverse primer (5' to 3') CTCAAGGTCTGAGAATGTTCCC.

The mCherry-TGNP-N-10 was a gift from Michael Davidson (Addgene plasmid #55145) and Rab7-RFP was a gift from Ari Helenius (Addgene plasmid #14436). Construction of scFv-furin construct is reported previously[12,17].

6. Reagents and buffers

CellMask™ reagents and TMR-Dextran were purchased from molecular probes/Life Technologies (USA). Maleylated Bovine serum albumin (mBSA) and fluorescent transferrin (Tf-Alexa546) were conjugated according to published protocols[5]. 1-palmitoyl-2-oleoyl-sn-glycero-3-phosphoethanolamine lipid was purchased from Avanti lipids (USA). Vacuolin-1 is purchased

from Cayman (USA). Dulbecco's minimal essential media (DMEM), Hank's balanced salt solution (HBSS) and Opti-MEM are purchased from ThermoFisher (USA).

1X Phosphate buffered Saline (PBS): 137 mM NaCl, 2.7 mM KCl, 10 mM Na_2HPO_4. 2 mM KH_2PO_4, pH adjusted to 7.0 using 1N HCl. The buffer was filtered using 0.22 µm filter and autoclaved prior use.

7. Maleylated-BSA preparation

Final concentration of 5 mg/ mL BSA (sigma, USA) was dissolved in 100 mM sodium carbonate/ bicarbonate buffer, pH 9.0. Maleic anhydride was added to BSA solution in 10 equivalent excess and stirred at room temperature for 3 h. In order to maintain optimal pH of the reaction mixture, sodium carbonate is added every 30 mins such that the pH is 9.0. After 4 h, the reaction mixture was diluted 10 times with 1X PBS and filtered using 3KDa amicon filters to remove maleic anhydride. The resultant mBSA was aliquoted and immediately frozen at -20°C.

8. Transferrin-Alexa 546 conjugation

Human holo-transferrin was dissolved in 100 mM sodium phosphate buffer, pH 7.4 to a final concentration of 10 mg/mL. Alexa 546-NHS ester (Life Technologies, USA) was added in 10 equivalent excess to transferrin and stirred at room temperature for 4 h. After 4 h, the reaction mixture is diluted 10 times with 10 mM sodium phosphate buffer, pH 7.4 and filtered using amicon filters to remove unreacted excess dye. The concentrated Alexa546-transferrin conjugate was quantified following UV absorbance at 280 nm and 546 nm, aliquoted and stored at -20°C.

9. Plasma membrane labeling

HEK 293T cells were washed with 1X PBS to remove cell debris and traces of complete media. 10 µM Voltair or 100 µM RVF sample was diluted to a final concentration of 500 nM with HBSS and added to the coverslip containing HEK 293T cells. Cells were incubated for 20 mins at room temperature and washed 3 times with 1X PBS and further incubated at room temperature for 15 mins. For plasma membrane colocalization experiments, Cell mask^{TM} diluted to 1000X were added along with DNA probes and above protocol was followed. Fluorescently labeled cells were then imaged at room temperature and same cells were followed over a period of time to record the dissociation of DNA-POPE conjugate from the plasma membrane.

10. Transfection

HEK 293T cells were transiently transfected with respective plasmids using *Trans*IT®-293 transfection reagent (MIRUS). Cells were washed and incubated with Opti-MEM, while preparing the transfection complex as per the manufacturer's instruction. Cells were incubated for 4 h with the transfected medium and was replaced with fresh medium. All Voltair labeling experiments were performed on cells 48 hours post transfection.

11. DNA uptake in mammalian cells expressing scavenger receptor

Mammalian cells endogenously expressing scavenger receptor or HEK 293T cells transiently expressed with macrophage scavenger receptor (MSR1) were washed with 1X PBS and incubated with 500 nM Voltair$_{mono}^{IM}$ in HBSS, for 30 mins at 37°C. The cells were then washed three times with 1X PBS and further incubated in complete media for 30 mins, at 37°C. Post incubation, cells were thoroughly washed with 1X PBS and replaced with Opti-MEM for imaging experiments.

12. Competition assay with mBSA

HEK 293T cells transfected with hMSR1-CFP and other cells endogenously expressed with scavenger receptors, were washed with 1X PBS, pH 7.4 prior to labeling with the $Voltair_{mono}^{IM}$. Cells were incubated with 20 μM maleylated BSA (mBSA) for 15 min, followed by a 20 min pulse of 500 nM $Voltair_{mono}$ and 20 μM mBSA to allow internalization by receptor mediated endocytosis. Control cells were washed and pulsed for 20 mins in 500 nM $Voltair_{mono}^{IM}$ without mBSA. Cells were then washed three times with 1X PBS and chased for 30 mins in complete DMEM media. Complete media was replaced with Opti-MEM solution (Thermofisher) and imaged by widefield microscopy for quantification and confocal microscopy for representative images. Similar pulse-chase protocol was followed for other cell types. Whole cell intensities in the Atto647N channel were quantified for cells expressing hMSR1-CFP observed in CFP channel. The mean intensity from three different experiments were normalized against the no mBSA control, for n~50 cells.

13. Co-localization assay with organelle markers

In order to find out the time points at which internalized DNA devices specifically label a defined organelle, colocalization experiments were performed with different organelle specific markers as a function of time in HEK 293T cells. Transferrin receptors are known to recycle to plasma membrane via early endosome (EE) and recycling endosome (RE), therefore we used fluorescent Transferrin to specifically label EE by pulsing it for 10 min prior to imaging and label RE with an additional chase time of 30 mins[19]. Rab7-mRFP is a well-established late endosome (LE) marker, and was transiently expressed in HEK 293T cells to label LE[20]. Transient expression of TGN46-mCherry specifically labels trans Golgi network (TGN)[21]. Finally, TMR-Dextran a specific marker

for lysosome (Ly), was pulsed for 1 hour, followed by 16 hours chase in complete media to label lysosomes[20].

To find out the trafficking time of DNA device in labeling EE, HEK 293T cells transfected with hMSR1, were pulsed with 500 nM $Voltair_{mono}^{IM}$ for 10 minutes and chased for indicated time. These cells were also pulsed with 100 nM Tf-Alexa546 for 10 mins to visualize the early endosomes. A stock solution of Tf-Alexa546 was prepared according to previously established methods[5]. Images of the Alexa546 channel and the Atto647N channel were acquired by confocal imaging (microscopy methods) and Pearson correlation coefficient (PCC) value were calculated using Fiji plugin coloc2[22].

To find out the trafficking time of DNA device in specifically labeling LE or Ly, HEK 293T-hMSR1 cells were transfected with Rab7-RFP for LE or pre-pulsed & chased with TMR-Dextran for Ly. These cells were then pulsed with 500 nM $Voltair_{mono}^{IM}$ for 30 mins and chased for indicated time. PCC of DNA device colocalization with EE, LE or Ly was plotted with respect to chase time. A maximum PCC value represents the time point at which DNA device is localized to the specific organelle. The trafficking time of DNA device with transferrin aptamer and $d(AT)_4$ tag in labeling RE and TGN, respectively, have been established previously[5,12]. Briefly, recycling endosomes are targeted by pulsing $Voltair^{RE}$ in 1X HBSS, for 10 mins at 37°C, followed by 30 mins of chase in complete media at 37°C. Trans Golgi network is targeted by pulsing $Voltair^{TGN}$ in complete media containing cycloheximide (CHX) for 90 mins at 37°C, followed by 90 mins chase in the same media.

14. Fluorescence microscopy

Wide field microscopy was carried out on an IX83 inverted microscope (Olympus Corporation of the Americas, Center Valley, PA, USA) using either a 100X or 60X, 1.4 NA, DIC oil immersion objective (PLAPON, Olympus) and Evolve Delta 512 EMCCD camera (Photometrics, USA). Filter wheel, shutter and CCD camera were controlled using Metamorph premier Ver 7.8.12.0 (Molecular Devices, LLC, USA). Images on the same day were acquired under the same acquisition settings (exposure 100 ms and EM gain at 100 for Atto647N, exposure 100 ms and EM gain 300 for RVF). All the images were background subtracted by taking mean intensity over an adjacent cell free area. Filter sets, purchased from Chroma, suitable for each fluorophore were selected to minimize excitation and emission from other dyes in the sample. RVF channel images were obtained using 500/20 band pass excitation filter, 535/30 band pas emission filter and 89016 dichroic. For Atto647N, images were obtained using the 640/30 band pass excitation filter, 705/72 band pass emission filter and 89016 dichroic.

Confocal images were captured with a Leica TCS SP5 II STED laser scanning confocal microscope (Leica Microsystems, Inc. Buffalo Grove, IL, USA) equipped with a 63X, 1.4 NA, Oil immersion objective. RVF was excited using an argon laser with 514 nm wavelength, CFP by 458 nm and Atto647N using a He-Ne laser with 633 nm wavelength. CellMask orange stain was excited by 543 nm and all emissions were filtered using Acousto Optical Beam Splitter (AOBS) with settings suitable for each fluorophore and recorded using hybrid detectors (HyD).

15. Coelomocyte labeling experiments

Coelomocyte labeling was performed with mVivo as per established methods[6]. For microinjections, mVivo were diluted to 500 nM using 1X Medium 1 (150 mM NaCl, 5 mM KCl,

1 mM $CaCl_2$, 1 mM $MgCl_2$, 20 mM HEPES, pH 7.2). Microinjections were performed in the pseudocoelom of one-day old PPK3 mutant hermaphrodites, at the dorsal side, opposite to the vulva. Microinjections are performed using an Olympus IX53 Simple Inverted Microscope (Olympus Corporation of the Americas, Center Valley, PA) equipped with 40X, 0.6 NA objective, and microinjection setup (Narishige, Japan). Injected worms were mounted on 2.0% agarose pad and anesthetized using 40 mM sodium azide in M9 buffer. Lysosomes labeled with mVivo is imaged after 1 h incubation at 22°C.

16. Colocalization - Image analysis

Pearson correlation coefficient (PCC) by Coloc2 ImageJ plugin is calculated with the equation (1), where R_i and G_i refer to the intensity of red and green channels, respectively of pixel i, and R_m and G_m refer to the mean intensities of the red and green channels, respectively, across the entire image.

$$\text{PCC} = \frac{\sum_i (R_i - R_m) \times (G_i - G_m)}{\sqrt{\sum_i (R_i - R_m)^2 \times \sum_i (G_i - G_m)^2}} \qquad (1)$$

PCC values range from 1 for two images whose fluorescence intensities are perfectly, and linearly related, to −1 for two images whose fluorescence intensities are perfectly, but inversely related, to one another. Values near zero reflect distributions of probes that are uncorrelated with one another.

To account for the comparative nature of colocalization in endocytosis, consistent with common practice, we performed two controls

(i) Pixel shift analysis: One of the images is translated by $x=x_i+15$ and $y=y_i+15$ in space (this number is 1.5 - 2X the size of the average puncta/spot) and the PCC is measured again. If the colocalization is real, and not random, then the pixel-shifted PCC will dramatically reduce.

However, if the colocalization occurs due to sheer randomness, then the PCC before and after pixel shifts will be comparable, or lower.

(ii) negative colocalization control, where PCC is measured between images of one specific organelle type (say early endosome) labeled with a molecule of interest (say, Voltair) and another organelle labeled by a tracer or an organelle protein marker. Negative colocalization controls in this case would be PCC's values for Voltair in the early endosomes against a Late endosome marker or a lysosome marker. One should observe PCC and pixel-shifted PCC values close to 0.

III.C: Results and Discussion

1. Targeting DNA-POPE to plasma membrane

To anchor DNA based probes to the outer membrane leaflet of cell, the DNA backbone was conjugated to 1-palmitoyl-2-oleoyl-sn-glycero-3-phosphoethanolamine lipid (POPE). POPE-DNA conjugates have been previously shown to effectively label the plasma membrane of cells[23]. For efficient insertion, the DNA duplex was coupled to POPE via tetraethylene glycol linker, providing additional flexibility and spacing (Fig II.4, III.2). DNA-lipid conjugates show reversibility in anchoring due to hydrophilicity of negatively charged DNA. We labeled the cells with 500 nM DNA-POPE or *Voltair*^{PM} for 20 mins at room temperature, washed the cells three times with 1X PBS and incubate the cells in extracellular buffer.

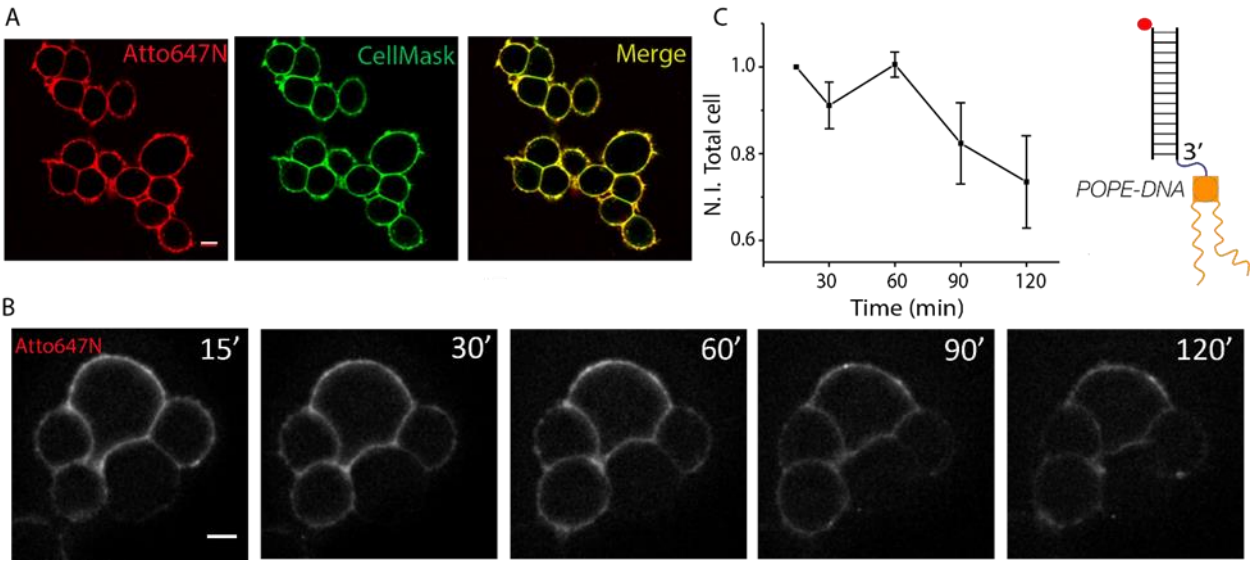

Figure III.2. Plasma membrane labeling with POPE-DNA. (a) Colocalization of Voltair^{PM} with plasma membrane marker CellMask^{TM} orange in HEK 293T cells. Scale = 10 µm. (b) Time lapse images of HEK 293T cells labelled with POPE-DNA (500 nM) as a function of time shows a loss of signal only beyond 60 min. Scale = 10 µm. (c) Normalized total cell intensity (N.I. Total cell) shown in (b) as a function of time. Error bar indicates mean ± s.d. of n = 15 cells.

2. DNA uptake in cells expressing scavenger receptors

The Voltair^{IM} variant labels intracellular organelles by leveraging the ability of duplex DNA to double as a ligand for scavenger receptors[4]. The DNA-based targeting motif imposes an over-riding trafficking signal that enables Voltair internalization into a specific intracellular organelle. The DNA duplex binds scavenger receptors at the plasma-membrane and undergoes scavenger receptor-mediated endocytosis, trafficking to early endosomes, which mature to late endosomes, and finally to lysosomes, in a time-dependent manner[5]. DNA-based probes can label endocytic organelles precisely and in diverse cell types that express scavenger receptors such as THP-1 (Human monocyte cell line), RAW 264.7 (Mouse macrophage cell line), T-47D (breast cancer cell

line), BHK-21 (Baby Hamster Kidney fibroblast), HDF (Human Dermal fibroblast) and COS-7 cells (Monkey kidney cells), as shown in figure III.3.

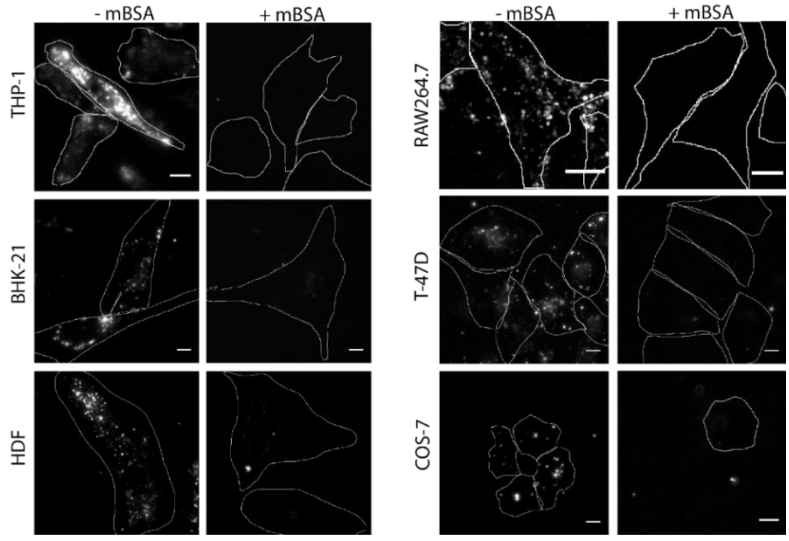

Figure III.3. DNA uptake by cell types expressing endogenous levels of scavenger receptor Representative images of different cell lines demonstrating uptake of DNA nanodevices to intracellular compartments, via endogenous scavenger receptor. Competitive inhibition of DNA - scavenger receptor interaction with maleylated BSA, decreases uptake in these cells. THP-1: human monocyte derived cell line; BHK-21: Baby Hamster Kidney cells; HDF: Human Dermal Fibroblast primary cells; RAW 264.7: Mouse macrophage cell line; T-47D: breast cancer cell line; COS-7: Monkey kidney cell line. Scale: 10 µm.

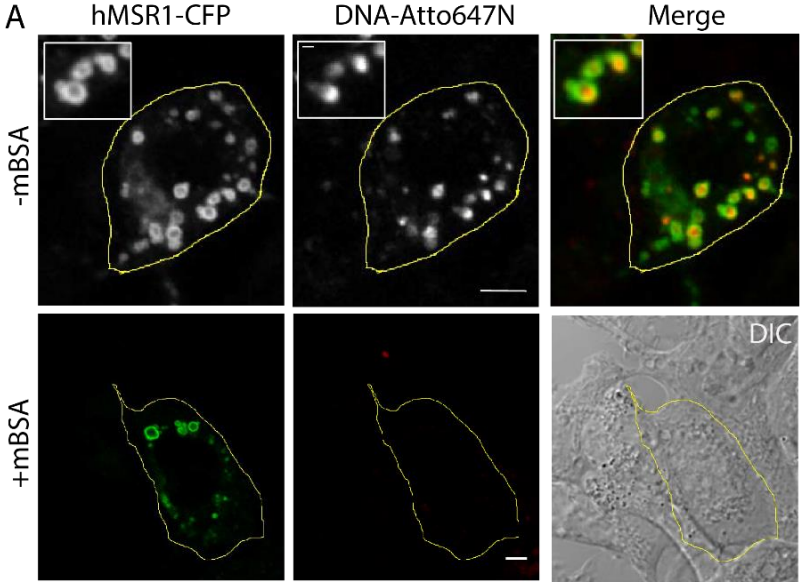

Figure III.4. Voltair^{IM} uptake by HEK cells expressing human scavenger receptor (hMSR1). (a) Upper Panels: Voltair^{IM} is endocytosed by HEK 293T cells expressing hMSR1-CFP. Colocalization of hMSR1 (CFP channel) with Voltair^{IM} (Atto647N channel) in punctate structures.

Lower panels (continued): Uptake of Voltair^{IM} is efficiently competed out in the presence of maleylated BSA (mBSA) a good ligand for hMSR1. Scale bar = 10 μm.

HEK 293T cells on the other hand, do not express scavenger receptors[24]. While this is ideal for plasma membrane immobilization of Voltair^{PM}, it prevents endosomal uptake of Voltair nanodevices. Therefore, we over-expressed human macrophage scavenger receptor (hMSR1) fused to CFP in HEK293T cells by transient transfection. These transfected cells effectively endocytosed Voltair^{IM} through receptor-mediated endocytosis (Fig III.4). Colocalization between hMSR1-CFP and Voltair^{IM} indicated uptake by scavenger receptors (Fig III.4). This was reaffirmed by competing out Voltair^{IM} uptake with excess maleylated BSA, a strong ligand for scavenger receptors (Fig III.4)[4].

3. Time dependent trafficking of DNA device along degradative pathway

DNA nanodevices are known to undergo receptor mediated endocytosis and traffics along degradative pathway to localize at terminal lysosomes[6,8]. Thus, we determined the timepoints of localization of internalized DNA nanodevices at each stage along the endo-lysosomal pathway in HEK 293T cells (Fig III.5). For this, we performed time-dependent colocalization with various well-known endocytic markers. Briefly, HEK 293T cells expressing hMSR1 were pre-labeled with endocytic markers such as Alexa546-labeled transferrin or TMR-Dextran, that each specifically labels early endosomes or lysosomes, respectively[19,20]. HEK 293T cells co expressing hMSR1 and Rab7-mRFP labels the late endosomes with fluorescent Rab7[20]. These cells were then pulsed with Voltair$_{mono}^{IM}$. Colocalization was monitored as a function of different chase times (Fig III.5). We found that Voltair$_{mono}^{IM}$ localized in early endosomes at ~10 min, showing 70% colocalization with Alexa546-Tf. Localized to late endosomes at ~60 min and to lysosomes at ~100 min, with 85% and 60% colocalization with Rab7 labeled vesicles and dextran positive lysosomes, respectively.

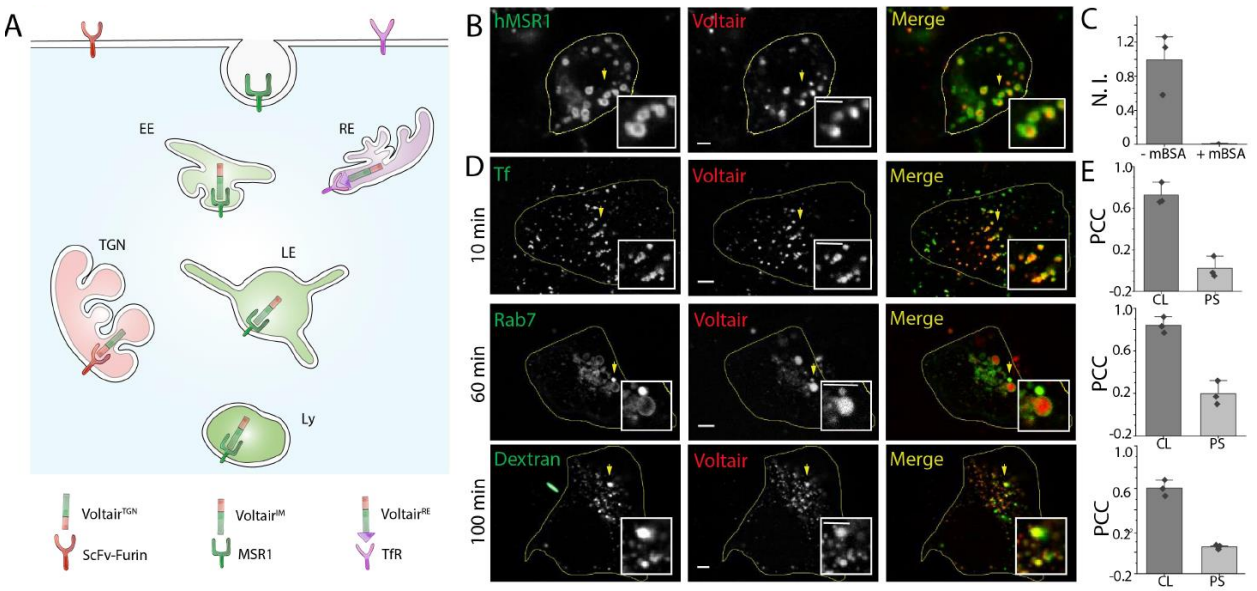

Figure III.5. Targeting Voltair^{IM} to membranes of specific endocytic organelles: (a) Schematic of targeting strategy: Voltair^{IM} undergoes scavenger receptor mediated endocytosis by binding scavenger receptors. Endocytosed Voltair^{IM} traffics in a time-dependent manner from the plasma membrane to the early endosome, the late endosome and then the lysosome. (b) Representative colocalization between internalized Voltair^{IM} (red channel) and human macrophage scavenger receptors (hMSR1-CFP, green channel) transfected in HEK 293T cells. (c) Normalized intensity of Voltair^{IM} uptake in cells, in absence and presence of mBSA (30 eq.) Error bar represents mean ± s.e.m. of three independent trials, n =30 cells (d) Representative colocalization between various endocytic organelle markers (green channel) and Voltair^{IM} (red channel) at the indicated chase times. Early endosomes are labelled with Transferrin-Alex¬a546 (Tf), late endosomes are labelled with Rab7-mRFP (Rab7) and lysosomes are labelled with TMR dextran (Dextrans). Scale bar = 5 μm. (e) Pearson's correlation coefficient (PCC) of Voltair colocalization (CL) with corresponding endocytic markers in (d) along with pixel shift (PS). Error bar represents mean ± s.e.m. of three independent trials, n = 20 cells.

Although the observed 60% colocalization between Voltair$_{mono}^{IM}$ and TMR dextran positive lysosomes is modest, it's similar to reported values in literature[25]. Pearson correlation coefficient (PCC) is sensitive to i) Pixel to pixel proportionality in the signal levels of two channels and ii) degree to which each pixel intensity (red and green) is either both above or below background. Although in an ideal case we expected a PCC of 1 for perfect colocalization, in cell biology and especially endocytosis biology is comparative, as shown by Dunn et al[26]. For instance, Dunn et al record a PCC of 0.944 when a binary mixture of transferrin carrying two different

fluorophores is internalized by cells via the transferrin receptor. However, PCC is 0.66 when two different endocytic ligands (transferrin and IgA) engage two different receptors (transferrin receptor and Ig receptor) and are then localized in early endosomes. Thus, heterogeneous receptor expression or heterogenous uptake of ligands under-represent the degree of correlation. Although every *Voltair*-containing compartment may be a lysosome, not every lysosome contains *Voltair*. This further lowers the PCC value. We demonstrate the sensitivity of PCC measurement with images shown in figure III.6. The heterogeneity in green to red intensity ratio primarily affects the PCC values as well as visually underestimate the colocalization levels in these images.

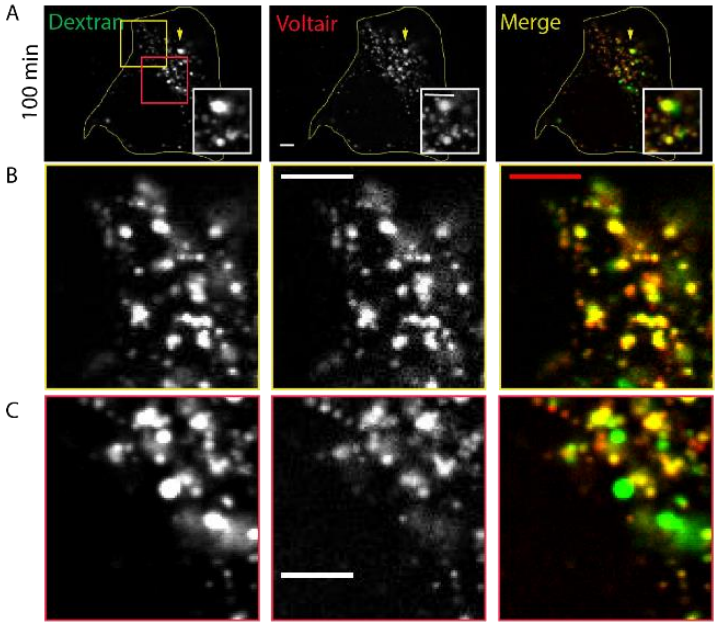

Figure III.6. Localization of Voltair^{IM} to lysosomes. (a) Representative colocalization of singly labeled VoltairIM (red) and lysosome marker TMR-dextran (green) in HEK 293T cells expressing hMSR1. (b, c) Magnified images in yellow and red boxes shown in (a), respectively. Scale = 5 μm

To further verify the temporal specificity of DNA nanodevice trafficking, we performed colocalization experiments with Voltair$_{mono}^{IM}$ positive vesicles w. r. t. organelle markers at various time points (10 to 120 mins) as shown in figure III.7. Time dependent trafficking of Voltair$_{mono}^{IM}$ can be clearly observed in figure III.7, where Voltair colocalizes with the vesicles positive for organelle marker only at specific time points.

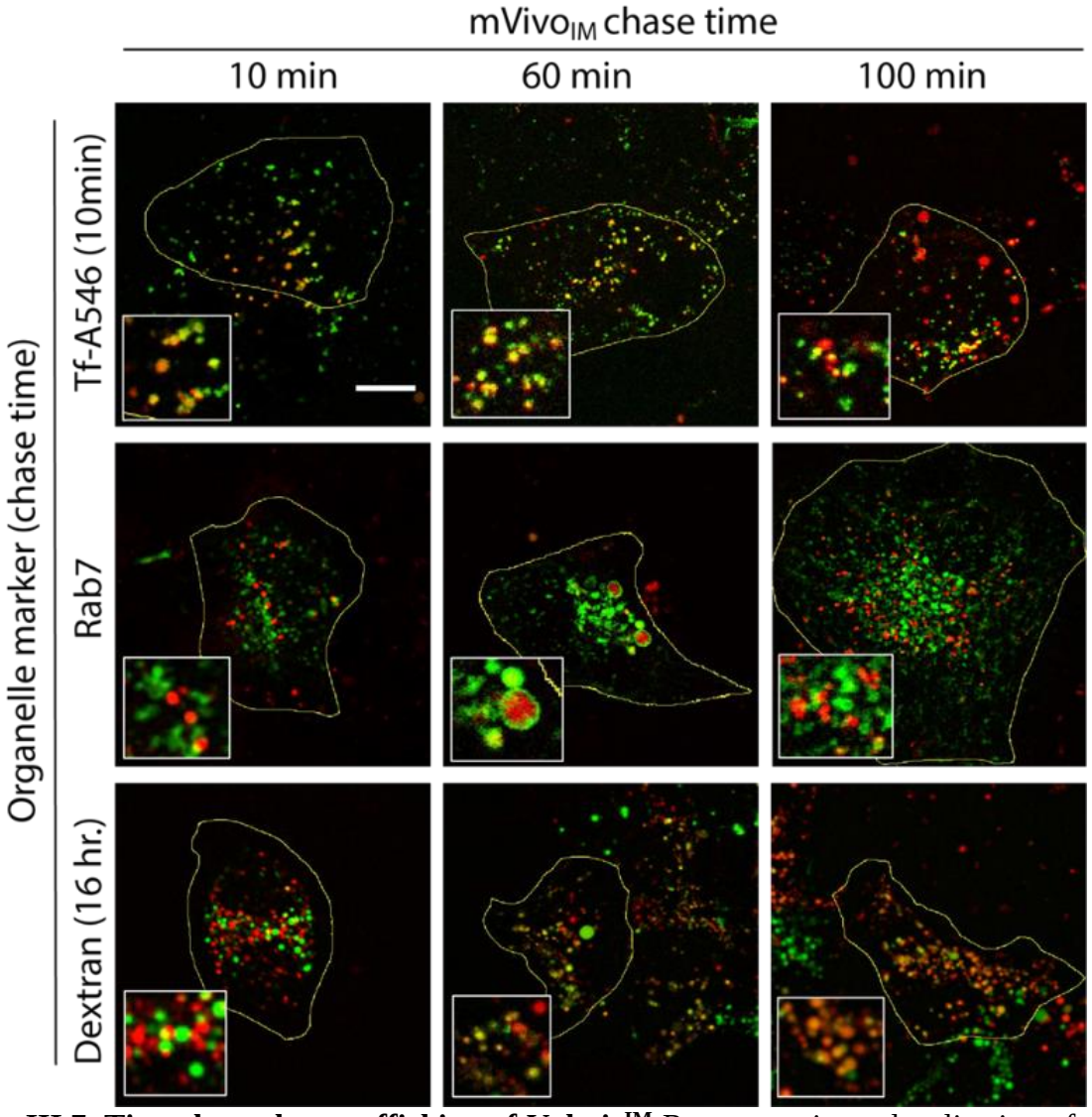

Figure III.7. Time dependent trafficking of Voltair^{IM} Representative colocalization of singly labeled VoltairIM (red) and endosomal markers (green) in HEK 293T cells expressing hMSR1. Early endosomes are labeled with 10 min pulse Alexa 546-labeled transferrin (Tf-A546). Late endosomes are labeled with Rab7-mRFP. Lysosomes are labeled by pulsing TMR-Dextran for 1 hour and chasing for 16 hours. VoltairIM was pulsed for 10 min and chased for indicated time and imaged accordingly. Pearson's correlation coefficients are shown in Fig 2 of the main manuscript. Scale bar = 10 μm.

4. DNA reprograms localization of RVF to intracellular membrane.

In Voltair^{IM}, the RVF moiety functions both as a voltage sensitive dye as well as a lipid anchor that tethers Voltair^{IM} to the lumenal face of the organelle membrane (Fig III.8b). In parallel, the duplex DNA moiety allows scavenger receptor binding and also allows RVF insertion into the intracellular membrane surrounding the receptor, and therefore overrides the affinity of RVF to the plasma membrane (Fig III.8b). Thus, integration onto a duplex DNA scaffold successfully imposes the scavenger receptor-mediated endocytic program on to RVF (Fig III.8b).

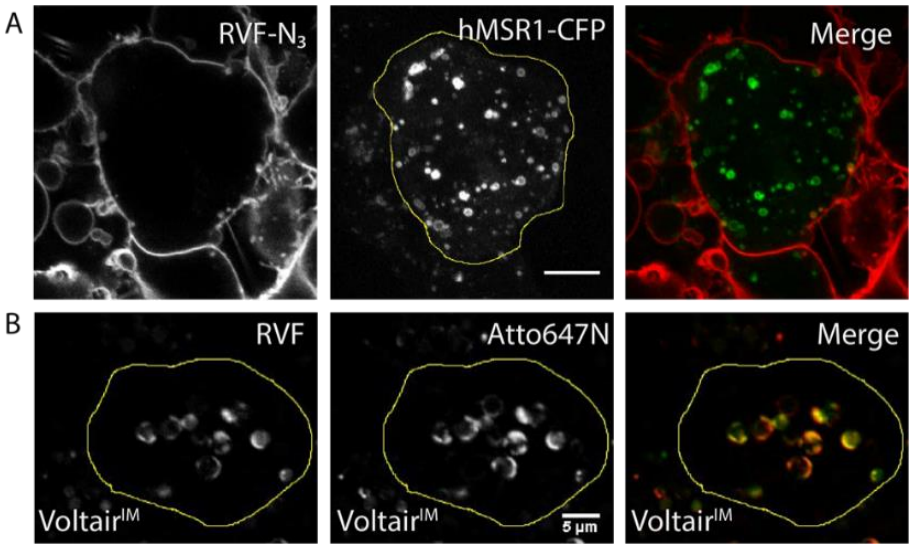

Figure III.8. Conjugation to the DNA duplex reprograms the affinity of RVF to intracellular membranes (a) Incubating RVF with hMSR1-CFP expressing HEK 293T cells results in RVF labeling only the plasma membrane. (b) RVF is conjugated to duplex DNA to give Voltair^{IM}. hMSR1 expressing HEK 293T cells incubated with Voltair^{IM} imaged in the RVF channel and the Atto647N channel (DNA) shows that RVF now labels organellar membranes. Cells were treated with Vacuolin-1 to swell the vesicles in order to confirm tethering to intracellular membranes. Scale: 5 µm.

In the absence of DNA moiety, voltage sensitive dye RVF do not internalize to localize at intracellular compartments (Fig III.8a). Thus, attaching targeting groups such as triphenyl phosphonium or morphlino groups that assist in mitochondria and lysosome labeling respectively, would fail in this scenario. In figure III.9, RVF can be specifically targeted to intracellular membrane when conjugated to endocytic ligand such as DNA. For accurate membrane potential

sensing, RVF is required to be membrane anchored, otherwise would sense zero membrane potential in free lumenal space. Thus, to verify the localization of RVF to intracellular membrane, lysosomes of HEK 293T cells were enlarged by treating the cells with overnight Vacuolin-1[27]. This allows us to observe the membrane localization in an organelle of size larger than diffraction limit.

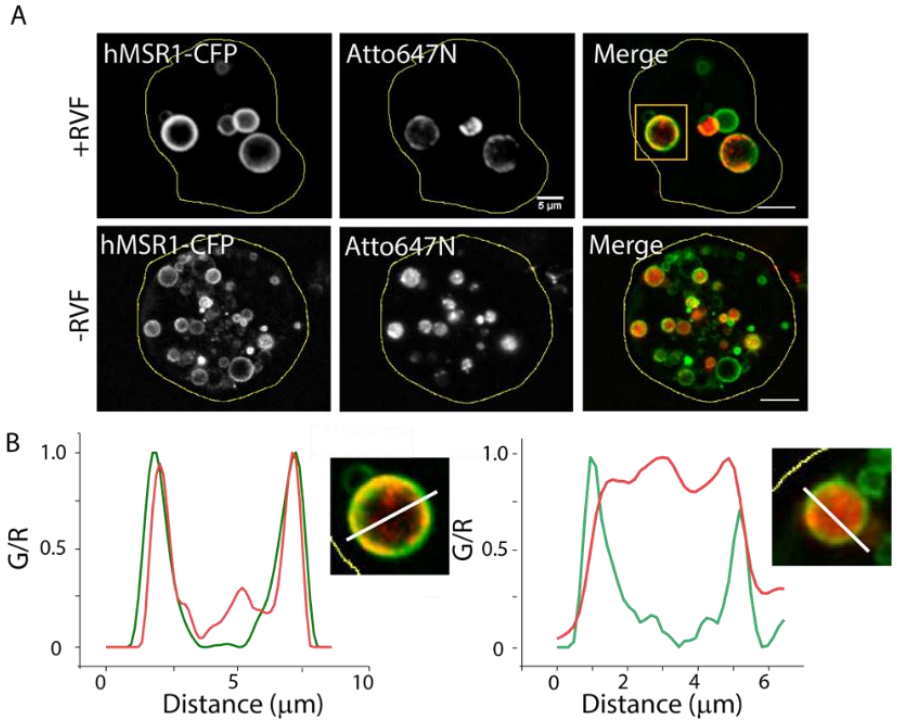

Figure III.9. Insertion of Voltair^{IM} into the membrane of the intracellular organelle: (a) Vacuolin-1 treated HEK 293T cells labeled with VoltairIM show the DNA probe insert into the lumenal leaflet of lysosomal membranes. When labeled with duplex DNA lacking lipophilic RVF, DNA probe fail to localize at the membrane. (b) Line profile of vacuolin-1 treated single lysosome shows the colocalization of DNA probe with hMSR1-CFP present on the endo-lysosomal membrane. Scale = 5μm.

When HEK 293T cells expressing scavenger receptors (hMSRI) are labelled with *Voltair^{PM}* (Fig III.10), cells do indeed begin to endocytose Voltair^{PM}. HEK 293T cells not expressing hMSR1 do not internalize Voltair^{PM} and the latter remains nicely and exclusively on the plasma membrane. This shows that the interaction of Voltair and the scavenger receptor is required for internalization. This internalization can be completely abolished by competitively inhibiting Voltair-hMSR1 interaction by carrying out Voltair labeling in the presence of 30 equivalents of mBSA Thus, to

exclusively label the plasma membrane in cells expressing scavenger receptors, one just has to carry out the Voltair^{PM} labeling and imaging in the presence of a passivator such as 30 eq mBSA (Fig III.10).

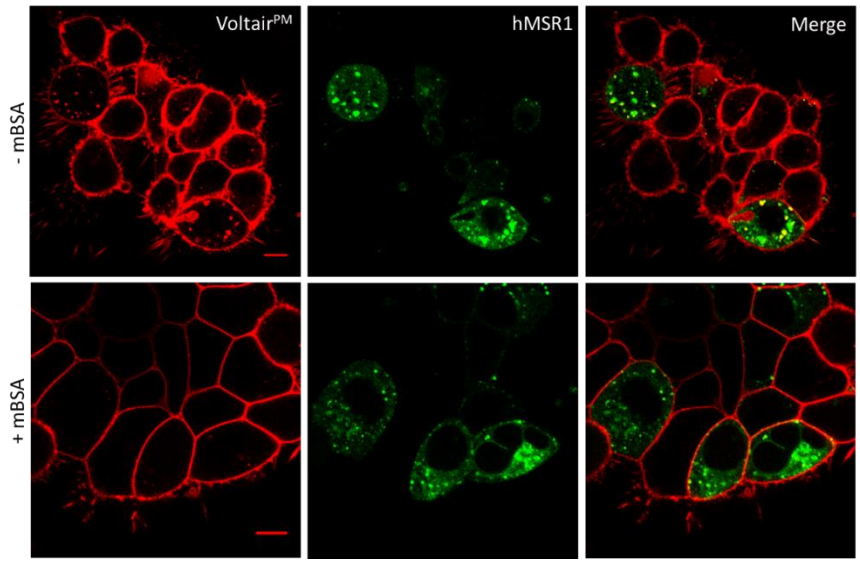

Figure III.10. Maleylated BSA blocks endocytosis of Voltair^{PM} in hMSR1 expressing HEK 293T cells. Representative images of VoltairPM localization in CFP-hMSR1 transfected HEK 293T cells, where 500nM VoltairPM was pulsed and chased for 30 mins in the presence and absence of 30eq. mBSA. Scale: 10 µm.

5. DNA localizes voltage probe to lysosomal membrane *in vivo*.

The nematode, C. elegans, possess six scavenger cells called Coelomocytes, that are known to endocytose foreign substances injected in the body cavity[28]. The negative backbone of DNA has been leveraged to target endolysosomal organelles in scavenger receptor expressing coelomocytes[7]. In order to demonstrate the requirement of DNA in specifically targeting voltage probes to intracellular membrane, 500 nM of VF2.1.Cl and DNA-Alexa647 was injected to the pseudocoelom of 1-day adult PPK3 mutant worms. Figure III.11a shows the specific localization of DNA at the vesicular organelle of Coelomocytes, whereas VF nonspecifically labeled all membranes. Microinjection of mVivo, where the CVF is coupled to DNA duplex, localizes both

the VF and DNA to the intracellular organelles. Figure III.11b shows the representative whole worm image acquired after irradiation with 400 nm light to photoactivate localized VF. The DNA's ability to govern the localization of membrane anchored voltage probe to lysosomal membrane was further demonstrated by acquiring images of mVivo labelled coelomocytes at higher magnification, post irradiation (Fig. III.11c).

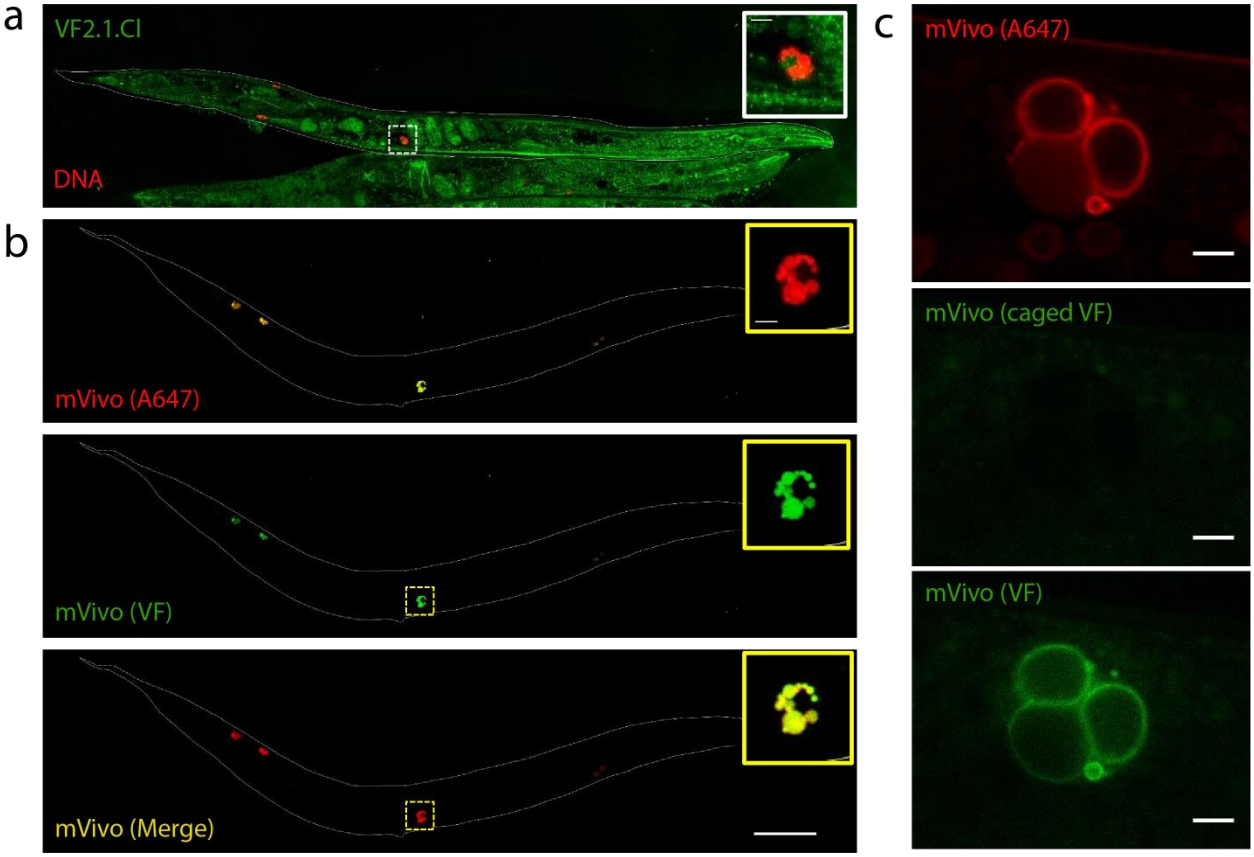

Figure III.11. Targeting mVivo to intracellular membranes in vivo. (a) Representative image of VF2.1.Cl and DNA – Alexa647 labeling when injected via pseudocoelom cavity of c. elegans. (b) Representative images of coelomocyte lysosomes labeled with mVivo. VF is imaged after irradiation with 400 nm light for 20 secs. Scale = 100 µm, Inset scale = 10 µm. (c) Representative image of mVivo localized to intracellular membrane of lysosomes in coelomocytes of PPK3 mutant worms. Irradiation with 400 nm light photoactivates the fluorescence from membrane localized VF. Scale = 10 µm.

6. Targeting Voltair to compartments in recycling and retrograde pathway.

Similar to programming DNA trafficking along the degradative pathway, we modified Voltair and cells to target compartments along recycling and retrograde trafficking pathway. We re-designed Voltair^{RE} to incorporate an RNA aptamer against human transferrin receptor, which was known to targeting recycling endosomes in mammalian cells (Fig. III.12). Voltair^{RE} localized to recycling endosomes at 30 mins in HEK 293T cells, evidenced by 80% colocalization observed with Alexa546-labeled transferrin.

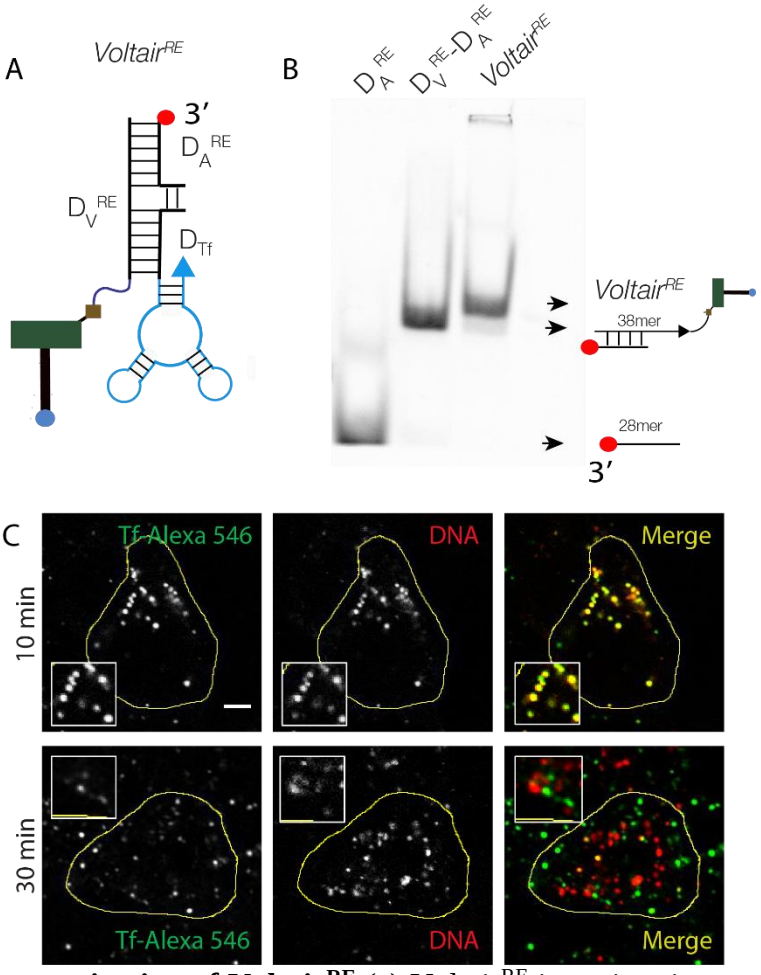

Figure III.12. Characterization of Voltair^{RE} (a) Voltair^{RE} is a trimeric complex comprising of voltage sensing strand DV^{RE}, normalizing strand DA^{RE} and targeting strand D^{Tf}. (b) 15% Native polyacrylamide gel electrophoresis imaged in Atto647N channel, showing the formation of Voltair^{RE}. (c) Colocalization of fluorescently labeled transferrin with early endosomes labeled by DNA-Atto647 duplex in 10 mins and 30 mins of chase time (Scale = 5 μm).

Voltair^{TGN} was targeted to the trans-Golgi network in HEK 293 cells expressing furin fused to a single-chain variable fragment recombinant antibody, scFv. The scFv domain selectively binds any DNA duplex containing a d(AT)$_4$ sequence. Voltair^{TGN} included a d(AT)$_4$ sequence in the duplex so that the scFv-Furin chimera acts as a carrier protein for the former. Voltair^{TGN} is thus trafficked along the retrograde pathway localizing in the trans Golgi network evidenced by 70% colocalization with TGN46-mCherry and absence of colocalization with endocytic organelles (Fig III.13).

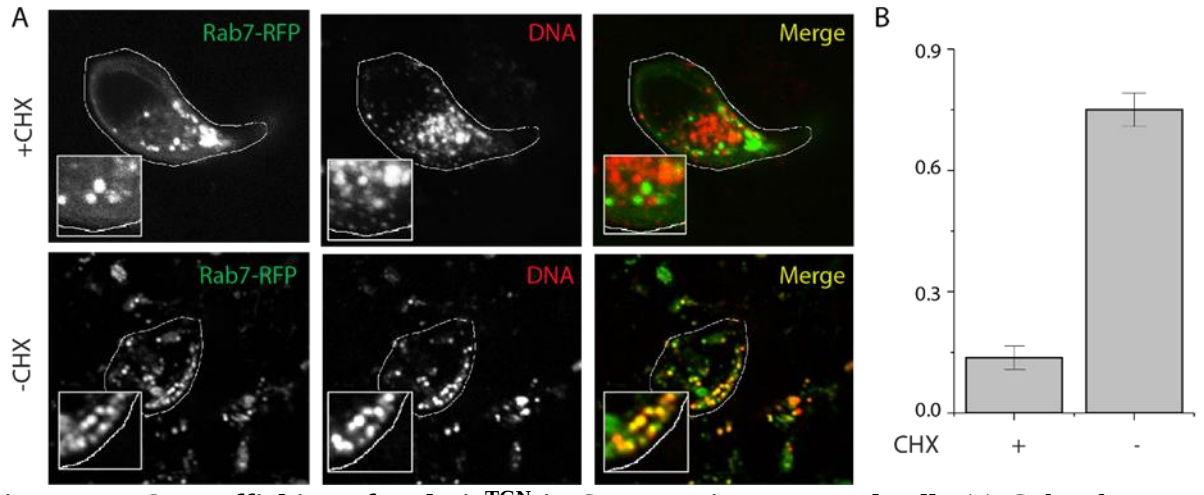

Figure III.13. Trafficking of Voltair^{TGN} in ScFv-Furin expressed cells (a) Colocalization of Voltair^{TGN} with late endosome marker Rab7-RFP in presence and absence of 125 µg/ mL cycloheximide (CHX). (scale = 5 µm). (c) Pearson's correlation coefficient (PCC) for (A). Error bar represents mean ± s.e.m of three independent experiments.

III.D: Conclusion

A key requirement for voltage reporters is robust membrane association. Genetically encoded voltage reporters access the membrane of interest from the cytosolic side, while voltage-sensitive dyes such as VF or RVF selectively orient themselves on the outer leaflet of the plasma membrane[29,30]. Voltair probes are embedded in the outer leaflet of the plasma membrane as well as in the lumenal leaflet of the organellar membrane of interest. Therefore, the direction of

membrane potential as measured by Voltair at the plasma membrane is consistent with conventional electrophysiology. Engineering Voltair to traffic via. endogenous pathways provide access to most transient organelles such as early, late and recycling endosomes, which cannot be specifically labeled using membrane protein targeting strategies.

Currently, Voltair can probe only those organelles that can be accessed based on membrane trafficking pathways originating from the plasma membrane. These include early endosomes, late endosomes, recycling endosomes, lysosomes and the trans Golgi network (TGN). Although these approaches can be directly applied to synaptic vesicles and secretory vesicles, the small size of these organelles may limit probe density, reducing signal to noise ratios and thus may require more sophisticated imaging modalities. In order to apply Voltair to organelles such as the medial or cis Golgi, endoplasmic reticulum, mitochondria, nucleus and peroxisomes, new knowledge of proteins that traffic to these organelles from the plasma membrane is required. Since DNA nanodevices can already be targeted to the TGN - represents the junction between the endocytic and secretory pathways - one can envisage the introduction of secondary targeting motifs to access the ER and thereby, other organelles on the secretory pathway.

III.E: References

1. Baid, K. *et al.* Direct binding and internalization of diverse extracellular nucleic acid species through the collagenous domain of class A scavenger receptors. *Immunol. Cell Biol.* **96,** 922–934 (2018).
2. PrabhuDas, M. R. *et al.* A consensus definitive classification of scavenger receptors and their roles in health and disease. *J. Immunol.* **198,** 3775–3789 (2017).
3. Platt, N. & Gordon, S. Scavenger receptors: diverse activities and promiscuous binding of polyanionic ligands. *Chem. Biol.* **5,** R193–203 (1998).
4. Modi, S. *et al.* A DNA nanomachine that maps spatial and temporal pH changes inside living cells. *Nat. Nanotechnol.* **4,** 325–330 (2009).
5. Saha, S., Prakash, V., Halder, S., Chakraborty, K. & Krishnan, Y. A pH-independent DNA nanodevice for quantifying chloride transport in organelles of living cells. *Nat. Nanotechnol.* **10,** 645–651 (2015).
6. Chakraborty, K., Leung, K. & Krishnan, Y. High lumenal chloride in the lysosome is critical for lysosome function. *Elife* **6,** e28862 (2017).
7. Surana, S., Bhat, J. M., Koushika, S. P. & Krishnan, Y. An autonomous DNA nanomachine maps spatiotemporal pH changes in a multicellular living organism. *Nat Commun* **2,** 340 (2011).
8. Leung, K., Chakraborty, K., Saminathan, A. & Krishnan, Y. A DNA nanomachine chemically resolves lysosomes in live cells. *Nat. Nanotechnol.* **14,** 176–183 (2019).
9. Narayanaswamy, N. *et al.* A pH-correctable, DNA-based fluorescent reporter for organellar calcium. *Nat. Methods* **16,** 95–102 (2019).
10. Chakraborty, K., Veetil, A. T., Jaffrey, S. R. & Krishnan, Y. Nucleic Acid-Based Nanodevices in Biological Imaging. *Annu. Rev. Biochem.* **85,** 349–373 (2016).
11. Thekkan, S. *et al.* A DNA-based fluorescent reporter maps HOCl production in the maturing phagosome. *Nat. Chem. Biol.* **15,** 1165–1172 (2019).
12. Modi, S., Nizak, C., Surana, S., Halder, S. & Krishnan, Y. Two DNA nanomachines map pH changes along intersecting endocytic pathways inside the same cell. *Nat. Nanotechnol.* **8,** 459–467 (2013).
13. Bhatia, D. *et al.* Quantum dot-loaded monofunctionalized DNA icosahedra for single-particle tracking of endocytic pathways. *Nat. Nanotechnol.* **11,** 1112–1119 (2016).
14. You, M. *et al.* DNA probes for monitoring dynamic and transient molecular encounters on live cell membranes. *Nat. Nanotechnol.* **12,** 453–459 (2017).
15. Zhao, B. *et al.* Visualizing Intercellular Tensile Forces by DNA-Based Membrane Molecular Probes. *J. Am. Chem. Soc.* **139,** 18182–18185 (2017).

16. Veetil, A. T. *et al.* DNA-based fluorescent probes of NOS2 activity in live brains. *Proc. Natl. Acad. Sci. USA* **117,** 14694–14702 (2020).

17. Modi, S., Halder, S., Nizak, C. & Krishnan, Y. Recombinant antibody mediated delivery of organelle-specific DNA pH sensors along endocytic pathways. *Nanoscale* **6,** 1144–1152 (2014).

18. Jani, M. S., Zou, J., Veetil, A. T. & Krishnan, Y. A DNA-based fluorescent probe maps NOS3 activity with subcellular spatial resolution. *Nat. Chem. Biol.* **16,** 660–666 (2020).

19. Magadán, J. G., Barbieri, M. A., Mesa, R., Stahl, P. D. & Mayorga, L. S. Rab22a regulates the sorting of transferrin to recycling endosomes. *Mol. Cell. Biol.* **26,** 2595–2614 (2006).

20. Rosenfeld, J. L. *et al.* Lysosome proteins are redistributed during expression of a GTP-hydrolysis-defective rab5a. *J. Cell Sci.* **114,** 4499–4508 (2001).

21. Van Galen, J. *et al.* Sphingomyelin homeostasis is required to form functional enzymatic domains at the trans-Golgi network. *J. Cell Biol.* **206,** 609–618 (2014).

22. Schindelin, J. *et al.* Fiji: an open-source platform for biological-image analysis. *Nat. Methods* **9,** 676–682 (2012).

23. Van Lengerich, B., Rawle, R. J. & Boxer, S. G. Covalent attachment of lipid vesicles to a fluid-supported bilayer allows observation of DNA-mediated vesicle interactions. *Langmuir* **26,** 8666–8672 (2010).

24. Post, S. R. *et al.* Class A scavenger receptors mediate cell adhesion via activation of G(i/o) and formation of focal adhesion complexes. *J. Lipid Res.* **43,** 1829–1836 (2002).

25. Vanlandingham, P. A. & Ceresa, B. P. Rab7 regulates late endocytic trafficking downstream of multivesicular body biogenesis and cargo sequestration. *J. Biol. Chem.* **284,** 12110–12124 (2009).

26. Dunn, K. W., Kamocka, M. M. & McDonald, J. H. A practical guide to evaluating colocalization in biological microscopy. *Am. J. Physiol. Cell Physiol.* **300,** C723–42 (2011).

27. Wang, X. *et al.* TPC proteins are phosphoinositide- activated sodium-selective ion channels in endosomes and lysosomes. *Cell* **151,** 372–383 (2012).

28. Tahseen, Q. Coelomocytes: Biology and Possible Immune Functions in Invertebrates with Special Remarks on Nematodes. *International Journal of Zoology* **2009,** 1–13 (2009).

29. Kulkarni, R. U. *et al.* Voltage-sensitive rhodol with enhanced two-photon brightness. *Proc. Natl. Acad. Sci. USA* **114,** 2813–2818 (2017).

30. Yang, H. H. *et al.* Subcellular imaging of voltage and calcium signals reveals neural processing in vivo. *Cell* **166,** 245–257 (2016).

IV. Calibration of Voltair across cellular membrane

IV.A: Introduction

Although membrane potential can be measured using physical electrodes, fluorescent imaging reporters are often more convenient due to their noninvasive method of interrogating voltage dynamics in high throughput[1,2]. Recent progress in the development of such imaging tools suggests that optical electrophysiology is a viable option and that it could become a routine method of use in the future. Fundamentally, all membrane potential indicators that are localized across the transmembrane region sense the local electric field, proportional to membrane potential. Electrophysiological techniques on the other hand, directly report transmembrane potential difference. Local electric field can arise even in the absence of transmembrane potential[3]. Surface potential difference, that arises due to asymmetry in ionizable surface charge across the membrane and dipole potential, that arises due to dipolar zwitterionic lipids at the interface of lipid-solution, could contribute to total membrane potential[4]. This explains how voltage gated ion channels depend on local lipid or ionic environment.

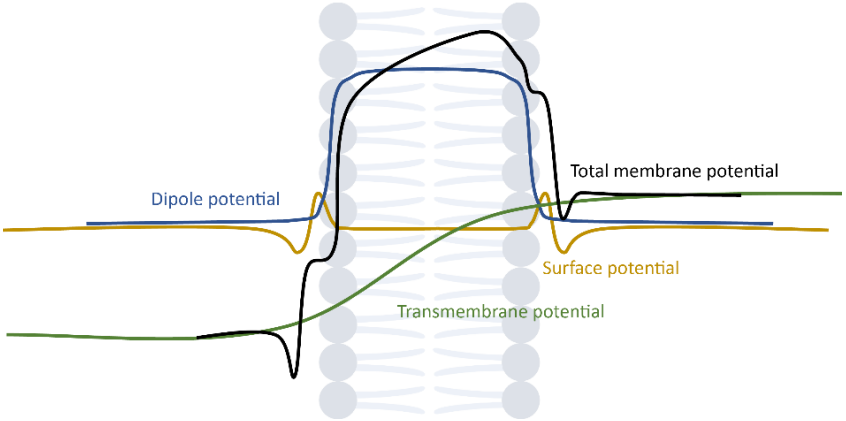

Figure IV.1. Contributions of transmembrane, dipole and surface potential to the total electrical potential across a membrane.

Thus, optical and electrode-based voltage measurements might not be in perfect agreement and that's why it's essential that optical method used to compare voltage across different membranes are based on same sensing domain and oriented in same direction.

IV.B: Materials and methods

1. Oligonucleotides:

Modified DNA oligonucleotides were purchased from IDT (USA). PAGE purified and lyophilized oligonucleotides were dissolved in Milli-Q water of recommended volume to approximately prepare 100 µM stocks. Concentration of oligonucleotides are accurately quantified by collecting UV absorbance spectra and using Beer Lambert's law with absorbance at 260nm for DNA. In the case of fluorescently labeled oligonucleotides, equation 1 is used to quantify the concentration.

$$\text{Concentration} = (Abs_{260} \times \text{dilution factor}) / (\varepsilon_{oligo} - \varepsilon_{dye}) \quad \text{Eq. 1}$$

Where, molecular extinction coefficients of all oligonucleotides ε_{oligo} are provided in the specification sheet by IDT and molecular extinction coefficient of the fluorescent dye at 260nm ε_{odye} is referred from literature references.

Table IV.1. List of modified oligonucleotides used in chapter 4

S. No	Strand	Sequence (5' to 3')	Comment
1	D_V	ATCAACACTGCACACCAGACAGCAA GATCCTATATATA-ispacer18-DBCON	Sensing stand – conjugated to RVF

2	D_V^{POPE}	ATCAACACTGCACACCAGACAGCAA GATCCTATATATA-ispacer18-DBCON	PM labeling - conjugated to POPE
3	D_T	DBCO-TEG-TATATATAGGATCTTGCTGTCT	Targeting strand – conjugated to POPE
4	D_A	Atto647N – GGTGTGCAGTGTTGAT	Normalizing strand – PM
5	D_A'	TATATATAGGATCTTGCTGTCTGGTG TGCAGTGTTGAT-Atto647N	Normalizing strand – Intracellular Membrane (IM)
6	$D_V^{5'}$	DBCO-TEG-ATCAACACTGCACACCAGACAGCAA GATCCTATATATA	$Voltair_{short}$ sensing strand – conjugated to RVF

Table IV.1. List of modified oligonucleotides used in chapter 4 (continued).

2. Sample preparation:

Stock solution of $Voltair^{PM}$ was prepared at a final concentration of 10 µM by mixing D_V, D_T and D_A (Atto647N – 5' modified strand) at an equimolar ratio in 10 mM sodium phosphate buffer, pH 7.4. $Voltair_{mono}^{PM}$, monolabeled variant of Voltair with only Atto647N label is used to study the voltage insensitivity of normalizing dye, Atto647N. Stock solution of $Voltair_{mono}^{PM}$ was prepared at a final concentration of 10 µM by mixing D_V^{POPE} (unlabeled) and D_A' (Atto647N – 3' modified 38 mer strand) at an equimolar ratio in 10 mM sodium phosphate buffer, pH 7.4. $Voltair_{short}^{PM}$ is assembled at a final concentration of 10 µM by hybridizing $D_v^{5'}$, DT and DA (Atto647N – 5' modified strand) at an equimolar ratio in 10 mM sodium phosphate buffer, pH 7.4. For all samples, annealing was performed by heating the reaction mixture to 95°C for 15 min and gradually cooling to RT, at 1°C/ 3 min. Annealed samples were equilibrated at 4°C overnight.

3. Cell culture

Human embryonic kidney cells (HEK 293T) were a kind gift from Dr. Bryan Dickinson (Department of Chemistry, University of Chicago). COS-7 cells were purchased from ATCC. Cells were cultured in Dulbecco's Modified Eagle's Medium (Invitrogen Corporation, USA) containing 10% heat inactivated Fetal Bovine Serum (FBS) (Invitrogen Corporation, USA), 100 U/mL penicillin and 100 µg/mL streptomycin and maintained at 37ºC under 5% CO_2. HEK 293T cells were passaged and plated at a confluency of 20 – 30% for electrophysiology experiments.

4. Reagents and buffers

1-palmitoyl-2-oleoyl-sn-glycero-3-phosphoethanolamine lipid was purchased from Avanti lipids (USA). Vacuolin-1 is purchased from Cayman (USA). All other reagents were purchased from Sigma-Aldrich (USA) unless otherwise specified.

1X Phosphate buffered Saline (PBS): 137 mM NaCl, 2.7 mM KCl, 10 mM Na_2HPO_4. 2 mM KH_2PO_4, pH adjusted to 7.0 using 1N HCl. The buffer then filtered using 0.22 µm filter and autoclaved.

Extracellular solution (Whole cell clamping): 145 mM NaCl, 20 mM glucose, 10 mM HEPES, pH 7.4, 3 mM KCl, 2 mM $CaCl^2$, 1 mM $MgCl_2$ (310 mOsm).

Intracellular solution (whole cell clamping):115 mM potassium gluconate, 10 mM EGTA tetrapotassium salt, 10 mM HEPES, pH 7.2, 5 mM NaCl, 10 mM KCl, 2 mM ATP disodium salt, 300 µM GTP trisodium salt (290 mOsm).

Bath solution (Lysosome clamping): 140 mM K-gluconate, 4 mM NaCl, 1mM EGTA, 20 mM HEPES, pH 7.2, 0.39 mM $CaCl_2$, 2 mM $MgCl_2$, 2 mM ATP disodium salt, 300 µM GTP trisodium salt.

Pipette solution (Lysosome clamping: 145 mM NaCl, 2mM $CaCl_2$, 1mM $MgCl_2$, 10 mM HEPES, 10 mM MES pH 4.6, 10 mM glucose, 5 mM KCl.

5. Whole cell voltage clamping

A schematic of the electrophysiology equipment used for whole cell patch clamp recording is shown in figure IV.2. Recordings of Voltair^{PM} labelled HEK 293T cells were performed with an Axopatch 200A amplifier (Molecular Devices). The signals were digitized using an NI-6251 DAQ (National Instruments). The amplifier and digitizer were controlled using WinWCP software (Strathclyde Electrophysiology Software). Patch pipettes were pulled using a Sutter P-97 Micropipette puller. Borosilicate glass capillaries (Sutter) of dimension 1.5 mm x 0.86 mm (OD/ID) were pulled using the program: Heat – Ramp, Pull – 0, Vel – 21, Time – 1(Delay), Loops – 5. Patch pipettes with resistances between 5-10 MOhm were used in voltage clamping experiments. The patch pipette was positioned using an MP325 motorized manipulator (Sutter). Image Acquisition software Metamorph premier Ver. 7.8.12.0 was linked to an NI-6501 DAQ to enable voltage triggered image acquisition. When applying a voltage pulse across the cell membrane a digital output pulse was generated by WinWCP to trigger imaging. For all measurements the extracellular solution composition was 145 mM NaCl, 20 mM glucose, 10 mM HEPES, pH 7.4, 3 mM KCl, 2 mM $CaCl_2$, 1 mM $MgCl_2$ (310 mOsm) and the intracellular solution composition was 115 mM potassium gluconate, 10 mM EGTA tetrapotassium salt, 10 mM HEPES, pH 7.2, 5 mM NaCl, 10 mM KCl, 2 mM ATP disodium salt, 300 µM GTP trisodium salt (290 mOsm).

For plasma membrane voltage clamping experiments, 1 µM RVF or 500 nM Voltair^{PM} was incubated with HEK 293T cells for 30 mins in Hank's Balanced Salt Solution (Thermofisher) at room temperature. Labelled cells were washed three times with 1X PBS and incubated in extracellular solution for whole cell voltage clamping. Whole cell voltage clamping was performed according to an established protocol[5]. Electrophysiological measurements were made from a single HEK 293T cell, without physical interaction with nearby cells to avoid interference from gap junctions. For background subtraction, bleaching correction and lamp fluctuation compensation, imaging field was chosen with at least one more HEK 293T cell that is not clamped. Once clamped, membrane potential is changed from -100 mV to +100 mV in 10mV increments at 1000 ms intervals. Around 200 ms after the voltage is changed three images are taken in quick succession.

Voltage clamp experiments were also performed with extracellular solutions of different pH, to study the effect of pH on voltage sensitivity of RVF. For cholesterol modulation experiments, HeLa cells were incubated with either 5 mM Methyl-β-cyclodextrin (MβCD) in HBSS alone or 4.5mM MβCD complexed with 0.5mM cholesterol for 1 h. The former treatment depletes cholesterol levels in the plasma membrane while the latter treatment increases cholesterol levels in the plasma membrane[6]. HeLa cells treated thus, were then labeled with Voltair^{PM} in HBSS for 20 mins and voltage clamped from -100 to +100 mV and simultaneously imaged in the red and green channels.

6. Ionophore based voltage clamping

Ionophores selectively permeabilize specific ions across the membrane and have been used to manipulate the membrane potential of purified lysosomes[7]. Three well established ionophore sets have been used previously, (i) Valinomycin, a K^+ ionophore which gives the lysosome a membrane potential of +40 mV when incubated for 10 mins at RT[8], (ii) An equimolar concentration of

valinomycin and monensin, in presence of 150 mM K^+ which neutralizes lysosomal membrane potential[9]. (iii) FCCP, a H^+ ionophore which in absence of ATP shifts the lysosomal membrane potential to -90 mV[7]. Lysosomes of HEK 293T cells were labelled with 500 nM Voltair^{IM} as previously described above. Cells were treated with 10 µM digitonin for 2 mins in presence of an intracellular solution with one set of ionophores and washed three times with the same buffer in absence of digitonin. This replaces the cytosol with the intracellular solution containing ionophores which clamp lysosome voltage to known values. Pseudo color images shown in figure IV.11, were generated as described in image analysis section. Ratiometric G and R images were acquired to record G/R values of ~50 lysosomes for each experiment and plotted as a function of membrane potential (Fig. IV.11).

7. Lysosomal voltage clamping

COS-7 cells were treated with 1 µM vacuolin-1 overnight to increase the size of lysosomes to 1-3 µm[10]. Enlarged lysosomes of COS-7 cells were labeled with 500 nM Voltair^{IM}, by 30 mins pulse in HBSS followed by 2 hr. chase in complete media containing 1 µM vacuolin-1. Patch pipettes used for whole cell voltage clamping, was briefly pressed against the edge of the cell and quickly pulled away in the direction perpendicular to axis of pipette to rupture the cell membrane. Enlarged endolysosome containing Voltair^{IM} was pushed out of the ruptured cell using the same patch pipette. Borosilicate glass capillaries (Sutter) of dimension 1.5 mm x 0.86 mm (OD/ID) were pulled using the program: Heat – 520, Pull – 0, Vel – 20, Time – 200, Loops – 4. Fire polished patch pipettes with resistances between 15-20 MOhm were used in voltage clamping experiments. After giga-ohm seal formation, break in was performed by a zap protocol (5V: 0.5-5s) till appearance of capacitance transients. In order to minimize fluorescence interference from other lysosomes, patched lysosome is moved away from the cell prior to imaging. For all measurements

the cytoplasmic solution composition was 140 mM K-gluconate, 4 mM NaCl, 1mM EGTA, 20 mM HEPES, pH 7.2, 0.39 mM $CaCl_2$, 2 mM $MgCl_2$, 2 mM ATP disodium salt, 300 µM GTP trisodium salt and the composition of pipette solution was 145 mM NaCl, 2mM $CaCl_2$, 1mM $MgCl_2$, 10 mM HEPES, 10 mM MES pH 4.6, 10 mM glucose, 5 mM KCl. The voltage clamping and imaging protocol was followed as discussed in electrophysiology section above.

8. Fluorescence microscopy

Wide field microscopy was carried out on an IX83 inverted microscope (Olympus Corporation of the Americas, Center Valley, PA, USA) using either a 100X or 60X, 1.4 NA, DIC oil immersion objective (PLAPON, Olympus) and Evolve Delta 512 EMCCD camera (Photometrics, USA). Filter wheel, shutter and CCD camera were controlled using Metamorph premier Ver 7.8.12.0 (Molecular Devices, LLC, USA). Images on the same day were acquired under the same acquisition settings (exposure 100 ms and EM gain at 100 for Atto647N, exposure 100 ms and EM gain 300 for RVF). All the images were background subtracted by taking mean intensity over an adjacent cell free area. The mean intensity in each endosome/lysosome was measured in the sensing channel (G) and the normalizing channel (R). RVF channel images were obtained using 500/20 band pass excitation filter, 535/30 band pas emission filter and 89016 dichroic. For Atto647N, images were obtained using the 640/30 band pass excitation filter, 705/72 band pass emission filter and 89016 dichroic. Pseudo-color images were generated by calculating the G/R ratio per pixel in Fiji using the Image calculator module. FITC dextran images were acquired using a 480/20 band pass excitation filter, 520/40 band pass emission filter and 89016 dichroic.

IV.C: Results and Discussion

1. Optical electrophysiology set up

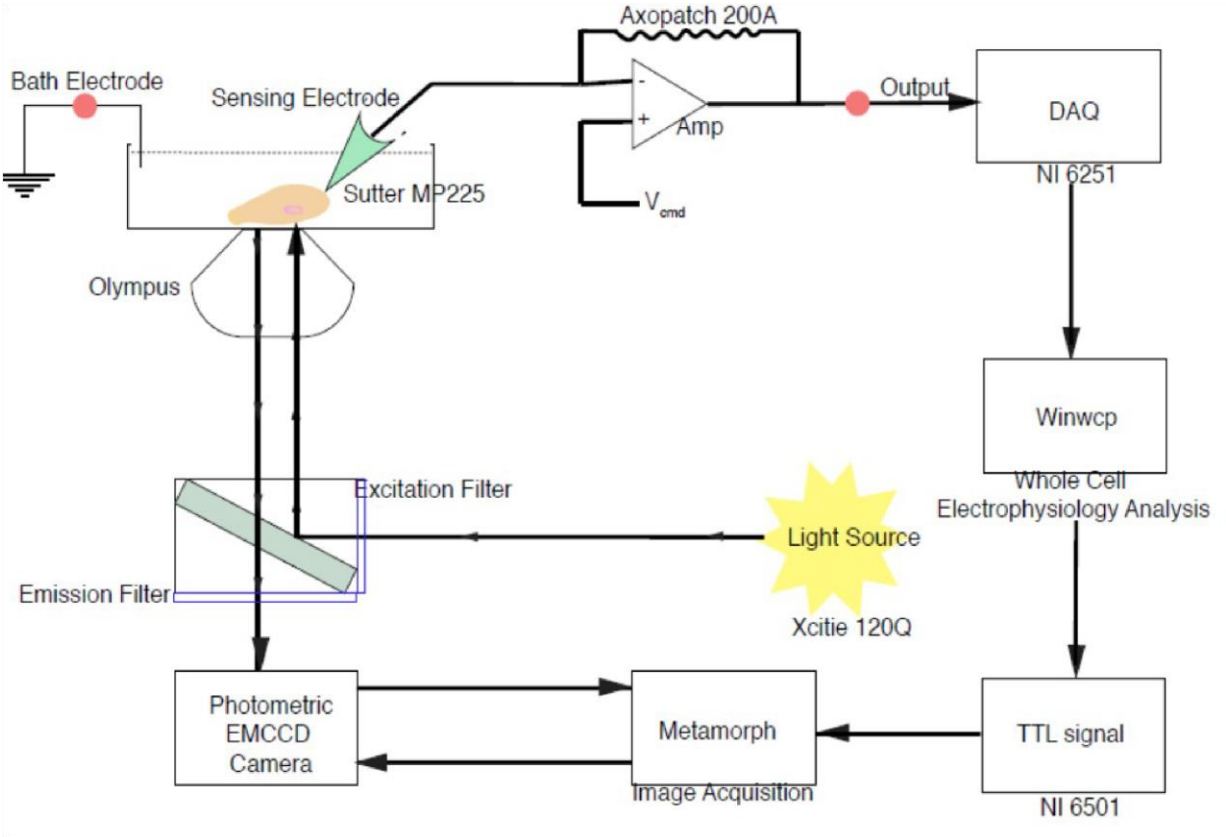

Figure IV.2. Optical electrophysiology set up for single cell voltage clamping. Schematic shows the equipment workflow of electrophysiology measurements. Recordings were performed with an Axopatch 200A amplifier. The signals were digitized with NI-6251 DAQ and recorded using WinWCP software (Strathclyde Electrophysiology Software). The patch pipette was positioned using MP325 motorized manipulator. Image Acquisition software Metamorph premier Ver. 7.8.12.0 was linked to an NI-6501 to enable voltage triggered image acquisition. When applying a voltage pulse across the cell membrane a digital output pulse was generated by WinWCP to trigger imaging. Images are acquired using IX83 widefield microscope, 60X, 1.4 NA.

Schematic shows the equipment workflow of electrophysiology measurements (Fig. IV.2). Recordings were performed with an Axopatch 200A amplifier. The signals were digitized with NI-6251 DAQ and recorded using WinWCP software (Strathclyde Electrophysiology Software). The patch pipette was positioned using MP325 motorized manipulator. Image Acquisition

software Metamorph premier Ver. 7.8.12.0 was linked to an NI-6501 to enable voltage triggered image acquisition. When applying a voltage pulse across the cell membrane a digital output pulse was generated by WinWCP to trigger imaging. Images are acquired using IX83 widefield microscope, 60X, 1.4 NA, Oil objective.

2. Membrane potential sensitivity of voltage sensitive probes.

Membrane potential sensitivity is characterized by the whole cell voltage clamping performed in combination with fluorescence microscopy. Plasma membrane of HEK 293T cells were labeled with voltage sensitive probes, VoltageFluor (VF), caged VoltageFluor (CVF) or RVF and membrane potential clamped from -100 mV to +100mV (Fig. IV. 3a, b).

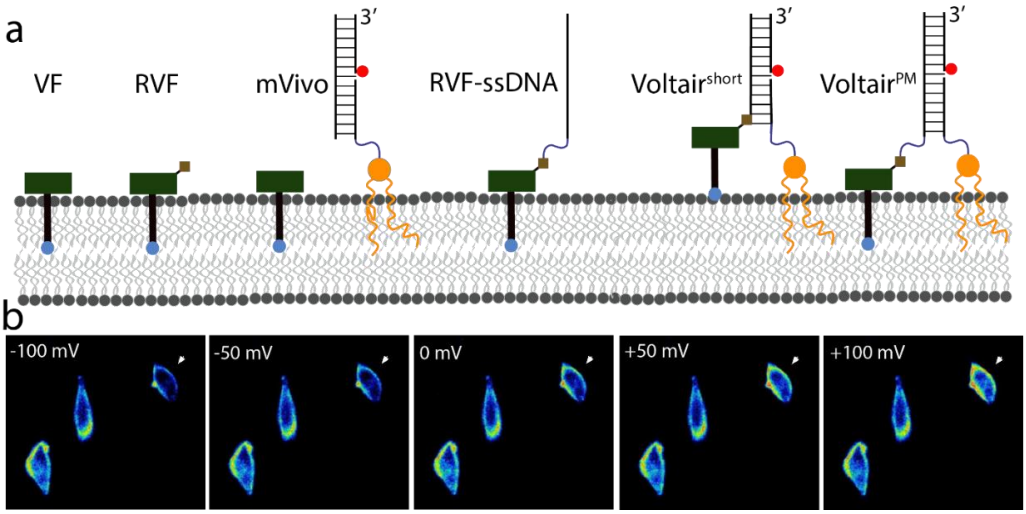

Figure IV.3. Variants of membrane potential sensors. (a) Different variants of probes were assembled to investigate the effect of DNA on voltage sensitivity of PeT probes. (b) Pseudo colored images of RVF labeled HeLa cells, voltage clamped from -100 to +100 mV (white arrow). Pseudo color scale: 0 to 255.

Voltage sensitivity of these PeT based dyes highly depend on the orientation angle of the fluorophore-bridge-quencher axis w.r.t. plasma membrane, as the change in PeT signal depends on the cosine of orientation angle. According to recent report, VF dyes insert across the membrane at an angle of 30°, whereas further modification of additional sulfonate group decreases the orientation angle to 19° and thus shows improved sensitivity[11]. Conjugation of DNA to the voltage sensing dye could affect the orientation angle, in addition to increasing the dissociation constant or perturb the PeT mechanism. Thus, in order to study the effect of DNA on voltage sensitivity of these dyes, whole cell voltage clamping was performed on different variants of DNA based voltage probes (Fig IV.3). Plasma membrane of HEK293T cells were labeled with (i) VF2.1.Cl, (ii) RVF, (iii) mVivo, (iv) single strand DNA coupled to RVF (RVF-ssDNA), (ii) Voltair scaffold coupled to RVF using a short TEG linker, and as a control (iv) Voltair^{PM}, DNA duplex coupled to membrane anchor POPE and normalizing dye Atto647N.

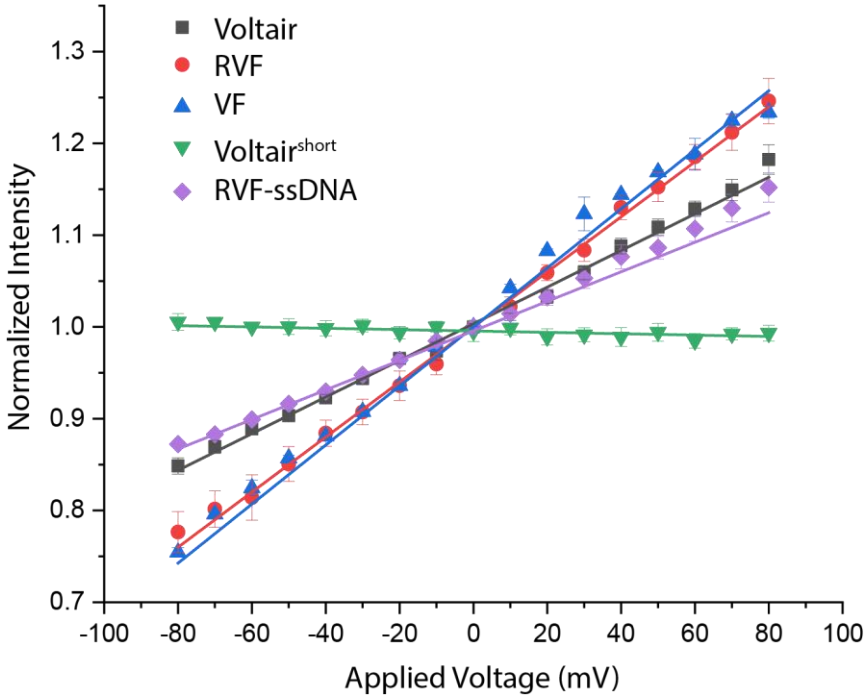

Figure IV.4. Voltage sensing characteristics of DNA coupled voltage sensors: Normalized intensity of voltage sensing variants described in Fig 4.3. Probe labelled HEK 293T cells were voltage clamped from -80 mV to +80 mV. Error bars indicate mean ± s. e. m. of n = 4 cells.

In comparison to the voltage sensitivity of RVF or VF (25% per 100 mV), RVF coupled to ssDNA shows 40% reduction in their membrane potential sensitivity when clamped from -80 to +80 mV (Fig IV.4). This was expected, as the 38mer long flexible ssDNA could hinder the orientation of RVF across the membrane. Coupling RVF to a more rigid duplex strand and further strengthening the membrane association with POPE labeling, improves the voltage sensitivity

(20% per 100 mV). In order to show the significance of the linker length connecting the DNA to RVF dye, $Voltair_{short}^{PM}$ was constructed, which uses a triethylene glycol linker to connect RVF to DNA instead hexaethylene glycol linker used in $Voltair^{PM}$. Interestingly, $Voltair_{short}^{PM}$ shows efficient labeling due to POPE, but failed to show any voltage sensitivity (Fig IV.3, IV.4). Thus, anchoring the DNA duplex to the membrane with a help of lipid anchor or receptor protein improves the voltage sensitivity, in addition to longer linker between voltage sensitive dye and DNA scaffold (Fig IV.3).

3. Voltage calibration of *Voltair* and *mVivo* across plasma membrane of HEK 293T cells.

$Voltair^{PM}$ report on membrane potential by sequentially exciting RVF and Atto647N and monitoring their emission intensities at λem = 540 nm (G) and λem = 665 nm (R). The plasma membrane of HEK293T cells were labeled by $Voltair^{PM}$ and were voltage clamped from -100 mV to +100 mV, at increments of 10 mV, and fluorescence images of RVF and Atto647N were sequentially acquired at each clamped voltage, from which the pseudo-colored G/R images were generated as described. Notably, the whole-cell intensity images in the G channel of voltage-clamped cells changed as a function of the applied voltage, while the R channel was constant (Fig IV.5). Unclamped cells showed negligible variation in either channel. The uniform 1:1 ratio of RVF: Atto647N in $Voltair^{PM}$ yield highly reproducible G/R values as a function of applied voltage as seen in the calibration plot of $Voltair^{PM}$ (Fig IV.5). The fold change in G/R signal from 0 mV

to +100 mV (ΔG/R) was found to be 1.2 for Voltair^{PM} which matched well with that of unconjugated RVF.

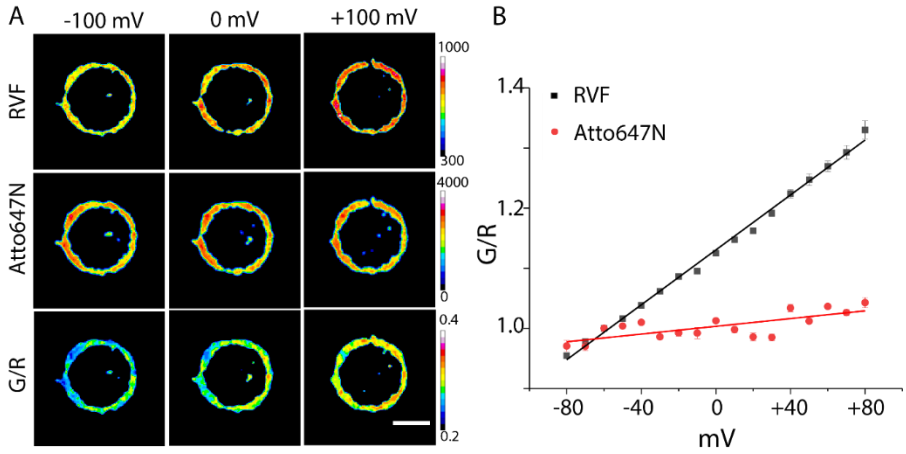

Figure IV.5. Voltage sensitivities of RVF and Atto647N in Voltair^{PM}: (a) Representative images of Voltair^{PM} labelled HEK 293T cells voltage clamped from -100mV to +100mV, pseudocolored according to the pixel-wise fluorescence intensities of RVF (G), Atto647N (R) and ratio G/R. Scale bar = 10 µm. (b) Normalized RVF (black) and Atto647N (red) intensities of Voltair^{PM} labelled HEK 293T cells voltage clamped from -80 mV to +80 mV. Error bars indicate mean ± s. e. m. of N = 3 experiments, n = 6 cells.

Unlike Voltair^{PM}, mVivo does not report absolute membrane potential. Due to inefficient photoactivation of nitrobenzyl cages, mVivo reports relative changes in membrane potential across specific membrane of choice. Similar to Voltair^{PM}, HEK 293T cells labeled with mVivo was irradiated with 400 nm and voltage clamped from -100 to + 100 mV. Figure 4.6a shows the increase in fluorescence of only voltage clamped cell when membrane was depolarized from 100 mV to +100 mV. Figure 4.6b shows the voltage sensitive fluorescence of uncaged VF in comparison to voltage insensitive normalizing dye, Atto647N.

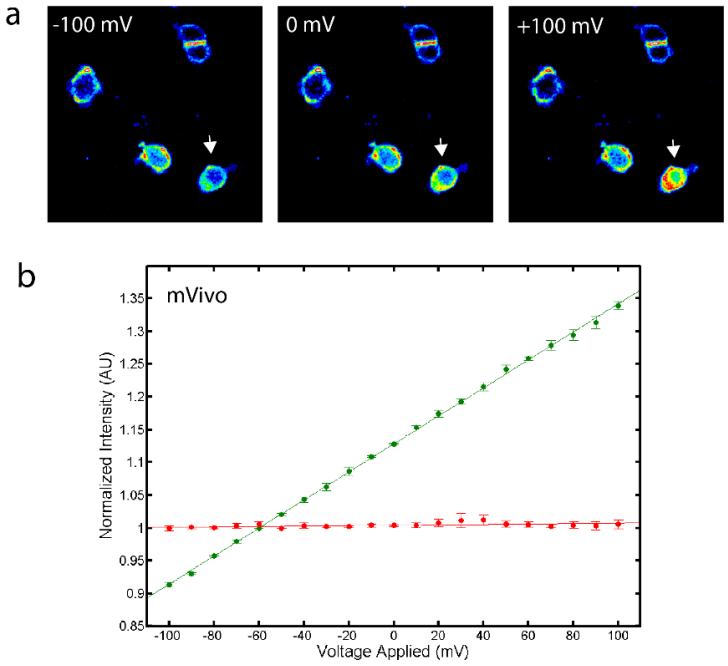

Figure IV.6. Voltage sensitivities of uncaged VF and Atto647N in mVivo: (a) Representative images of mVivo labelled HEK 293T cells voltage clamped from -100mV to +100mV, pseudocolored according to the pixel-wise fluorescence intensities of uncaged VF, after irradiation with 400 nm for 30 secs. Pseudo color scale: 0 to 255. (b) Normalized RVF (green) and Atto647N (red) intensities of mVivo labelled HEK 293T cells voltage clamped from -80 mV to +80 mV. Error bars indicate mean ± s. e. m. of N = 3 experiments, n = 6 cells

4. Membrane composition and pH sensitivity of RVF

Photoinduced electron transfer (PeT) based voltage dyes are significantly different from the charge shift voltage sensitive dyes that are based on Stark shift or electrochromism. Unlike charge shift dyes, the fluorescence spectra of PeT-based dyes are expected to be insensitive to the effect of lipid composition since sulfo-fluorescein (the voltage-sensitive fluorophore in Voltair) is perched outside the outer leaflet of the plasma membrane due to anionic nature of the sulfonate group[11]. However, to check whether this was indeed the case, we performed experiments on Voltair^{PM}-labeled cells and checked the response characteristics of the probe as a function of lipid composition of the plasma membrane (Fig IV.7). Our studies showed that Voltair performance characteristics is independent of lipid composition of the membrane, and depends strictly on the

membrane potential across the membrane. Cholesterol is a major component of plasma membrane and intracellular membranes, with 35% at plasma membrane, 20% at lysosome and 10% at Golgi. We therefore modulated the cholesterol levels on the plasma membrane of Hela cells and performed whole cell voltage clamping from -100 mV to +100 mV. Fluorescence intensity ratios (G/R) as a function of membrane potential in cells reveal that Voltair performance characteristics were insensitive to cholesterol levels in the membrane, i.e., lipid composition of the membrane (Fig IV.7).

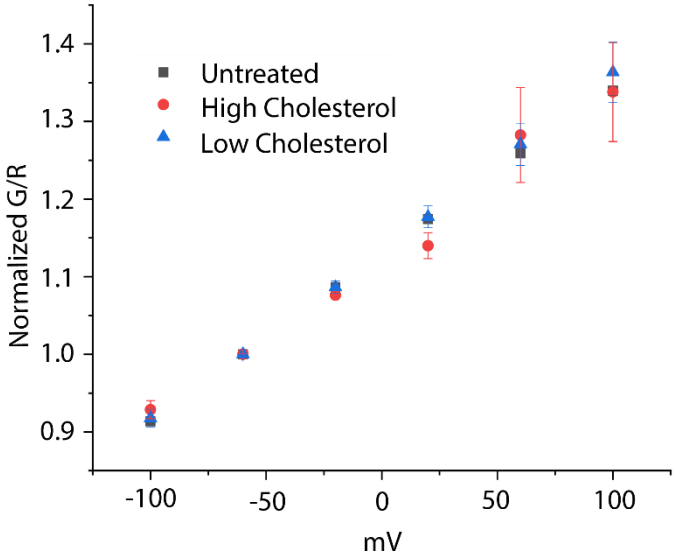

Figure IV.7. RVF fluorescence characteristics are insensitive to changes in cholesterol levels. Voltage sensing characteristics, fluorescence ratio G/R w.r.t. clamped voltage -100 mV to +100 mV, of VoltairPM on the plasma membrane of Hela cells with altered levels of cholesterol. G/R values are normalized to -60 mV. Error bars indicate mean ± s. e. m. of n = 3 experiments.

Endocytic compartments show increasing levels of lumenal acidity along the maturation pathway, ranging from pH 6.5 at EE to pH 4.5 at Ly in mammalian cells[12]. Most fluorescein-based probes are sensitive to acidic pH. Protonation of phenolic -OH moiety (pKa = 6.4) of fluorescein-based chromophore decreases the fluorescence and hence used as well-established pH sensors. This aspect of pH interference makes it difficult to uncouple the probes ability to sense signals.

Thus, we chose a voltage sensitive dye (RVF) that could reliably sense at acidic pH. RVF comprise of dichlorosulforhodol dye, which is expected to have very low pKa due to two reasons. (i) dichlorofluorescein derivatives have lower pKa (~4.5) than fluorescein due to the negative inductive effect of chloro substitution at the ortho position of the phenolic OH. 18. (ii) rhodol fluorophores have lower pKa than fluorescein (pKa of Rhodal = 5.5). To confirm the pH independence of RVF in sensing voltage, HEK 293T cells were labeled with 1 µM RVF and voltage clamped from -100 mV to +100 mV with extracellular solutions of pH 4.5, 5 and 7 (Fig IV.8).

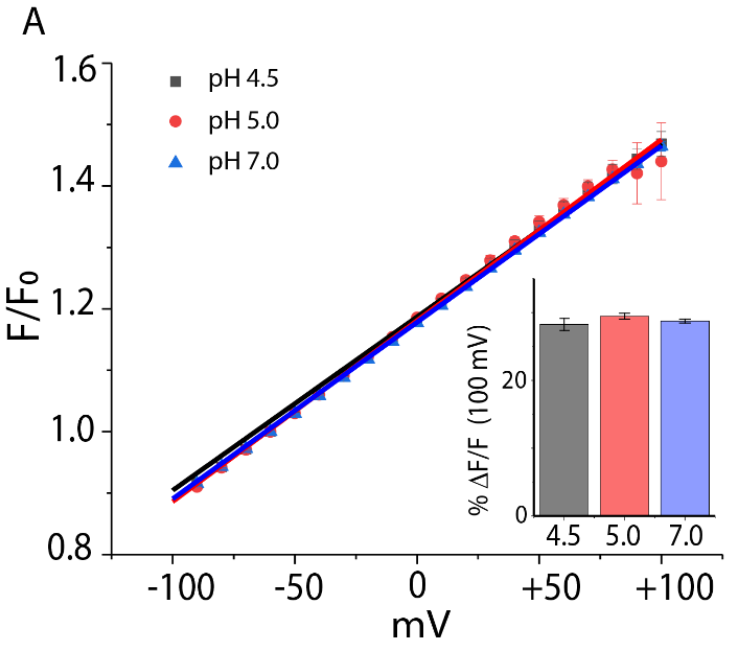

Figure IV.8. RVF fluorescence characteristics are insensitive to changes in physiological pH: (a) Voltage sensing characteristics of RVF in the plasma membrane of HEK 293T cells in extracellular UB4 buffer, pH 7, 5 and 4.5. A linear fit to each dataset is plotted. Inset shows the percentage fold change per 100 mV at indicated pH. Error bars indicate s. e. m. of n = 3 independent experiments.

5. Intracellular calibration using selective permeabilization of plasma membrane

Next, we mapped the response characteristics of Voltair in intracellular membranes. To achieve this, we developed a method to substitute the cytosol with buffer of a desired composition without affecting the integrity of fluorescently labeled lysosomes (Fig IV.9). This uses digitonin treatment of labeled cells in the presence of a buffer of desired ion concentrations. Digitonin treatment creates 30 nm wide pores on the plasma membrane through which small molecules such as ATP and ion content of the cytosol and the external buffer rapidly equilibrate (Fig IV.9)[13,14]. In order to verify the digitonin facilitated selective permeabilization of plasma membrane of HEK cells, plasma membrane was labeled with CellMask^{TM} red, and lysosomes were labeled with TMR-Dextran. Digitonin treatment to labeled cells, shows CellMaskTM red's labeling of intracellular membranes, whereas TMR-Dextran remains confined to lysosomes, showing lysosomal membrane are not permeabilized.

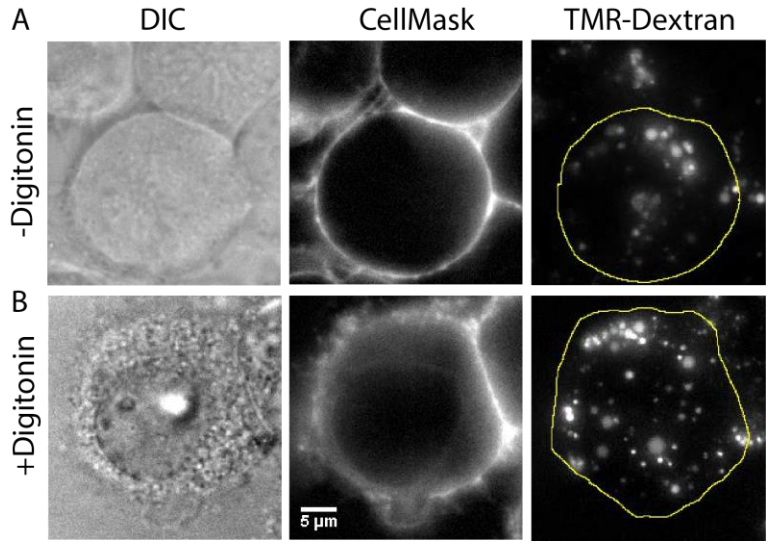

Figure IV.9. Digitonin selectively permeabilizes the plasma membrane: (A) HEK cells incubated with CellMaskTM red shows only plasma membrane labeling. Lysosomes labeled with TMR-Dextran are shown for reference. (B) HEK cells treated with digitonin and incubated with CellMaskTM red now shows labeling of intracellular membranes by CellMaskTM red. Note that TMR-Dextran labeled lysosomes are still retained in punctate structures, showing lysosomes are not permeabilized. Scale = 5 µm.

Further, to examine the functionality of lysosomal membrane integrity, lysosomal pH is monitored using FITC dextran in presence and absence of ATP in the dialyzing solution. The pH of native lysosomes labeled with FITC-dextran imaged using dual excitation method, gives low 480/430 ratio corresponding to acidic lysosomal pH[15]. Digitonin treatment and incubation in intracellular buffer without ATP increases lysosomal pH as V-ATPases cannot function under ATP-depleted conditions. External addition of 2 mM ATP during digitonin treatment decreases lysosomal pH, showing lysosomal pumps and transporters to be functional and can actively maintain lysosomal membrane potential in these digitonin treated cells.

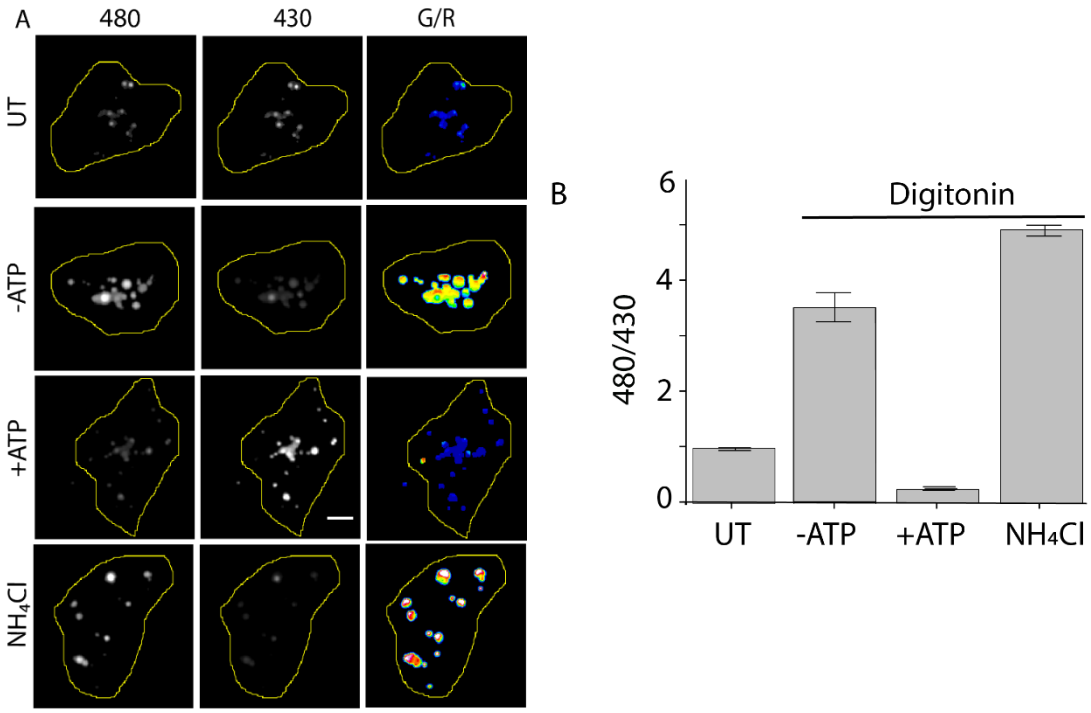

Figure IV.10. Ion-pumps on lysosomes are fully functional post digitonin treatment: (A) pH of native lysosomes labeled with FITC-dextran imaged using dual excitation method, gives low 480/430 ratio corresponding to native lysosomal pH. (B) Digitonin treatment and incubation in intracellular buffer without ATP increases lysosomal pH as V-ATPases cannot function under ATP-depleted conditions (C) Digitonin treatment in intracellular buffer containing 2 mM ATP decreases lysosomal pH as V-ATPases can now function. (D) Adding NH4Cl to the buffer in (C) elevates lysosomal pH as expected for functionally intact lysosomes. Scale =10 µm, error bars indicate s. e. m. of n = 3 experiments.

We constructed an in-cell calibration plot of membrane potential which reveals that reporter characteristics of Voltair^{IM} in intracellular membranes quantitatively recapitulates that of Voltair^{PM} at the plasma membrane (Fig IV.11).

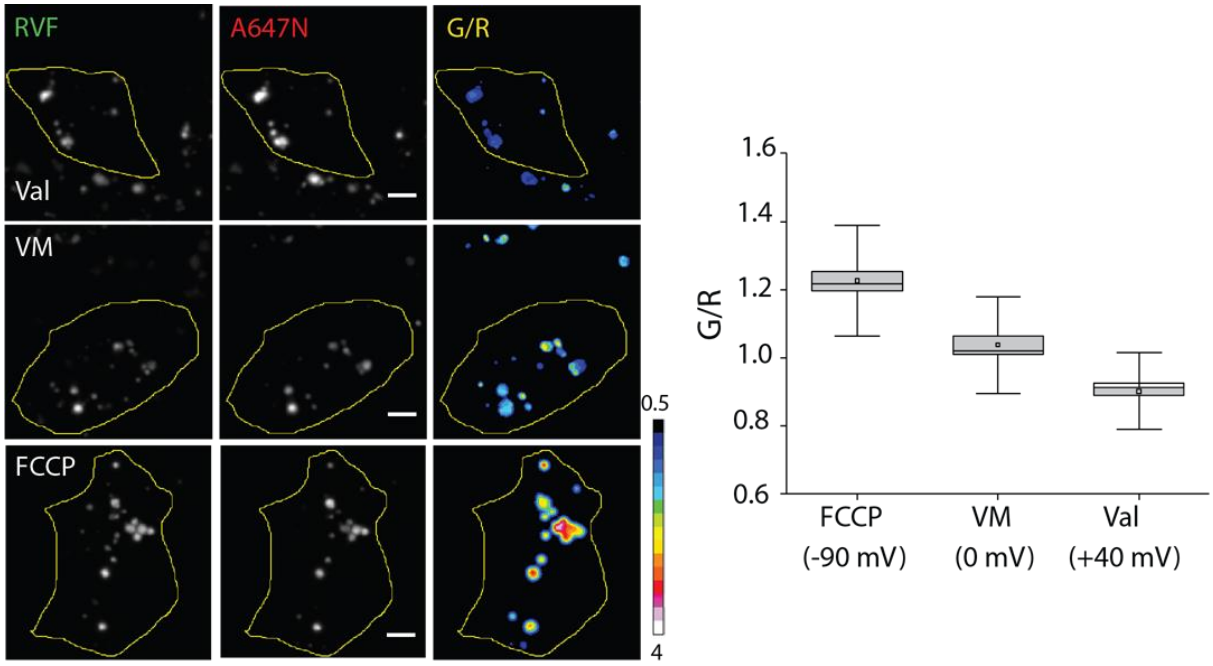

Figure IV.11. Intracellular voltage clamping of Voltair^{IM}. (A) Fluorescence images of VoltairIM labeled lysosomes, voltage clamped using ionophores, in the G and R channels as well as the corresponding pseudocolor G/R images. VoltairIM labeled cells were treated with digitonin, incubated with intracellular buffer containing the indicated ionophores to clamp lysosomal membrane potential. (Val – Valinomycin, VM – Valinomycin and Monensin) (B) Normalized G/R intensity ratios of each voltage clamped condition in (A). G/R values were normalized to valinomycin and monensin treated cells. Scale = 10 µm, error bars indicate SD of n = 50 lysosomes.

To achieve this, we labeled lysosomes with Voltair^{IM} and, using digitonin treatment, substituted the cytosol with buffers containing specific ionophores that have previously been shown to create well-defined values of membrane potential in isolated lysosomes. Valinomycin (50 µM) results in a membrane potential of +40 mV considering the lumen to be positive[8], a cocktail of valinomycin and monensin (50 µM) with 150 mM K+ neutralizes lysosomal membrane potential[9], while FCCP (50 µM) in the absence of ATP creates a membrane potential of -90 mV across the lysosomal membrane[7]. G/R values for ~50 Voltair^{IM} labeled lysosomes for each of these

conditions were plotted as a function of the expected lysosomal membrane potential (Fig. IV.11). Voltair^{IM} shows 25%-fold change in G/R signal per 100 mV, which is highly consistent with the reporter response of Voltair^{PM} (Fig. IV.4).

6. Voltage calibration of *Voltair* in lysosomes

Lysosomes of COS-7 cells treated with 1 µM vacuolin-1 were labeled with 500 nM Voltair^{IM}, as described in methods section. Figure IV.12 shows that the enlarged endo-lysosomal membrane can be labeled with Voltair^{IM}. Overnight chase of Voltair^{IM} results in degradation of DNA scaffold, releasing RVF and Atto647N, which can be observed by selective labeling of RVF at the lumenal membrane and Atto647N in the lumenal space (Fig IV.12).

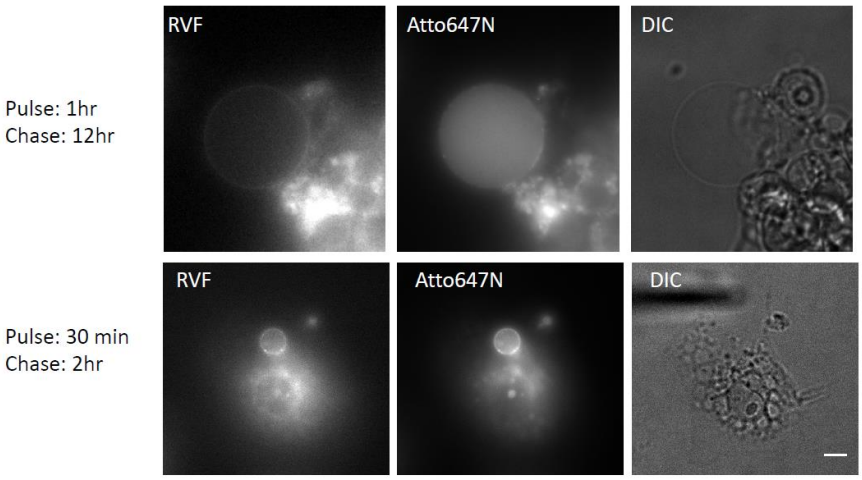

Figure IV.12. Isolation of enlarged lysosomes containing Voltair^{IM}: Upper panel: Localization of Voltair^{IM} components RVF and Attor647N labeled DNA on lysosomal membrane of Cos7 cells treated with 1 µM Vacuolin-1, post overnight chase. Lower panel: Isolation of Voltair^{IM} containing endolysosome using patch pipette for voltage clamping experiments. Scale: 5 µm.

Such enlarged, labeled lysosomes were isolated using a patch pipette and voltage clamped from -100 mV to +100 mV, as shown in figure IV.13 (Methods section). Fluorescence images of RVF and Atto647N were acquired sequentially at the indicated clamped membrane potential and the G/R heat maps of the patched lysosome (white box) were generated from the G and R images (see methods Endo-lysosomal electrophysiology). Figure IV.13c shows G/R values of Voltair^{IM}-labeled lysosomes as a function of lysosomal membrane potential (red trace). As a comparison we show the calibration plot of Voltair^{PM}-labeled plasma membrane at difference clamped voltages (grey trace). The results reveal that the response characteristics of Voltair on the plasma membrane does not change when it is present in a small intracellular organelle. Further, the overall fold changes in signal are preserved with Voltair^{IM} showing 20%-fold change per 100 mV, as observed with Voltair^{PM}.

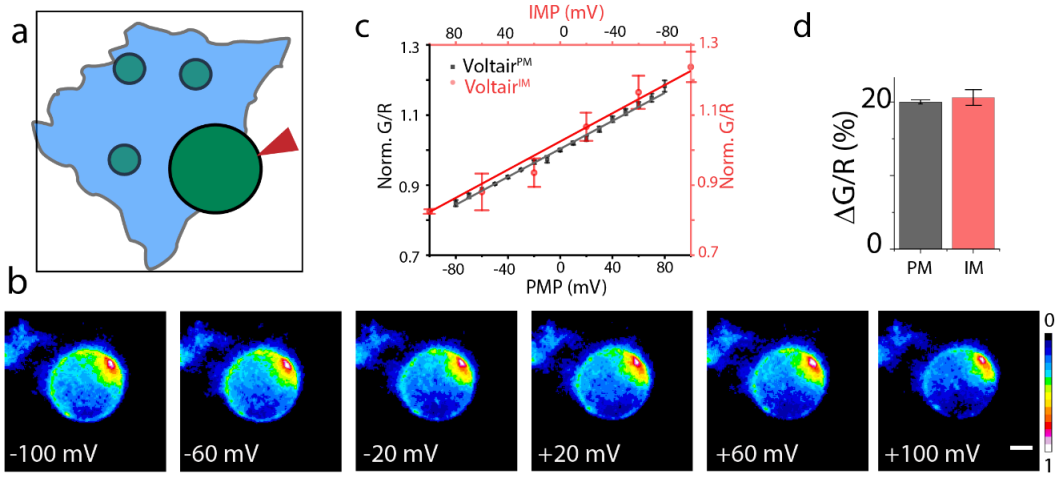

Figure IV.13. Voltair sensitivity response of Voltair as a function of lysosomal membrane potential: (a) Schematic showing voltage clamping of enlarged lysosome labeled with Voltair^{IM}. Red arrowheads indicate patch pipette. (b) Pseudo-color images show pixel-wise G/R ratio of Voltair^{IM} labelled on the inner leaflet of lysosomes as a function of membrane potential applied by whole lysosome voltage clamping. (c) Sensor response of Voltair^{PM} (gray trace, square) and Voltair^{IM} (red trace, circle) as a function of membrane potential (PMP: Plasma membrane potential, IMP: Intracellular membrane potential). Gray error bars indicate mean ± s.d., n = 6 cells. Red error bars indicate mean± s.d., n = 4 lysosomes. (d) Percentage change in signal of Voltair^{PM} (black) and Voltair^{IM} (red) from 0 to 100 mV in (c).

7. Comparsion of *Voltair*'s membrane potential sensitivity.

Voltage sensitive dye, RVF, shows 30%-fold change per 100 mV on the plasma membrane and addition of DNA scaffold onto RVF seem to decrease the voltage sensitive to 20% (Fig IV.14). This decrease, could be attributed to DNA affecting the orientation of the RVF dye across the membrane, as the voltage sensitivity is proportional to its orientation. Voltage clamping enlarged lysosomes labeled with Voltair^{IM} at longer chase times allowed us to interrogate the voltage sensitivity of RVF at the lysosomal membrane. Similar to plasma membrane, RVF shows 30%-fold change per 100 mV at the lysosomal membrane and complete voltair probe shows 20%-fold change per 100 mV (Fig IV.14). Ionophore based clamping shows Voltair^{IM} sensitivity to be around 25%-fold change at lysosomal membrane. It's an assumption that lysosomal membrane potential is + 40 mV in Valinomycin (K+ ionophore) –treated cells, and -90 mV in FCCP (H+ ionophore)-treated cells and it is not very clear how reliable these literature values are.

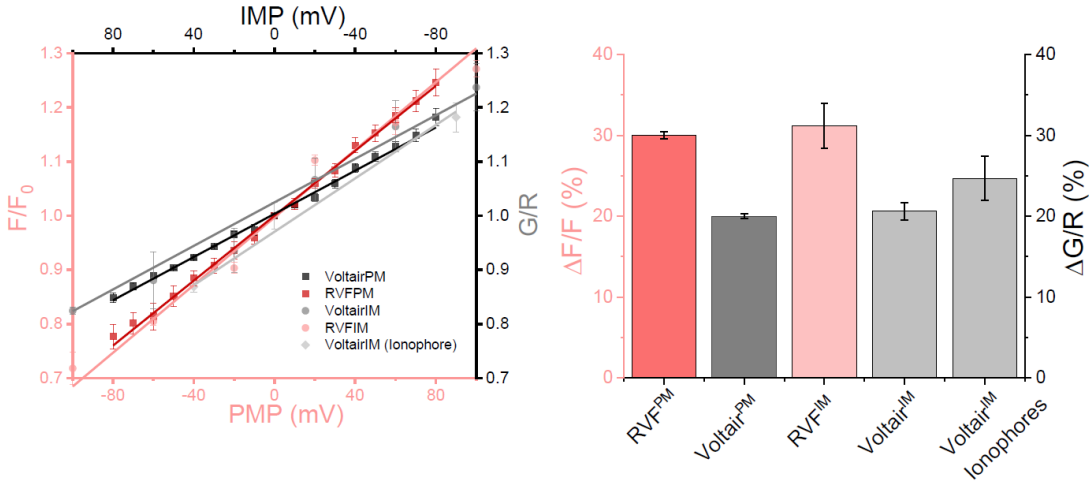

Figure IV.14. Comparison of voltage sensitivity of RVF and Voltair across different techniques: Left - Normalized intensity of voltage probe as a function of applied membrane potential. RVF^{PM} and Voltair^{PM} are voltage clamped on the plasma membrane of HEK 293T cells. RVF^{IM} and Voltair^{IM} are voltage clamped on the lysosomal membrane of COS7 cells, Voltair^{IM} (Ionophore) represents voltage clamped performed using ionophores and selective PM permeabilization. Error bars indicate mean ± s. e. m. of n = 4 cells. Right: Percentage change in signal of voltage probes from 0 to 100 mV.

IV.D: Conclusion

Genetically encoded voltage reporters access the membrane of interest from the cytosolic side, while voltage-sensitive dyes such as RVF or Voltair^{PM} selectively orient themselves on the outer leaflet of the plasma membrane. Voltair probes are embedded in the outer leaflet of the plasma membrane as well as in the lumenal leaflet of the organelle of interest. Therefore, the direction of membrane potential as measured by Voltair at the plasma membrane is consistent with the conventional electrophysiology. However, in organelles the sign convention is inverted with respect to lysosomal electrophysiology since the membrane topology is inverted in organelle interrogation. Although, there is a start contrast in terms of the membrane composition and morphology across intracellular organelles, insensitivity to membrane cholesterol as well as the similarity in voltage sensitivity of RVF and Voltair on both plasma membrane and lysosomal membrane, strengthens the basis that one could use lysosomal calibration to quantify membrane potential across all other organelles in live cells.

IV.E: References

1. Knöpfel, T. Genetically encoded optical indicators for the analysis of neuronal circuits. *Nat. Rev. Neurosci.* **13,** 687–700 (2012).

2. Knöpfel, T. & Song, C. Optical voltage imaging in neurons: moving from technology development to practical tool. *Nat. Rev. Neurosci.* **20,** 719–727 (2019).

3. Cohen, A. E. & Venkatachalam, V. Bringing bioelectricity to light. *Annu. Rev. Biophys.* **43,** 211–232 (2014).

4. Wang, L. Measurements and implications of the membrane dipole potential. *Annu. Rev. Biochem.* **81,** 615–635 (2012).

5. Grimm, C., Vierock, J., Hegemann, P. & Wietek, J. Whole-cell Patch-clamp Recordings for Electrophysiological Determination of Ion Selectivity in Channelrhodopsins. *J. Vis. Exp.* (2017). doi:10.3791/55497

6. Zhang, Q. *et al.* Functional relevance of Golgi- and plasma membrane-localized endothelial NO synthase in reconstituted endothelial cells. *Arterioscler. Thromb. Vasc. Biol.* **26,** 1015–1021 (2006).

7. Johnson, R. G. & Scarpa, A. Protonmotive force and catecholamine transport in isolated chromaffin granules. *J. Biol. Chem.* **254,** 3750–3760 (1979).

8. Yamashiro, D. J., Fluss, S. R. & Maxfield, F. R. Acidification of endocytic vesicles by an ATP-dependent proton pump. *J. Cell Biol.* **97,** 929–934 (1983).

9. Małecki, J., Wiedłocha, A., Wesche, J. & Olsnes, S. Vesicle transmembrane potential is required for translocation to the cytosol of externally added FGF-1. *EMBO J.* **21,** 4480–4490 (2002).

10. Wang, X. *et al.* TPC proteins are phosphoinositide- activated sodium-selective ion channels in endosomes and lysosomes. *Cell* **151,** 372–383 (2012).

11. Kulkarni, R. U. *et al.* A Rationally Designed, General Strategy for Membrane Orientation of Photoinduced Electron Transfer-Based Voltage-Sensitive Dyes. *ACS Chem. Biol.* **12,** 407–413 (2017).

12. Modi, S. *et al.* A DNA nanomachine that maps spatial and temporal pH changes inside living cells. *Nat. Nanotechnol.* **4,** 325–330 (2009).

13. Vercesi, A. E., Bernardes, C. F., Hoffmann, M. E., Gadelha, F. R. & Docampo, R. Digitonin permeabilization does not affect mitochondrial function and allows the determination of the mitochondrial membrane potential of Trypanosoma cruzi in situ. *J. Biol. Chem.* **266,** 14431–14434 (1991).

14. Bradley, M. P., Rayns, D. G. & Forrester, I. T. Effects of filipin, digitonin, and polymyxin B on plasma membrane of ram spermatozoa—an EM study. *Arch Androl* **4,** 195–204 (1980).

15. Bhatia, D., Surana, S., Chakraborty, S., Koushika, S. P. & Krishnan, Y. A synthetic icosahedral DNA-based host-cargo complex for functional in vivo imaging. *Nat Commun* **2,** 339 (2011).

V. Quantification of membrane potential across intracellular membranes

V.A: Introduction

Intracellular organelles have diverse compositions and cellular functions, yet one common feature of these organelles is the steady state maintenance of ionic gradients across their membranes[1]. Numerous reports that selectively probe the ionic concentration within these organelles show the existence of large ionic gradient between the organelle lumen and cytoplasm[2–5]. Although, the membrane transporters and channels responsible for maintenance of these ionic gradients are known to some extent, its near impossible to explain the magnitude of these gradients[6,7]. For instance, it is very well known that V-ATPase acidifies lysosomal lumen with the expense of cytosolic ATP. But it's still unclear how it generates a pH difference of only 2.5 units w.r.t. cytoplasm, when at thermodynamic equilibrium it is capable of acidifying the lumen up to ΔpH of 4.5 units[8]. Discovery of novel channels and transporters in these organelles, further complicates our understanding of dynamics in ion homeostasis. Imbalance in ionic homeostasis results in numerous diseases such as lysosomal storage disorders, neurodegenerative diseases due to ER stress, Golgi congenital diseases etc[9,10].

Unlike plasma membrane, organellar membranes are still relatively a black box, where some of the basic information are still unknown, such as lumenal ionic composition, organellar membrane potential, membrane lipid composition etc[1]. Organelle isolation techniques and fluorescent reporters for inorganic ions are constantly improving our knowledge on this front, but very little effort has been put to probe membrane potential across organellar membranes[11,12]. In addition to the most extensively interrogated organelle, mitochondria, electrochemical understanding of lysosome is on the rise due to lysosome electrophysiology[13]. Measurement of

lysosomal membrane potential from electrophysiology as well as FRET based probes show lysosomes to have a broad range of resting membrane potential (-30 to +110 mV)[14]. This huge variation could be due to numerous factors, ranging from differences in techniques to different cell types[15–17]. Thus, we use Voltair to map the membrane potential across various intracellular organelles within a given cell type.

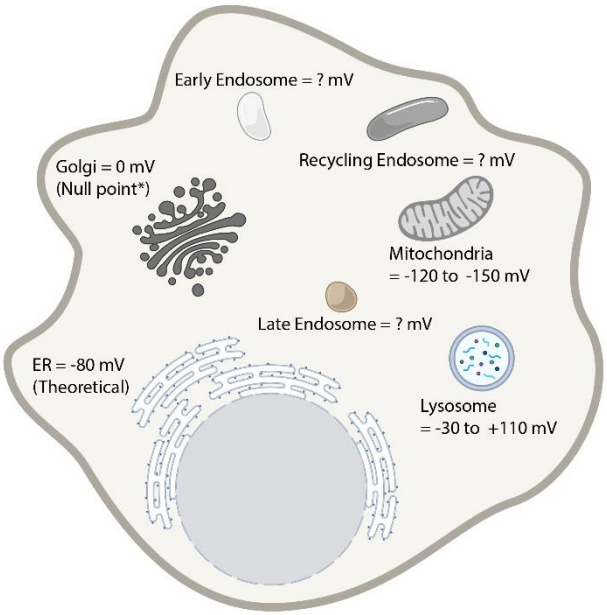

Figure V.1: Reported membrane potential of individual cellular organelles and compartments in a mammalian cell.

V.B: Materials and methods

1. Oligonucleotides

Modified DNA oligonucleotides were purchased from IDT (USA). PAGE purified and lyophilized oligonucleotides were dissolved in Milli-Q water of recommended volume to approximately prepare 100 µM stocks. Concentration of oligonucleotides are accurately quantified by collecting

UV absorbance spectra and using Beer Lambert's law with absorbance at 260nm for DNA. In the case of fluorescently labeled oligonucleotides, equation 1 is used to quantify the concentration.

$$\text{Concentration} = (Abs_{260} \times \text{dilution factor}) / (\varepsilon_{oligo} - \varepsilon_{dye}) \quad \text{Eq. 1}$$

Where, molecular extinction coefficients of all oligonucleotides ε_{oligo} are provided in the specification sheet by IDT and molecular extinction coefficient of the fluorescent dye at 260nm ε_{odye} is referred from literature references.

2. Sample preparation:

Stock solution of Voltair^{PM} was prepared at a final concentration of 10 µM by mixing D_V, D_T and D_A (Atto647N – 5' modified strand) at an equimolar ratio in 10 mM sodium phosphate buffer, pH 7.4. For Voltair^{IM} samples, D_V (Voltage sensing strand of Voltair^{PM}) and D_A' (Atto647N – 3' modified 38 mer strand) were mixed at an equimolar ratio with a final concentration of 10 µM. For Voltair^{RE} samples, 10 µM of D_V^{RE}, D^{Tf} and D_A^{RE} were mixed at an equimolar ratio. For all samples, annealing was performed by heating the reaction mixture to 95°C for 15 min and gradually cooling to RT, at 1°C/ 3 min. Annealed samples were equilibrated at 4°C overnight.

3. Cell culture

Human embryonic kidney cells (HEK 293T), BHK-21 cells, human dermal fibroblasts (HDF), RAW 264.7, THP-1 and T-47D cells were a kind gift from Dr. Bryan Dickinson (Department of Chemistry, University of Chicago), Dr. M. Gack (Department of Microbiology, the University of Chicago), J. Rowley's lab (University of Chicago), Dr. Christine A. Petersen (Department of Epidemiology, University of Iowa), Dr. D. Nelson (Department of Pharmacological and Physiological Sciences, the University of Chicago) and G. Greene (The Ben May Department for Cancer Research, the University of Chicago), respectively. COS-7 cells were purchased from

ATCC. Cells were cultured in Dulbecco's Modified Eagle's Medium (Invitrogen Corporation, USA) containing 10% heat inactivated Fetal Bovine Serum (FBS) (Invitrogen Corporation, USA), 100 U/mL penicillin and 100 µg/mL streptomycin and maintained at 37ºC under 5% CO2. HEK 293T cells were passaged and plated at a confluency of 20 – 30% for electrophysiology experiments, and 50 – 70% for transfection and intracellular measurements.

4. Reagents and buffers

All reagents were purchased from Sigma-Aldrich (USA) unless otherwise specified. HBSS and DMEM were purchased from Thermoscientific (USA).

1X Phosphate buffered Saline (PBS): 137 mM NaCl, 2.7 mM KCl, 10 mM Na_2HPO_4. 2 mM KH_2PO_4, pH adjusted to 7.0 using 1N HCl. The buffer then filtered using 0.22 um filter and autoclaved.

5. *Voltair* labeling

Specific labeling of Voltair across endocytic organelles (EE, LE and Ly) is achieved by transfecting HEK293T cells with hMSR1. Transfected cells were pulsed with 500 nM Voltair for 10 minutes and chased for 10 mins to label early endosomes. To label late endosomes and lysosomes, transfected cells were pulsed with Voltair for 30 mins and chased for 30 mins to label LE and 90 mins to label lysosomes respectively. The trafficking time of DNA device with transferrin aptamer and d(AT)4 tag in labeling RE and TGN, respectively, have been established previously. Briefly, recycling endosomes are targeted by pulsing $Voltair^{RE}$ in 1X HBSS, for 10 mins at 37°C, followed by 30 mins of chase in complete media at 37°C. Trans Golgi network is targeted by pulsing $Voltair^{IM}$ in complete media containing cycloheximide (CHX) for 90 mins at 37°C, followed by 90 mins chase in the same media.

6. Pharmacological drug treatments

Organelles of HEK 293T or COS-7 cells were labeled with Voltair^{IM} according to labeling protocols discussed above. Labelled cells were treated with ML-SA1 (20 µM), NS1619 (15 µM) or trans-ned-19 (1 µM) for 15 mins in HBSS solution at room temperature. Torin-1 (1 µM) was treated to labelled cells during the chase period (50 mins), to inhibit mTOR. Bafilomycin-A1 (500 nM) was added to cells for 30 mins in 1X HBSS and incubated at 37C prior organellar voltage measurements. After acquisition of G and R images of drug treated cells, intracellular membrane potential was neutralized (~ 0 mV) by adding 50 µM valinomycin and monensin in high K+ buffer, for 20 mins at room temperature. A set of G and R images of same cells were acquired after valinomycin and monensin treatment, where these images of neutralized organelles were used as a baseline measurement for internal control.

7. Fluorescence microscopy

Wide field microscopy was carried out on an IX83 inverted microscope (Olympus Corporation of the Americas, Center Valley, PA, USA) using either a 100X or 60X, 1.4 NA, DIC oil immersion objective (PLAPON, Olympus) and Evolve Delta 512 EMCCD camera (Photometrics, USA). Filter wheel, shutter and CCD camera were controlled using Metamorph premier Ver 7.8.12.0 (Molecular Devices, LLC, USA). Images on the same day were acquired under the same acquisition settings (exposure 100 ms and EM gain at 100 for Atto647N, exposure 100 ms and EM gain 300 for RVF). All the images were background subtracted by taking mean intensity over an adjacent cell free area. The mean intensity in each endosome/lysosome was measured in the sensing channel (G) and the normalizing channel (R). Filter sets, purchased from Chroma, suitable for each fluorophore were selected to minimize excitation and emission from other dyes in the sample. RVF channel images were obtained using 500/20 band pass excitation filter, 535/30 band

pas emission filter and 89016 dichroic. For Atto647N, images were obtained using the 640/30 band pass excitation filter, 705/72 band pass emission filter and 89016 dichroic. Pseudo-color images were generated by calculating the G/R ratio per pixel in Fiji using the Image calculator module. For cytosolic calcium recording, fluorescence of Fluo-4 was recorded by exciting at 480 nm and collecting emission at 520 nm. Images were acquired using a 480/20 band pass excitation filter, 520/40 band pass emission filter and 89016 dichroic.

Intracellular membrane potential measurements were performed by recording images in the sensing channel (G) and the normalizing channel (R) in cells where each specific compartment was labeled. After acquisition of G and R images, intracellular membrane potential was neutralized (~ 0 mV) by adding 50 µM valinomycin and monensin in high K+ buffer, for 20 mins at room temperature. A set of G and R images of same cells were acquired after valinomycin and monensin or pharmacological treatments as shown in Fig. S17. These images of neutralized endosomes were used as a baseline measurement to correct for variations in autofluorescence. To record all endo-lysosomal compartments in the cell, Z-stacks (30 planes, Z distance = 0.8 µm) were captured and a maximum intensity projection was used to produce a single image for analysis.

8. Time lapse imaging

Lysosomes of COS-7 cells labeled with Voltair^{IM} were sequentially imaged on a widefield microscope with 60X magnification in G and R channel at 10-20s interval for a duration of 20 mins. Image acquisition was briefly paused at indicated time for addition of chemicals (ML-SA1, Baf-A1, ATP or DMSO) to cells. To minimize bleaching, time-lapse imaging was done at single focal plane. Z-drift compensator module from IX83 was applied to minimize out of focus drift during time lapse imaging. The extracellular ATP induced cytosolic calcium increase was imaged by labeling COS-7 cells with cell permeable calcium sensitive dye Fluo4-AM ester 12. Time-lapse

imaging of Fluo-4 labeled COS-7 cells were acquired using a 480/20 band pass excitation filter, 520/40 band pass emission filter and 89016 dichroic, at 1s interval for 20 mins.

9. Image analysis

Images were analyzed with Fiji or imageJ (NIH, USA). For organellar voltage measurements, regions of cells containing single isolated endosomes/lysosomes in each Atto647N (R) image were manually selected and the coordinates saved in the ROI plugin in ImageJ. Similarly, for background computation, a nearby region outside endosomes/lysosomes were manually selected and saved as an ROI. The same regions were selected in the RVF (G) image by recalling the ROIs. After background subtraction, mean intensity for each endosome (G and R) was measured and exported to OriginPro (OriginLab, USA). A ratio of G to R intensities (G/R) was obtained from these values by dividing the mean intensity of a given endosome in the G image with the corresponding intensity in the R image. We used the same protocol for individual endosomes in the calibration, therefore G/R ratio correspond to membrane potential calibrated intracellularly. To minimize the measurement error due to low fold change of Voltair probes, the same endosomes or lysosomes are measured post addition of valinomycin and monensin which neutralizes the membrane potential in presence of 150 mM KCl. For TGN voltage measurements, total cell intensity was recorded and background subtraction was performed by manually selecting a region outside the cell. For a given experiment, membrane potential of an organelle population was determined by converting the mean $[G/R]_V$ - $[G/R]_O$ value of the distribution to voltage values according to intracellular voltage calibration profile. The mean value of each organelle population across three trials on different days is determined and the final data is presented as mean ± S.E.M. Representative images are shown in pseudo-color images, where G and R images were modified

by thresholding in ImageJ to get G' and R' images. Using ImageJ's Image calculator module, G' images were divided by R' images to generate an image where each pixel represents $[G/R]_V$.

10. Statistical analysis

For statistical analysis between two samples, two-sample two tailed test assuming unequal variance were used. For comparison of multiple samples, one-way ANOVA with a post hoc Tukey test or Fischer test was used. All statistical analysis was performed in Origin (Student version). Violin plots show the Kernel smooth distribution of data points and embedded box plots indicate 25-75% percentile, with median shown as white circle and error bars represents standard deviation.

V.C: Results and Discussion

1. In situ measurement of absolute lysosomal membrane potential

Voltair probes were specifically labeled to lysosomes using the pulse chase protocol as shown in Figure V.2.

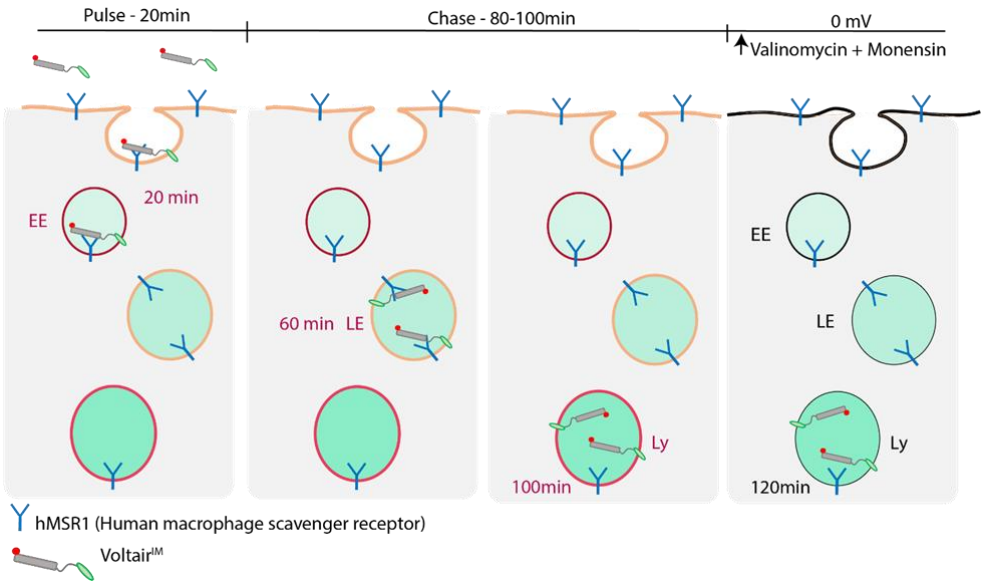

Figure V.2. Schematic representation of pulse-chase protocol for organellar measurements. HEK cells transfected with hMSR-1 were incubated with VoltairIM, washed and chased for the indicated chase times to achieve localization in the early endosome (EE), late endosome (LE) and lysosome (Ly) respectively. Images are recorded at indicated chase times. This followed by the addition of a cocktail of valinomycin and monensin to neutralize the membrane potential across all organelles, after which, images are again recorded to obtain the G/R value for 0 mV. G/R values of every organelle are normalized to the G/R value at 0 mV from which organelle membrane potential is quantified.

We first validated Voltair^{IM} performance in lysosomes in situ, given that this organelle has been rigorously addressed using electrophysiology. Fluorescence images in the G and R channels of Voltair^{IM} labeled lysosomes in HEK293T cells were acquired and the pseudo colored G/R images were computed (Fig V.3).

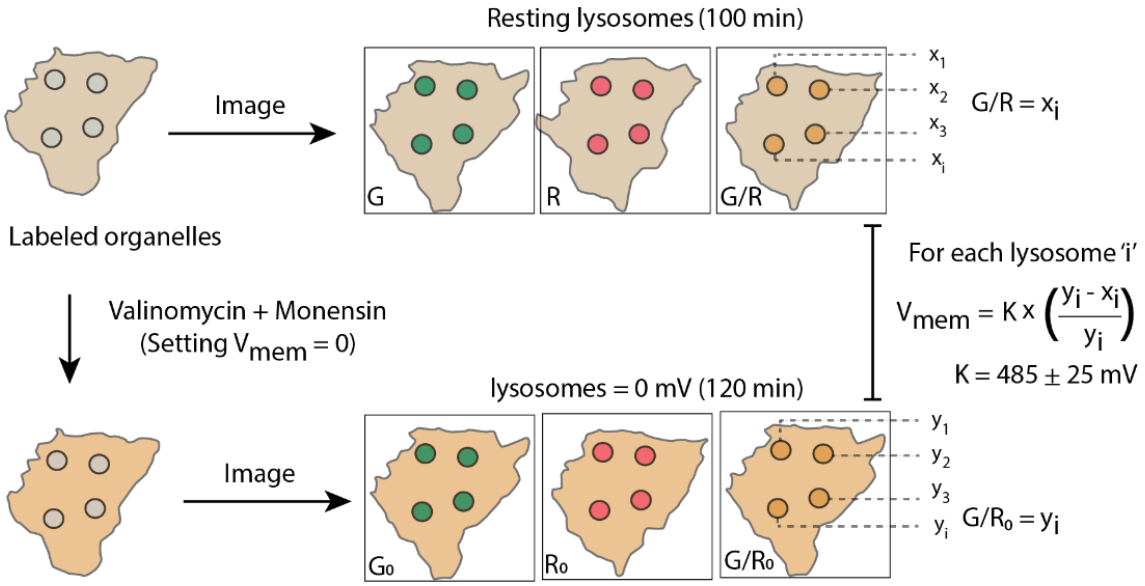

Fig V.3. Schematic of Lysosomal V_{mem} measurement: Imaging protocol of organelles labeled with VoltairIM. resting organelles are imaged in G and R channels, neutralized with valinomycin-monensin and second set of images are acquired in G and R channels. Resting membrane potential of the organelle is calculated by normalizing G/R values from untreated lysosomes (xi) to neutralized lysosomes (yi).

Figure V.4 shows the distribution of G/R values in lysosomes and from the intracellular calibration plot we could determine the corresponding membrane potential. Considering the lumen to be positive and the cytoplasmic face negative, the membrane potential of lysosomes (V_{Ly}) was found to be +114 mV in HEK 293T cells. This is in line with other electrophysiological studies of lysosomal membrane potential in different cell types that were found to lie between -30 mV to +110 mV[14]. We then compared the lysosomal membrane potential across different cell lines (Fig V.4). We found that COS-7 and BHK-21 cells showed slightly lower overall values of membrane potential +80 mV (lumen positive) compared to HEK 293T cells. Those in RAW macrophages were even more depolarized with values centered at +40 mV (lumen positive), comparable to +20

mV reported in previous literature (Fig V.4)[11]. Such variations in the mean resting potential in different cell types could arise from the differential lysosomal membrane protein composition across these cell types[7].

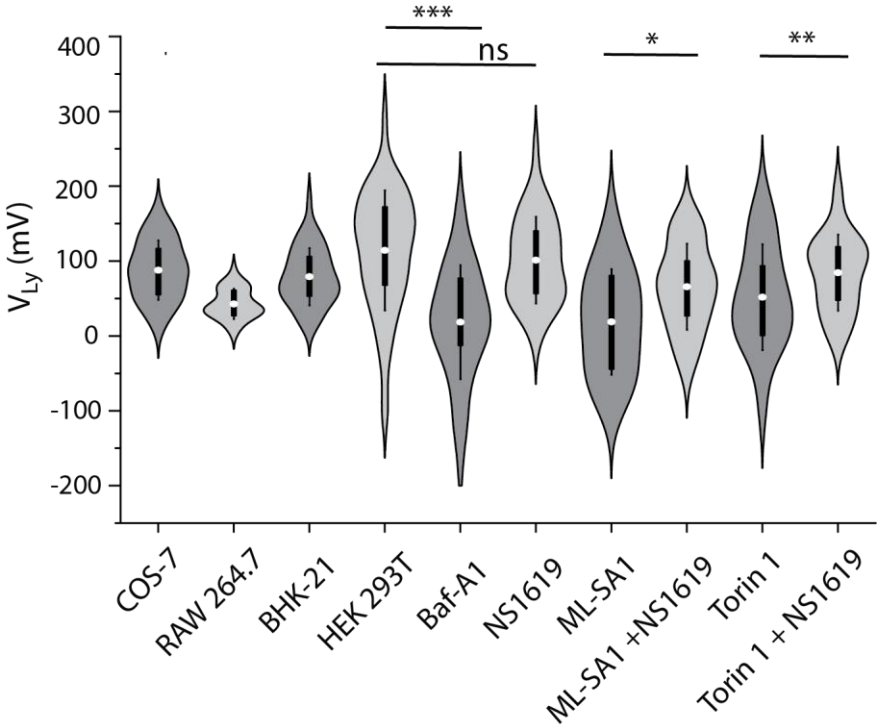

Figure V.4. Quantification of lysosomal membrane potential: Measured lysosomal resting membrane potential values (V_{Lys}) of COS-7, RAW 264.7, BHK-21 cells and HEK 293T values in presence of V-ATPase inhibitor Bafilomycin (Baf-A1, 500 nM), mTORC1 inhibitor Torin-1 (1 µM), the TRPML1 activator ML-SA1 (20 µM), and the Slo1 activator, NS1619 (15 µM). Violin plots show kernel smooth distribution, box indicates interquartile range 25-75; Error bars indicate mean ± s.d. of 100 lysosomes; ns, not significant ($P > 0.05$); **$P < 0.01$; *$P < 0.05$ (Unpaired two sample t-test).

2. Changes in lysosomal mV upon pharmacological perturbations

Next, we checked whether Voltair^{IM} had the sensitivity to report changes in lysosomal membrane potential upon treatment with common pharmacological reagents that activate pumps, channels and transporters on the lysosomal membrane. Voltair^{IM} quantitatively reports membrane potential up to 1h post reaching lysosomes in HEK293T cells. The electrogenic proton pump V-

ATPase acidifies many organelles by hydrolyzing ATP and generating membrane potential across organelle membranes[18]. Inhibiting V-ATPase with bafilomycin A1 stops proton transport, which neutralizes membrane potential in purified, highly acidic synaptic vesicles[19]. We found that Voltair^{IM} labeled lysosomes showed a large increase in G/R values upon bafilomycin A1 treatment (500 nM) compared to untreated cells, revealing that lysosomal membrane potential (V_{Ly}) was dissipated by inhibiting V-ATPase (Fig V.4). From the in-cell calibration plot (Fig V.14), V_{Ly} was reduced by ~100 mV from the resting membrane potential, consistent with studies on other highly acidic V-ATPase regulated organelles such as synaptic vesicles[19] (Fig V.4).

Next, we tested the effect of modulating specific channels on the lysosomal membrane. While on the lysosome, the mTORC1 complex inhibits both TPC2 and TRPML1 channels (Fig V.5a)[20,21]. When nutrient levels plummet, mTORC1 dissociates from the lysosome, relieving the inhibition on TPC2 and TRPML1 channels. This triggers lysosomal Ca^{2+} release and is expected to reduce V_{Ly}. Low V_{Ly} is expected to activate the voltage dependent channel Slo1, which would promote K^+ influx into the lysosome and activate TRPML1[22]. Cytosolic Ca^{2+} elevation caused by TRPML1 channel opening is expected to induce a positive feedback loop to release lysosomal Ca^{2+} and drive further K^+ influx[22].

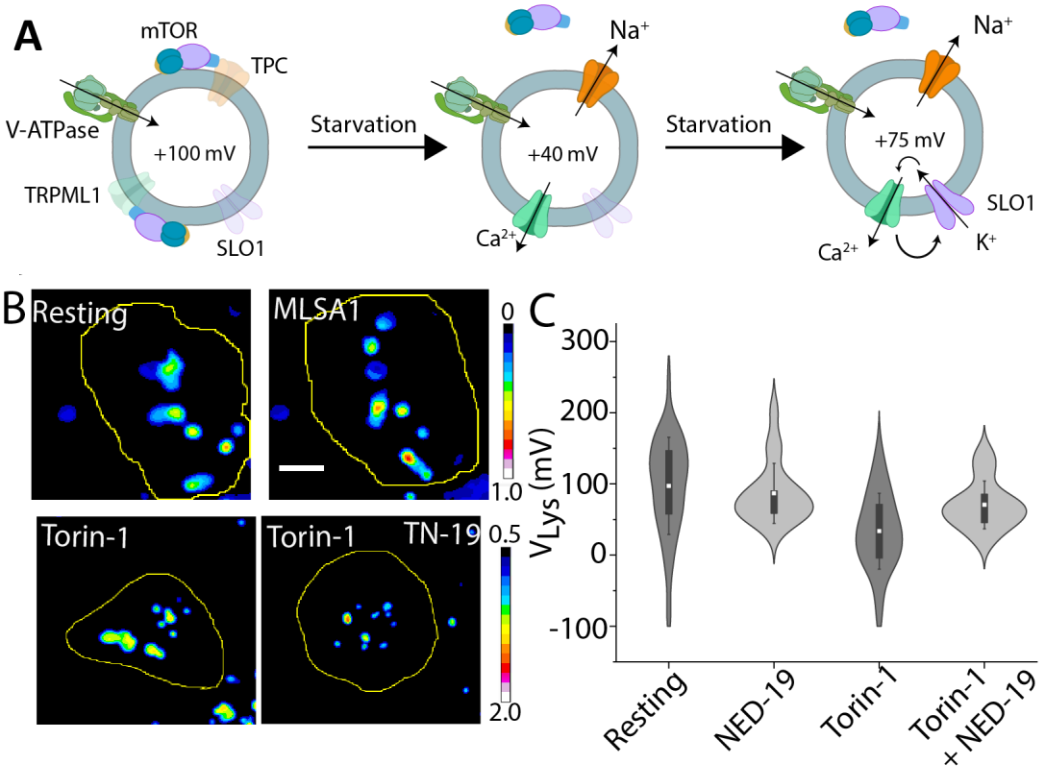

D

Protein	Inhibition	Activation	$\lvert\Delta V_{lys}\rvert$ (Initial – Final)	
			Electrophysiology	Voltair
TPC2	ATP	-	20 mV[21]	-
	trans NED-19	-	-	35 mV
TRPML1	-	ML-SA1	30 mV[23]	90 mV
Slo1	-	cyto-Ca^{2+}	40 mV[22]	-
		NS1619	-	50 mV
mTORC1	Torin-1	-	n.d.	60 mV

Figure V.5. Lysosomal membrane potential changes under starvation (a) Model: Starvation promotes dissociation of mTORC1 from lysosomes, activating TPC and TRPML1 channels that release cations and depolarize lysosomes. Low lysosomal membrane potential (VLys) as well as released Ca2+ promote the opening of the voltage activated channel Slo1, which, by coupling to TRPML1 releases lysosomal Ca2+ by positive feedback. (b) Representative pseudo-color G/R images of lysosomes in HEK 293T cells in presence of indicated pharmacological agents (1 µM). Scale = 5 µm. (c) Violin plot of lysosomal membrane potential in presence of indicated pharmacological chemicals. (d) Table comparing the changes in VLys measured by electrophysiology and by VoltairIM when indicated ion channels are inhibited or activated.

Treating HEK 293T cells with ML-SA1 as well as the BK channel agonist, NS1619 gave ΔV_{Ly} of 50 mV (Fig V.4). These values are in good agreement with electrophysiological studies that inhibited TRPML1 or activated Slo1[13,22]. Inhibiting mTORC1 with Torin-1 (1 μM) reduced V_{Ly}, by nearly 60 mV from the resting V_{Ly}, presumably due to TPC2 and TRPML1 channel activation (Fig V.5). In the presence of Torin-1 and a TPC2 channel inhibitor (trans-ned-19, 1 μM), V_{Ly} was reduced to +80 mV giving ΔV_{Ly} of 35 mV due to TPC2 channel inhibition (Fig V.4, V.5). This is in excellent agreement with analogous measurements by electrophysiology on isolated lysosomes where TPC2 channel inhibition gave ΔV_{Ly} of 20 mV[20].

3. Membrane potential as a function of endosomal maturation

Encouraged by the accuracy in absolute membrane potential afforded by Voltair in lysosomes, we proceeded to measure the resting membrane potential of other endocytic organelles as a function of endosomal maturation. Although, the membrane potential of lysosomes has been measured on isolated organelles, no prior values are known for early or late endosomes. Early endosomes, late endosomes and lysosomes were each specifically labelled with Voltair^{IM}, as described in earlier chapter. The G/R values of ~200 organelles were computed for each endosomal stage and from the intracellular calibration plot we could determine the corresponding organelle membrane potential (Fig V.6) Measurements with Voltair^{IM} revealed the membrane potential of early endosomes (V_{EE}) and late endosomes (V_{LE}) to be +153 mV and +46 mV respectively. We observed a spread in values of membrane potential in endocytic organelles (Fig V.6b). At least for endo-lysosomes, we know that they are heterogenous and comprise subpopulations that enclose different ionic concentrations[23]. This could in part explain the observed spread in organellar membrane potential.

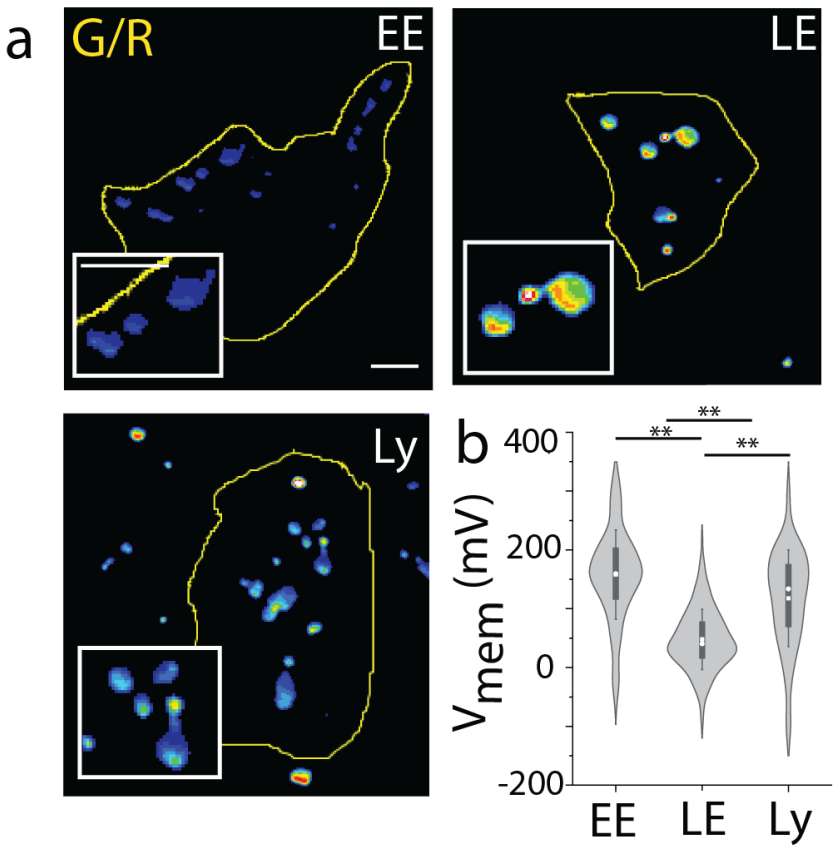

Figure V.6. Membrane potential of organelles along endocytic pathway: (a) Representative pseudocolor G/R images of the indicated organelles labeled with VoltairIM. Scale: 5 µm. (b) Measured membrane potentials of early endosomes (EE), late endosomes (LE) and lysosomes (Ly). Violin plots show kernel smooth distribution, box indicates interquartile range 25-75; Error bars indicate mean ± s.d. of 200 vesicles; **P < 0.01 (one-way ANOVA with Tukey post hoc test).

Surprisingly the gradient of membrane potential accompanying endosomal maturation did not reflect that of ion gradients that have been previously mapped (Fig V.7). The concentrations of protons, chloride and calcium increase progressively during endosomal maturation[2–5] (Fig V.7). In contrast, membrane potential is highest in the early endosome, drops ~3 fold in the late endosome and increases again in lysosomes. With respect to cytoplasmic concentrations, the levels of lumenal [Ca^{2+}] and [Cl^{-}] for the early endosome or the lysosome, are very similar i.e., ~10^2-10^3 fold higher [Ca^{2+}], 1-2-fold higher [Cl^{-}] (Fig V.7). However, the lysosome lumen has ~10^3 fold higher [H^{+}], while the early endosome lumen has only ~10 fold higher [H^{+}] than the cytosol . Yet

the observed membrane potentials for both these organelles are consistent with lower rather than higher membrane potential compared to the early endosome (V_{EE} = +153 mV; V_{LY} = +114 mV). Considering the low abundances of other free ions, this provides a compelling case for Na^+ and K^+ transporters or exchangers in maintaining the high positive membrane potential of the early endosome[24]. In fact, late endosomes are posited to contain high K^+, which is consistent with our observations[25]. Our hypothesis is supported by observations at the plasma membrane. The differences in [Ca^{2+}] and [Cl^-] across the plasma membrane are comparable, yet its membrane potential is set by the differences in [Na^+] and [K^+] across the membrane[24,26].

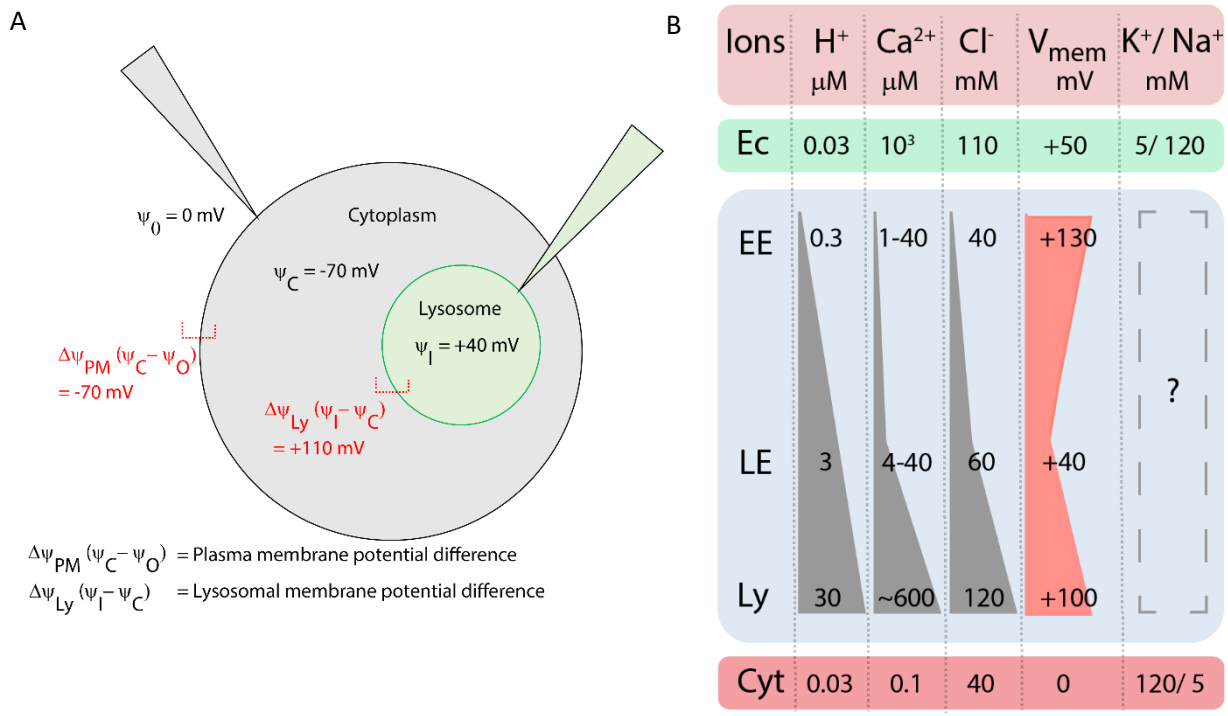

Figure V.7. (a) Schematic showing the convention followed in representing organellar membrane potential. (b) Tabular column summarizing approximate ionic concentration7–9 and voltage difference in organelles along the endosomal pathway. Cytosolic (Cyt), extracellular (Ec) and organellar concentrations of main ions that maintain membrane potential.

4. Membrane potential of recycling endosomes and trans Golgi network

We then sought to measure membrane potential in organelles that were off the endolysosomal pathway by targeting Voltair to these organelles. We re-designed Voltair to give Voltair^{RE} and Voltair^{TGN} that could access the recycling and retrograde pathways and measure the membrane potential of these respective organelles. Recycling endosomes and the trans-Golgi network have been only hypothesized to have membrane potential which is thought to be regulated by the electrogenic activity of vacuolar H^+-ATPases[27]. We then measured the resting membrane potential of the recycling endosome and trans-Golgi network, neither of which has been previously possible, and evaluated the contribution of V-ATPase to membrane potential in each organelle. Voltair^{RE} labelled cells were imaged in the G and R channels, and G/R values of ~50 recycling endosomes were computed (Fig V.8). We found that the membrane potential of recycling endosome (V_{RE}) was +65 mV (lumen positive), similar to plasma membrane (cytosol negative). When V-ATPase activity was inhibited by treating cells with 500 nM bafilomycin A1, V_{RE} showed no change revealing a negligible contribution of V-ATPase in recycling endosome membranes[28]. The magnitude and the V-ATPase dependence of membrane potential in the recycling endosome mirrors that of the plasma membrane, indicating that both membranes share similar electrical characteristics. Voltair^{TGN} labelled cells were similarly imaged and G/R values of the TGN in ~30 cells were computed. We found that the membrane potential of the trans Golgi network (V_{TGN}) was +121 mV (lumen positive) (Fig V.8). The high membrane potential of the trans-Golgi network is surprising as the Golgi has been envisaged to have negligible membrane potential, since its high permeability to K^+ ions could electrically balance the H^+ influx needed to acidify its lumen[16]. In contrast to what we observed for recycling endosomes, V-ATPase inhibition substantially reduced V_{TGN}. However, unlike in lysosomes, the membrane potential of the TGN could not be completely

neutralized and still showed +75 mV across the membrane. This suggests that other electrogenic transporters at the TGN, possibly Na^+/K^+ ATPases could significantly contribute to the V_{TGN}[29]. It also reveals that different organelle membranes have distinct electrochemical behaviors.

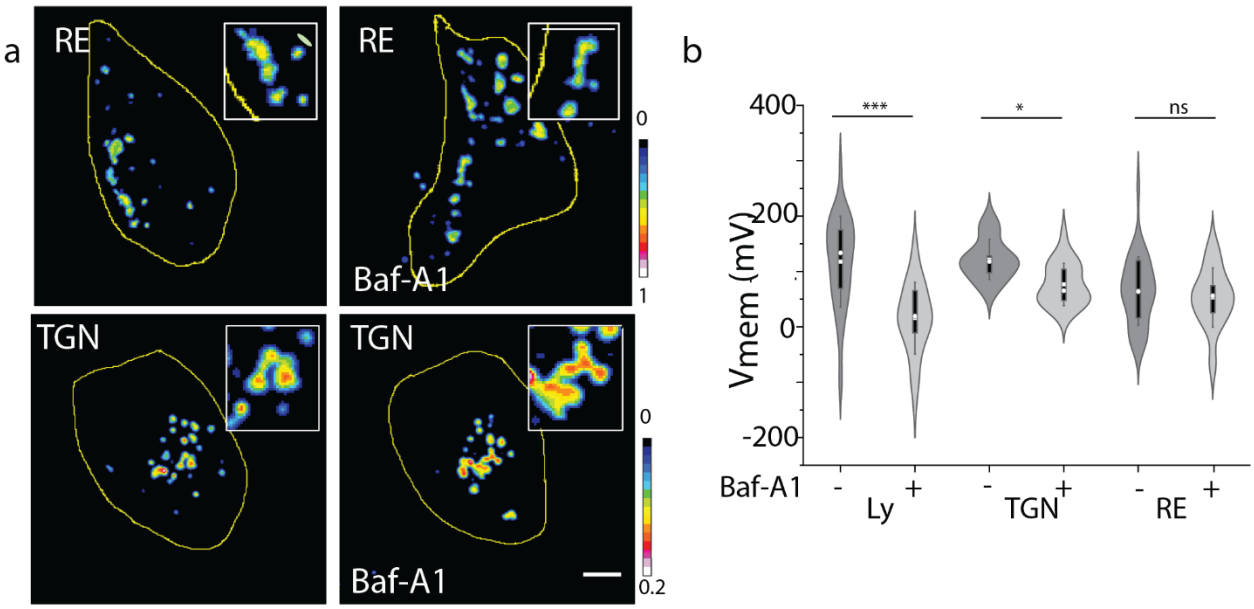

Figure V.8. Membrane potential of organelles along endocytic, recycling and retrograde trafficking pathway: Representative pseudo-color G/R images of RE and TGN of HEK 293T cells in absence and presence of bafilomycin A1 (500 nM). Scale = 5 µm. (h) Violin plot of resting membrane potential of organelles and changes upon inhibition of V-ATPase. Box indicates interquartile range 25-75; Error bars indicate mean ± s.d; ns, not significant ($P > 0.05$); ***$P < 0.001$, *$P < 0.05$ (one-way ANOVA with Tukey post hoc test). (i) Representative pseudo-color time lapse images of ATP induced cytosolic calcium increase imaged using Fluo-4 AM dye. Scale = 10 µm.

5. Time lapse imaging of membrane potential changes in lysosomes

Finally, to test the ability of Voltair technology to provide temporal information, we sought to map membrane potential of large numbers of intact lysosomes in situ in response to acute pharmacological triggers. Treating HEK 293T cells with an activator of TRPML1 (ML-SA1, 20 µM) gave a ΔV_{Ly} of 90 mV using Voltair^{IM} (Fig V.4). This decrease in membrane potential was

specific to the lysosome, because time-lapse imaging of membrane potential in early endosomes (V_{EE}) stayed constant upon ML-SA1 treatment, unlike that of lysosomes (Fig V.9).

Cytosolic Ca^{2+} levels are stringently regulated by various intracellular organelles such as endoplasmic reticulum, mitochondria and plasma membrane[30]. Lysosomes are also hypothesized to buffer cytosolic Ca^{2+}, which, when increased is expected to perturb electrochemical homeostasis of the lysosome[31]. We therefore elevated cytosolic Ca^{2+} using a physiological trigger such as ATP and measured lysosomal membrane potential along with cytosolic Ca^{2+} levels in COS-7 cells labeled with Voltair^{IM} and Fluo-4-AM. Extracellular ATP increases cytosolic Ca^{2+} by interacting with P2 purinergic receptors on the plasma membrane, generating Ins(1,4,5)P_3 or IP_3. This activates IP_3 receptors on the endoplasmic reticulum, releasing calcium[32].

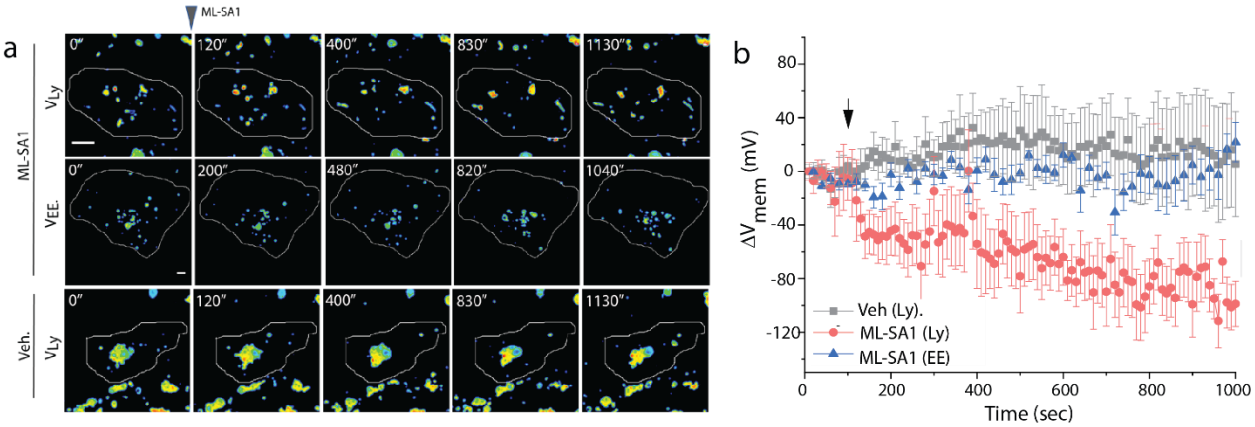

Figure V.9. Perturbation of lysosomal V_{mem}: (a) Representative pseudo-color time lapse images of lysosomal and early endosomal G/R intensity ratios in presence of TRPML1 activator, ML-SA1 at t = 100s (Veh. = DMSO); Pseudo colored images represents the computed intensity ratio of VoltairIM in G (RVF) and R (Atto647N) channel. The cell of interest is represented by white ROI (region of interest). Scale = 10 µm. (b) Time-lapse plot of ΔVmem vs time upon TRPML1 activation in VoltairIM labeled lysosomes (red trace), in VoltairIM labeled Endosome (blue trace). DMSO (Veh.) treatment (black trace), Error bar represents mean ± s.d. from n = 10 cells. Experiments were repeated thrice independently with similar results.

We followed cytosolic Ca^{2+} levels as a function of time by continuously imaging the whole cell intensity of Fluo-4 and lysosomal membrane potential by imaging whole cell intensity from

Voltair^{IM} labeled cells (Fig V.10a). As expected, cytosolic Ca^{2+} levels reach the maximum ~5 seconds after ATP addition (Fig V.10c). Interestingly, ~80 seconds after maximal cytosolic Ca^{2+} elevation we observed an acute hyperpolarization of the lysosomal membrane by +75 mV. This hyperpolarization lasted for ~100 seconds, before it reverted to normal resting lysosomal membrane potential (Fig V.10b, d). Further, the lysosomal membrane potential is restored when cytosolic Ca^{2+} levels are also restored.

The correlation between the cytosolic Ca^{2+} surge and the ensuing abrupt lysosomal hyperpolarization suggests the activation of lysosome-resident transporters that import Ca^{2+} in order to restore cytosolic Ca^{2+} levels, along with other Ca^{2+} buffering organelles of the cell. For example, the activity of a transporter such as a lysosomal Ca^{2+}/H^{+} exchanger (CAX) could elevate lysosome membrane potential because it would lead to the asymmetric accumulation of positive charge in the lysosome due to dicationic Ca^{2+} influx versus monocationic H^{+} efflux[33]. Membrane potential variations are ~10^3-fold faster than Ca^{2+} transients and the small size of lysosomes compared to the plasma membrane are possible reasons for the abrupt nature of the observed membrane potential variations.

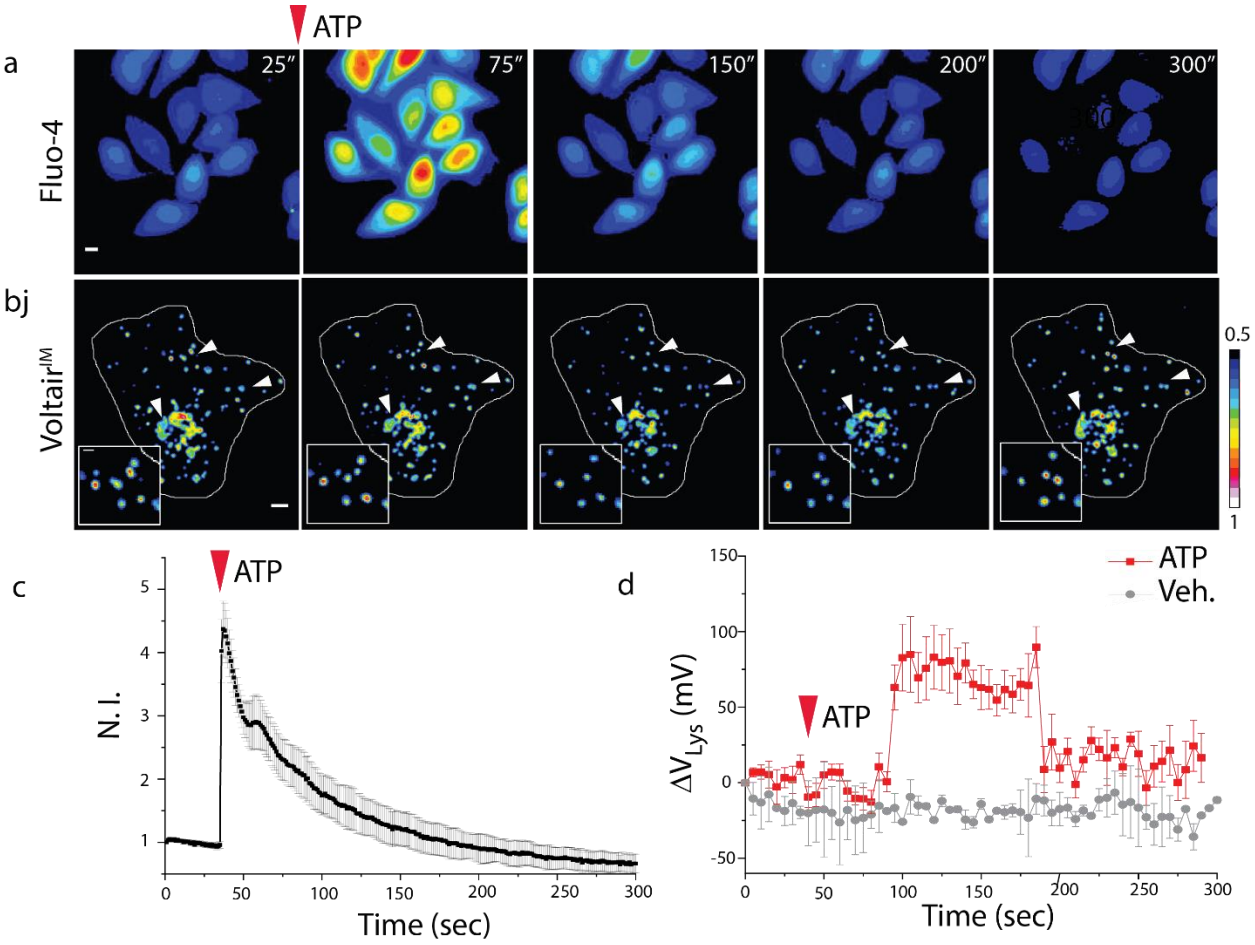

Figure V.10. Dynamic changes in lysosomal V_{mem}: (a) Representative pseudo-color time lapse images of ATP induced cytosolic calcium increase imaged using Fluo-4 AM dye. Scale = 10 µm. (b) Representative pseudo-color time lapse images of G/R ratio from VoltairIM in presence of 100 µM ATP. White arrowheads highlight the lysosomes undergoing ATP induced hyperpolarization. (c) Quantification of (a) as a fluorescent intensity vs time plot, error bar represents standard deviation from n = 10 cells; Scale = 10 µm. (d) Quantification of (b) as a normalized G/R ratio from whole cell vs time plot, 100 µM ATP treated (Black trace), Untreated (red trace). Decrease in G/R (observed in movie) represents increase in positive membrane potential. Error bar represents standard deviation from n = 6 cells; Scale = 10 µm. Experiments were repeated thrice independently with similar results.

V.D: Conclusion

The resting membrane potential for transient organelles such as early, late and recycling endosomes were previously not known. The dynamic maturation of these organelles in real time, makes it difficult to probe membrane potential using existing techniques. We have demonstrated that Voltair, when exogenously added, mimics as a receptor ligand and traffics along these challenging organelles, probing membrane potential. Our measurements provide compelling evidence for either Na^+ or K^+ in establishing the high membrane potential of the early endosome and in playing a significant role in establishing the ionic lumen. Magnitude of membrane potential and V-ATPase activity suggests membranes of recycling endosomes (+65 mV) and plasma membrane could be electrochemically similar at resting state. The membrane potential of the trans Golgi network (+121 mV), previously hypothesized to be negligible, is revealed to be as hyperpolarized as the lysosomal membrane (+114 mV). Yet, unlike the lysosome, membrane potential of trans Golgi network is only partially generated by V-ATPase. Similar to ATP being the chemical energy source of the cell, intracellular membrane potential could be the physical energy source for various organellar process. Non-invasive interrogation of this organellar membrane potential could offer the capacity to uncover how these organelles exploit membrane potential to regulate their function.

V.E: References

1. Xu, H., Martinoia, E. & Szabo, I. Organellar channels and transporters. *Cell Calcium* **58,** 1–10 (2015).
2. Saha, S., Prakash, V., Halder, S., Chakraborty, K. & Krishnan, Y. A pH-independent DNA nanodevice for quantifying chloride transport in organelles of living cells. *Nat. Nanotechnol.* **10,** 645–651 (2015).
3. Narayanaswamy, N. *et al.* A pH-correctable, DNA-based fluorescent reporter for organellar calcium. *Nat. Methods* **16,** 95–102 (2019).
4. Modi, S. *et al.* A DNA nanomachine that maps spatial and temporal pH changes inside living cells. *Nat. Nanotechnol.* **4,** 325–330 (2009).
5. Christensen, K. A., Myers, J. T. & Swanson, J. A. pH-dependent regulation of lysosomal calcium in macrophages. *J. Cell Sci.* **115,** 599–607 (2002).
6. Ishida, Y., Nayak, S., Mindell, J. A. & Grabe, M. A model of lysosomal pH regulation. *J. Gen. Physiol.* **141,** 705–720 (2013).
7. Xu, H. & Ren, D. Lysosomal physiology. *Annu. Rev. Physiol.* **77,** 57–80 (2015).
8. Grabe, M. & Oster, G. Regulation of organelle acidity. *J. Gen. Physiol.* **117,** 329–344 (2001).
9. Khosrowabadi, E. & Kellokumpu, S. Golgi ph and ion homeostasis in health and disease. *Rev Physiol Biochem Pharmacol* (2020). doi:10.1007/112_2020_49
10. Xiong, J. & Zhu, M. X. Regulation of lysosomal ion homeostasis by channels and transporters. *Sci China Life Sci* **59,** 777–791 (2016).
11. Koivusalo, M., Steinberg, B. E., Mason, D. & Grinstein, S. In situ measurement of the electrical potential across the lysosomal membrane using FRET. *Traffic* **12,** 972–982 (2011).
12. Steinberg, B. E., Touret, N., Vargas-Caballero, M. & Grinstein, S. In situ measurement of the electrical potential across the phagosomal membrane using FRET and its contribution to the proton-motive force. *Proc. Natl. Acad. Sci. USA* **104,** 9523–9528 (2007).
13. Zhong, X. Z. & Dong, X.-P. Lysosome electrophysiology. *Methods Cell Biol.* **126,** 197–215 (2015).
14. Dong, X.-P., Wang, X. & Xu, H. TRP channels of intracellular membranes. *J. Neurochem.* **113,** 313–328 (2010).
15. Zorova, L. D. *et al.* Mitochondrial membrane potential. *Anal. Biochem.* **552,** 50–59 (2018).
16. Schapiro, F. B. & Grinstein, S. Determinants of the pH of the Golgi complex. *J. Biol. Chem.* **275,** 21025–21032 (2000).
17. Qin, Y., Dittmer, P. J., Park, J. G., Jansen, K. B. & Palmer, A. E. Measuring steady-state and dynamic endoplasmic reticulum and Golgi Zn2+ with genetically encoded sensors. *Proc. Natl. Acad. Sci. USA* **108,** 7351–7356 (2011).

18. Maxson, M. E. & Grinstein, S. The vacuolar-type H^+-ATPase at a glance - more than a proton pump. *J. Cell Sci.* **127,** 4987–4993 (2014).

19. Farsi, Z. *et al.* Single-vesicle imaging reveals different transport mechanisms between glutamatergic and GABAergic vesicles. *Science (80-.).* **351,** 981–984 (2016).

20. Cang, C. *et al.* mTOR regulates lysosomal ATP-sensitive two-pore Na(+) channels to adapt to metabolic state. *Cell* **152,** 778–790 (2013).

21. Sun, X. *et al.* A negative feedback regulation of MTORC1 activity by the lysosomal Ca2+ channel MCOLN1 (mucolipin 1) using a CALM (calmodulin)-dependent mechanism. *Autophagy* **14,** 38–52 (2018).

22. Wang, W. *et al.* A voltage-dependent K+ channel in the lysosome is required for refilling lysosomal Ca2+ stores. *J. Cell Biol.* **216,** 1715–1730 (2017).

23. Leung, K., Chakraborty, K., Saminathan, A. & Krishnan, Y. A DNA nanomachine chemically resolves lysosomes in live cells. *Nat. Nanotechnol.* **14,** 176–183 (2019).

24. Anbari, M., Root, K. V. & Van Dyke, R. W. Role of Na,K-ATPase in regulating acidification of early rat liver endocytic vesicles. *Hepatology* **19,** 1034–1043 (1994).

25. Hover, S. *et al.* Bunyavirus requirement for endosomal K+ reveals new roles of cellular ion channels during infection. *PLoS Pathog.* **14,** e1006845 (2018).

26. Peluffo, R. D., Argüello, J. M. & Berlin, J. R. The role of Na,K-ATPase alpha subunit serine 775 and glutamate 779 in determining the extracellular K+ and membrane potential-dependent properties of the Na,K-pump. *J. Gen. Physiol.* **116,** 47–59 (2000).

27. Kellokumpu, S. Golgi ph, ion and redox homeostasis: how much do they really matter? *Front. Cell Dev. Biol.* **7,** 93 (2019).

28. Gagescu, R. *et al.* The recycling endosome of Madin-Darby canine kidney cells is a mildly acidic compartment rich in raft components. *Mol. Biol. Cell* **11,** 2775–2791 (2000).

29. Numata, M. & Orlowski, J. Molecular cloning and characterization of a novel (Na+,K+)/H+ exchanger localized to the trans-Golgi network. *J. Biol. Chem.* **276,** 17387–17394 (2001).

30. Raffaello, A., Mammucari, C., Gherardi, G. & Rizzuto, R. Calcium at the Center of Cell Signaling: Interplay between Endoplasmic Reticulum, Mitochondria, and Lysosomes. *Trends Biochem. Sci.* **41,** 1035–1049 (2016).

31. Atakpa, P., Thillaiappan, N. B., Mataragka, S., Prole, D. L. & Taylor, C. W. IP3 Receptors Preferentially Associate with ER-Lysosome Contact Sites and Selectively Deliver Ca2+ to Lysosomes. *Cell Rep.* **25,** 3180–3193.e7 (2018).

32. Russa, A. D. *et al.* Microtubule remodeling mediates the inhibition of store-operated calcium entry (SOCE) during mitosis in COS-7 cells. *Arch Histol Cytol* **71,** 249–263 (2008).

33. Lloyd-Evans, E. On the move, lysosomal CAX drives Ca2+ transport and motility. *J. Cell Biol.* **212,** 755–757 (2016).